

**NEAR-INFRARED AUTOFLUORESCENCE IMAGING  
AND SPECTROSCOPY FOR EARLY DETECTION OF  
PRECANCER AND CANCER IN THE COLON**

**SHAO XIAOZHUO**

**A THESIS SUBMITTED  
FOR THE DEGREE OF DOCTOR OF PHILOSOPHY  
DIVISION OF BIOENGINEERING  
NATIONAL UNIVERSITY OF SINGAPORE**

**2011**

# Acknowledgements

This thesis would not have been possible, or at least not what it looks like now, without the guidance and help of many people.

Foremost, I would like to show my sincere gratitude to my advisor Assistant Professor Huang Zhiwei. It was July in the year of 2006, when Prof Huang offered me the opportunity to pursue the PhD degree in his group. I appreciate his professional advice, guidance, and patience throughout my studies. His financial support on my experiments boosted the overall progress greatly. As an exemplary teacher and mentor, his influence has been truly beyond the research aspect of my life.

I would also like to thank Dr. Seow – Choen for his generous support and guidance on my experiments, and nurses for their assistance on the data collection.

Many labmates and colleagues in Optical Bioimaging Laboratory have helped me in the past five years. I would like to thank Dr. Zheng Wei, Dr. Bevin Lin, Dr. Lu Fake, Dr. Mo Jianhua, Teh Seng Knoon, Lin Kan, Lin Jian, Mads Bergholt, and Shiyamala Duraipandian for the inspiring brainstorming, valuable suggestions, and enlightening feedbacks on my work.

I would also like to acknowledge the financial supports from Academic Research Fund from the Ministry of Education of Singapore, the Biomedical Research Council, the National Medical Research Council, and the Faculty Research Fund from the National University of Singapore.

Last but not least, I would like to thank my parents and my husband. For their selfless care, endless love, and unconditional support, my gratitude is truly beyond words.

# Table of Contents

|                                                                    |            |
|--------------------------------------------------------------------|------------|
| <b>Acknowledgements .....</b>                                      | <b>I</b>   |
| <b>Table of Contents .....</b>                                     | <b>II</b>  |
| <b>Abstract.....</b>                                               | <b>IIV</b> |
| <b>List of Figures.....</b>                                        | <b>VI</b>  |
| <b>List of Tables.....</b>                                         | <b>X</b>   |
| <b>List of Abbreviations.....</b>                                  | <b>XI</b>  |
| <b>Chapter 1 Introduction.....</b>                                 | <b>1</b>   |
| 1.1 Overview of Colon Cancer .....                                 | 1          |
| 1.2 Screening Tests for Colon Cancer.....                          | 4          |
| 1.2.1 Conventional colon cancer screening methods.....             | 4          |
| 1.2.2 New colonoscopy techniques.....                              | 8          |
| 1.3 Challenges for Colonoscopy Screening .....                     | 12         |
| 1.4 Thesis Organization .....                                      | 13         |
| <b>Chapter 2 Fluorescence Imaging and Spectroscopy .....</b>       | <b>15</b>  |
| <b>2.1 The Basis of Fluorescence .....</b>                         | <b>15</b>  |
| 2.1.1 Interaction of light with a molecule .....                   | 15         |
| 2.1.2 Properties of fluorescence.....                              | 18         |
| 2.1.3 Fluorescence polarization .....                              | 18         |
| 2.1.4 Fundamentals for fluorescence detection.....                 | 20         |
| 2.2 Application of Fluorescence in Clinical Diagnosis .....        | 24         |
| 2.2.1 Exogenous fluorescent contrast agents .....                  | 25         |
| 2.2.2 Autofluorescence .....                                       | 26         |
| 2.2.3 Near-infrared autofluorescence.....                          | 29         |
| 2.3 Motivations .....                                              | 31         |
| 2.4 Research Objectives.....                                       | 34         |
| <b>Chapter 3 Autofluorescence Imaging of Colonic Tissues .....</b> | <b>36</b>  |
| 3.1 Introduction.....                                              | 36         |
| 3.2 Experiments .....                                              | 37         |
| 3.2.1 Near-infrared autofluorescence imaging system.....           | 37         |
| 3.2.2 Tissue preparation .....                                     | 44         |
| 3.3 Results and Discussion .....                                   | 45         |

|                                                                                                                                    |            |
|------------------------------------------------------------------------------------------------------------------------------------|------------|
| 3.3.1 NIR autofluorescence and reflectance diffuse imaging .....                                                                   | 45         |
| 3.3.2 Polarization autofluorescence imaging .....                                                                                  | 48         |
| 3.3.3 Ratio imaging of NIR DR/NIR AF .....                                                                                         | 51         |
| 3.4 Conclusion .....                                                                                                               | 54         |
| <b>Chapter 4 Endoscopy Based Spectroscopy for in vivo Diagnosis of Colonic Polyps .....</b>                                        | <b>57</b>  |
| 4.1 Introduction.....                                                                                                              | 57         |
| 4.2 Experiments .....                                                                                                              | 60         |
| 4.2.1 Integrated NIR AF spectroscopy system.....                                                                                   | 60         |
| 4.2.2 Patients and procedure .....                                                                                                 | 62         |
| 4.2.3 Multivariate analysis.....                                                                                                   | 63         |
| 4.3 Results and Discussion .....                                                                                                   | 67         |
| 4.4 Conclusions.....                                                                                                               | 76         |
| <b>Chapter 5 Study of Origin of Endogenous Fluorophores for NIR Autofluorescence .....</b>                                         | <b>78</b>  |
| 5.1 Introduction of Endogenous Fluorophores .....                                                                                  | 78         |
| 5.2 Experiments .....                                                                                                              | 82         |
| 5.2.1 The partial least square model .....                                                                                         | 82         |
| 5.2.2 Tissue specimens spectra .....                                                                                               | 83         |
| 5.2.3 Basis reference biochemicals.....                                                                                            | 84         |
| 5.3 Results and Discussion .....                                                                                                   | 85         |
| 5.3.1 In vivo colonic tissues.....                                                                                                 | 85         |
| 5.3.2 Ex vivo colonic paired specimens.....                                                                                        | 93         |
| 5.4 Conclusion .....                                                                                                               | 98         |
| <b>Chapter 6 Integrated Visible and Near-infrared Diffuse Reflectance Spectroscopy for Improving Colonic Cancer Diagnosis.....</b> | <b>101</b> |
| 6.1 Introduction of Diffuse Reflectance Spectroscopy .....                                                                         | 101        |
| 6.2 Diffuse Reflectance Spectroscopy System .....                                                                                  | 102        |
| 6.3 Results and Discussion .....                                                                                                   | 103        |
| <b>Chapter 7 Conclusions and Future Directions .....</b>                                                                           | <b>111</b> |
| 7.1 Conclusions.....                                                                                                               | 111        |
| 7.2 Future Directions .....                                                                                                        | 114        |
| <b>List of Publications .....</b>                                                                                                  | <b>117</b> |
| <b>References.....</b>                                                                                                             | <b>118</b> |
| <b>Appendix.....</b>                                                                                                               | <b>137</b> |

## Abstract

Early diagnosis and identification of precancer in the colon remains a great challenge in conventional white-light endoscopic examination. In recent years, optical methods such as autofluorescence (AF) technique, which are capable of detecting the changes of endogenous fluorophores and morphological architectures, have shown promising diagnostic potential for *in vivo* detection of precancer at endoscopy. Moreover, the near-infrared (NIR) light (700-1000 nm) is non-carcinogenic, and it is safe for tissue diagnosis. Both the excitation light used and the resulting tissue AF are at NIR wavelengths that can penetrate deeper into the tissue. Thus NIR AF could potentially be useful for the noninvasive *in vivo* detection of lesions located deeper inside the tissue. This dissertation presents the investigation on the diagnostic utility of NIR AF imaging and spectroscopy to detect precancer and cancer in the colon.

We have developed a novel integrated NIR AF and NIR diffuse reflectance (DR) imaging technique for colon cancer detection. 48 paired colonic tissue specimens (normal *vs.* cancer) were tested to evaluate the diagnostic feasibility of NIR AF imaging for differentiating cancer from normal tissues. The results suggest that the colon cancer tissues can be well separated from normal colonic tissues. The polarization technique was also coupled into the integrated NIR AF imaging system to further improve the diagnostic accuracy for colon cancer demarcation. The ratio imaging of NIR DR to NIR AF with polarization conditions achieved the best diagnostic accuracy of 95.8% among the NIR AF and NIR DR imaging modalities, affirming the potential of the integrated NIR AF/DR imaging with polarization for improving the early detection and diagnosis of malignant lesions in the colon.

We have also developed an endoscope-based NIR AF spectroscopy technique to realize real-time *in vivo* NIR AF spectra measurements from colonic tissue during clinical colonoscopic examination. Under the guidance of conventional wide-field endoscopic imaging, a novel bifurcated flexible fiber-probe, which can pass down the instrument channel of medical endoscopes, has been developed and integrated into the NIR AF spectroscopy system to measure *in vivo* NIR AF spectra from different types of colonic tissues from 100 patients, including normal ( $n=116$ ), hyperplastic polyp (benign abnormalities) ( $n=48$ ), and adenomatous polyps (precancer) ( $n=34$ ). Multivariate statistical techniques (principal components analysis (PCA) combined with linear discriminate analysis (LDA)) are employed for developing effective diagnostic algorithms for classification of different colonic

tissue types. The diagnostic algorithms yield overall accuracies of 88.9%, 85.4% and 91.4% respectively, for classification of colonic normal, hyperplastic, and adenomatous polyps. This indicates that NIR AF spectroscopy is a unique diagnostic means for *in vivo* diagnosis and characterization of precancerous and cancerous colonic tissues.

To further investigate the origins of tissue biochemicals responsible for the differences of NIR AF among different types of colonic tissues, we have constructed a non-negativity-constrained least squares minimization (NNCLSM) biochemical model to estimate the biochemical compositions of colonic tissues. The NIR AF spectra from the nine representative biochemicals (i.e., collagen I, elastin,  $\beta$ -NADH, FAD, L-tryptophan, hematoporphyrin, 4-pyridoxic acid, pyridoxal 5'-phosphate, and water) were found the most significant in colonic tissue for optimally fitting the measured *in vivo* NIR AF spectra colonic tissue. Colonic precancer and cancer tissues show lower fit coefficients belonging to collagen I, FAD,  $\beta$ -NADH, L-tryptophan, and pyridoxal 5'-phosphate, and higher fit coefficients belonging to hematoporphyrin, 4-pyridoxic acid, and water as compared to benign tissues. We also compared the fitting results between *in vivo* and *ex vivo* datasets. NIR AF spectroscopy provides new insights into biochemical changes of colonic tissue associated with cell proliferation and metabolic rate during the cancer progression.

Moreover, we have also investigated the diagnostic ability of the integrated visible (VIS) and NIR DR spectroscopy technique for detection and diagnosis of colon cancer. High-quality integrated VIS-NIR DR spectra (400-1000 nm) from normal and cancer colonic mucosal tissue were acquired within 8 msec and significant differences are observed in DR spectra between normal (n=58) and cancer (n=48) colonic tissue, particularly in the spectral bands near 420, 540, 580 and 1000 nm, which are primarily correlated to absorption of hemoglobin and water. Best differentiation between normal and cancer tissues can be achieved using the integrated VIS-NIR DR spectroscopy as compared to VIS or NIR DR spectroscopy alone, indicating the potential of the integrated VIS-NIR DR together with PCA-LDA algorithms for improving early diagnosis of colon cancer.

The results of this dissertation establish a proof of principle that NIR AF/DR imaging and spectroscopy techniques have the potential to be a clinically useful tool to complement the conventional white light endoscopy for non-invasive *in vivo* diagnosis and detection of colonic precancer and cancer during clinical colonoscopic screening.

## List of Figures

|                 |                                                                                                                                                                                                                                                                                                                                                                                                                                                                     |    |
|-----------------|---------------------------------------------------------------------------------------------------------------------------------------------------------------------------------------------------------------------------------------------------------------------------------------------------------------------------------------------------------------------------------------------------------------------------------------------------------------------|----|
| <b>Fig. 1.1</b> | Anatomy of the colon.....                                                                                                                                                                                                                                                                                                                                                                                                                                           | 1  |
| <b>Fig. 1.2</b> | Conceptualization of morphologic progression through oncogenesis, incorporating altered cell relationships, and invasion through the basement membrane.....                                                                                                                                                                                                                                                                                                         | 2  |
| <b>Fig. 2.1</b> | Electromagnetic waves with the electric field in a vertical plane and the magnetic field in a horizontal plane .....                                                                                                                                                                                                                                                                                                                                                | 16 |
| <b>Fig. 2.2</b> | Simple Perrin-Jablonski diagram showing three electronic states, several vibrational states, absorption of electromagnetic radiation, and emission of fluorescence or phosphorescence .....                                                                                                                                                                                                                                                                         | 17 |
| <b>Fig. 2.3</b> | Interactions between tissue and light .....                                                                                                                                                                                                                                                                                                                                                                                                                         | 22 |
| <b>Fig. 2.4</b> | Absorption spectra for some tissues (aorta, skin) and tissue component (whole blood, melanosome, epidermis, and water).....                                                                                                                                                                                                                                                                                                                                         | 23 |
| <b>Fig. 3.1</b> | Schematic diagram of the integrated NIR AF and NIR DR imaging system with polarization developed for tissue measurements.....                                                                                                                                                                                                                                                                                                                                       | 39 |
| <b>Fig. 3.2</b> | (a) NIR AF image of chicken muscle with melanin powder and (b) intensity profile along the line as indicated on the image (a).....                                                                                                                                                                                                                                                                                                                                  | 40 |
| <b>Fig. 3.3</b> | The mean NIR AF intensity ratio of the melanin over the chicken muscle $\pm 1$ standard error (SE) with the increasement of depth .....                                                                                                                                                                                                                                                                                                                             | 42 |
| <b>Fig. 3.4</b> | Polar diagrams displayed for a full sample rotation of every 20 degree for six paired colonic tissues, (a) NIR AF imaging, (b) NIR DR imaging. The error bars stand for the standard errors (SE).....                                                                                                                                                                                                                                                               | 42 |
| <b>Fig. 3.5</b> | Representative NIR DR and AF images of colonic tissues acquired using tungsten halogen light illumination and 785 nm laser excitation under different polarization conditions: (a) DR with non-polarization, (b) DR with parallel polarization, (c) DR with perpendicular polarization, (d) AF with non-polarization, (e) AF with parallel polarization, (f) AF with perpendicular polarization.....                                                                | 46 |
| <b>Fig. 3.6</b> | The average AF intensity for the normal and cancer colonic tissues based on the selected region on (a) NIR DR image and (b) NIR AF images.....                                                                                                                                                                                                                                                                                                                      | 47 |
| <b>Fig. 3.7</b> | Representative pseudocolor NIR AF images of colonic tissues acquired using 785 nm excitation under different polarization conditions: (a) non-polarization, (b) parallel polarization, and (c) perpendicular polarization. (d) Intensity profiles along the lines on the NIR AF images in (a-c). Note that the AF intensity profiles under the parallel and perpendicular polarizations have been magnified by 4 times in Fig. 3.7(d) for better visualization..... | 49 |

|                  |                                                                                                                                                                                                                                                                                                                                                                                                                                                                                                                                                                                                                                        |    |
|------------------|----------------------------------------------------------------------------------------------------------------------------------------------------------------------------------------------------------------------------------------------------------------------------------------------------------------------------------------------------------------------------------------------------------------------------------------------------------------------------------------------------------------------------------------------------------------------------------------------------------------------------------------|----|
| <b>Fig. 3.8</b>  | Pair-wise comparison of NIR AF intensities of all 48 paired (normal vs. cancer) colonic tissues under the three different polarization conditions: (a) non-polarization, (b) parallel polarization, and (c) perpendicular polarization.....                                                                                                                                                                                                                                                                                                                                                                                            | 50 |
| <b>Fig. 3.9</b>  | (a) The processed polarization ratio image $((I_{par}-I_{per})/(I_{par}+I_{per}))$ , where $I_{par}$ and $I_{per}$ are the NIR AF intensities under the parallel and perpendicular polarization conditions) of normal and cancer tissue. (b) Polarized ratio values along the line across normal and cancer colonic tissue as indicated on the polarization ratio image in Fig.3.9(a).....                                                                                                                                                                                                                                             | 52 |
| <b>Fig. 3.10</b> | NIR DR images of colonic tissues acquired using a broadband light source under different polarization illumination: (a) non-polarization, (b) parallel polarization, (c) perpendicular polarization, and (d) intensity profiles along the lines as indicated on the NIR DR images. Note that the AF intensity profiles under the parallel and perpendicular polarizations have been magnified by 12 times in Fig. 3.10(d) for better visualization.                                                                                                                                                                                    | 53 |
| <b>Fig. 3.11</b> | Ratio imaging of the NIR DR image to the NIR AF image under different polarization conditions: (a) non-polarization, (b) parallel polarization, (c) perpendicular polarization. (d) Comparison of ratio intensity profiles along the lines as indicated on the ratio images. Note that the ratio intensity profiles under parallel and perpendicular polarization have been magnified by 3 times in Fig. 3.11(d) for better visualization.....                                                                                                                                                                                         | 54 |
| <b>Fig. 4.1</b>  | Phenotypic stages in the adenoma-carcinoma sequence.....                                                                                                                                                                                                                                                                                                                                                                                                                                                                                                                                                                               | 58 |
| <b>Fig. 4.2</b>  | Schematic diagram of the integrated AF spectroscopy and wide-field endoscopic imaging system for <i>in vivo</i> tissue AF measurement at colonoscopy.....                                                                                                                                                                                                                                                                                                                                                                                                                                                                              | 62 |
| <b>Fig. 4.3</b>  | White-light reflectance (WLR) images of colonic tissues during clinical colonoscopy (a) normal, (b) polyp, and (c) cancer.....                                                                                                                                                                                                                                                                                                                                                                                                                                                                                                         | 63 |
| <b>Fig. 4.4</b>  | <i>In vivo</i> mean NIR AF spectra $\pm 1$ SE of normal (n=116), hyperplastic (n=48) and adenomatous polyps (n=34) colonic tissue. The shaded areas in tissue AF spectra stand for the respective standard error.....                                                                                                                                                                                                                                                                                                                                                                                                                  | 68 |
| <b>Fig. 4.5</b>  | The first eight significant principal components (PCs) (PC1~80.50%, PC2~10.08%, PC3~4.05%, PC4~2.52%, PC5~0.79%, PC6~0.42%, PC7~0.12%, and PC8~0.09%) accounting for ~99% of the total variance calculated from <i>in vivo</i> NIR AF spectra.....                                                                                                                                                                                                                                                                                                                                                                                     | 70 |
| <b>Fig. 4.6</b>  | Box charts of the eight significant principal component (PC) scores for the three colonic types (normal, hyperplastic polyp and adenomatous polyp): a PC1, b PC2, c PC3, d PC4, e PC5, f PC6, g PC7, and h PC8. The line within each notch box represents the median, and the lower and upper boundaries of the box indicate first (25 percent percentile) and third (75 percent percentile) quartiles respectively. Error bars (whiskers) represent the 1.5-fold interquartile range. * $p < 0.05$ (pairwise comparison of tissue types with <i>post hoc</i> multiple comparison tests (Fisher's least significant differences))..... | 71 |

|                 |                                                                                                                                                                                                                                                                                                                                                                                             |    |
|-----------------|---------------------------------------------------------------------------------------------------------------------------------------------------------------------------------------------------------------------------------------------------------------------------------------------------------------------------------------------------------------------------------------------|----|
| <b>Fig. 4.7</b> | Two-dimensional ternary plot of the posterior probability belonging to normal tissue, hyperplastic and adenomatous polyp, illustrating the good clusterings of the three different colonic tissue types achieved by PCA-LDA algorithms, together with the leave-one tissue site-out, cross validation method.....                                                                           | 73 |
| <b>Fig. 5.1</b> | <i>In vivo</i> mean NIR AF spectra $\pm 1$ SE of normal (n=116), hyperplastic polyps (n=48), adenomatous polyps (n=34), and cancer (n=65) colonic tissue. The shaded areas in tissue AF spectra stand for the respective standard error.....                                                                                                                                                | 86 |
| <b>Fig. 5.2</b> | The nine basis reference AF spectra form collagen I, elastin, $\beta$ -NADH, FAD, L-tryptophan, hematoporphyrin, 4-pyridoxic acid, pyridoxal 5'-phosphate and water are used for biochemical modeling of the colonic tissue.....                                                                                                                                                            | 87 |
| <b>Fig. 5.3</b> | Comparison of <i>in vivo</i> colonic AF spectra measured with the reconstructed tissue AF spectra through the employment of the nine basis reference AF spectra: (a) normal, (b) hyperplastic polyp, (c) adenomatous polyp, and (d) cancer colonic tissues. Residuals (measured spectrum minus reconstructed spectrum) are also shown in each plot.....                                     | 89 |
| <b>Fig. 5.4</b> | Histograms displaying the average compositions of the tissues diagnosed as normal, hyperplastic polyp, adenomatous polyp, and cancer. The one SE confidence intervals as shown for each model component. All nine biochemicals are for discriminating four different type of colonic tissues ( $p < 0.05$ ); the relative concentration of 4-pyridoxic acid times 0.5 and FAD times 10..... | 90 |
| <b>Fig. 5.5</b> | Ex vivo mean NIR AF spectra $\pm 1$ SE of normal (n=68) and cancer (n=32) colonic tissue. The shaded areas in tissue AF spectra stand for the respective standard error.....                                                                                                                                                                                                                | 94 |
| <b>Fig. 5.6</b> | Comparison of ex vivo colonic AF spectra measured with the reconstructed tissue AF spectra through the employment of the nine basis reference AF spectra: (a) normal and (b) cancer colonic tissues. Residuals (measured spectrum minus reconstructed spectrum) are also shown in each plot.....                                                                                            | 95 |
| <b>Fig. 5.7</b> | Histograms displaying the average compositions of the tissues diagnosed as normal and cancer. The one SE confidence intervals as shown for each model component. All biochemicals are significant for discriminating two different type of colonic tissues ( $p < 0.05$ ).....                                                                                                              | 96 |
| <b>Fig. 5.8</b> | Scatter plot of the posterior probabilities belonging to normal and cancer colonic tissue using the LDA algorithms. The separate line yields a diagnostic sensitivity of 84.3% (27/32) and 88.2% (60/68) for distinguishing cancer from normal colon tissues.....                                                                                                                           | 97 |
| <b>Fig. 5.9</b> | Receiver operating characteristic (ROC) curve of discrimination results of normal and cancer colonic tissue using the LDA algorithm based on relative concentration for nine biochemicals. The integration areas under the ROC curves are 94.5.....                                                                                                                                         | 98 |

|                 |                                                                                                                                                                                                                                                                                                                                                                                    |
|-----------------|------------------------------------------------------------------------------------------------------------------------------------------------------------------------------------------------------------------------------------------------------------------------------------------------------------------------------------------------------------------------------------|
| <b>Fig. 6.1</b> | The mean integrated visible and near-infrared (VIS/NIR) diffuse reflectance (DR) spectra $\pm 1$ standard error (SE) of normal (n=58) and cancer (n=48) colonic tissue. The shaded areas in tissue DR spectra stand for the respective standard error.....104                                                                                                                      |
| <b>Fig. 6.2</b> | The nine principal components (PCs) accounting more than 99% of the total variance calculated from the integrated VIS/NIR DR spectra (PC1~93.14%, PC2~4.64%, PC3~1.38%, PC4~0.48%, PC5~0.23%, PC7~0.02%, PC8~0.014%, PC9~0.01%, PC10~0.01%).....107                                                                                                                                |
| <b>Fig. 6.3</b> | Scatter plot of the posterior probability belonging to the normal and cancer colonic tissue calculated from the data sets of (a) integrated VIS/NIR, (b) VIS, and (c) NIR, respectively, using the PCA-LDA algorithms, together with the leave-one tissue site-out, cross validation method with three different spectral spaces.....108                                           |
| <b>Fig. 6.4</b> | Receiver operating characteristic (ROC) curve of discrimination results for integrated VIS/NIR, VIS, and NIR DR spectra, respectively, using PCA-LDA algorithms, together with the leave-one tissue site-out, cross validation method. The integration areas under the ROC curve are 0.973, 0.93, and 0.878, respectively, for integrated VIS/NIR, VIS, and NIR DR spectra.....109 |

## List of Tables

|                  |                                                                                                                                                                                                                                                                                                      |    |
|------------------|------------------------------------------------------------------------------------------------------------------------------------------------------------------------------------------------------------------------------------------------------------------------------------------------------|----|
| <b>Table 3.1</b> | Comparison of diagnostic accuracy and p-value (paired 2-sided Student's <i>t</i> -test) of different NIR imaging modalities (i.e., NIR AF imaging and NIR DR image under non-, parallel- and perpendicular polarization, and the ratio imaging of NIR DR to NIR AF for detection of colon cancer.... | 55 |
| <b>Table 4.1</b> | Classification results of <i>in vivo</i> NIR AF spectra prediction for the three colonic tissue groups using PCA-LDA algorithms, together with the leave-one tissue site-out, cross validation method .....                                                                                          | 74 |
| <b>Table 5.1</b> | Classification results of nine biochemicals for four colonic tissue groups using LDA algorithms.....                                                                                                                                                                                                 | 93 |

## List of Abbreviations

|        |                                                       |
|--------|-------------------------------------------------------|
| AF     | Autofluorescence                                      |
| AJCC   | American Joint Committee on Cancer                    |
| ANOVA  | Analysis of variance                                  |
| ANSI   | American National Standards Institute                 |
| CCD    | Charge coupled device                                 |
| CT     | Computed tomography                                   |
| DR     | Diffuse reflectance                                   |
| FAD    | Flavin adenine dinucleotide                           |
| FIT    | Fecal immunochemical tests                            |
| FMN    | Flavin mononucleotide                                 |
| FOBT   | Fecal occult blood testing                            |
| G-FOBT | Guaiac-FOBT                                           |
| ICG    | Indocyanine green                                     |
| IRB    | Institutional Review Board                            |
| LDA    | Linear discriminate analysis                          |
| NADH   | Nicotinamide adenine dinucleotide                     |
| NBI    | Narrow Band Imaging                                   |
| NHG    | National Healthcare Group                             |
| NIR    | Near infrared                                         |
| NNCLSM | Non-negativity-constrained least squares minimization |
| QDs    | Quantum dots                                          |
| PC     | Principal components                                  |
| PCA    | Principal components analysis                         |
| PLP    | Pyridoxal 5'-phosphate                                |
| PLS-DA | Partial least square – discriminant analysis          |
| ROC    | Receiver operating characteristic                     |
| SE     | Standard error                                        |
| UV     | Ultraviolet                                           |
| VIS    | Visible                                               |
| VR     | Vibrational relaxation                                |
| WLR    | White-light reflectance                               |

# Chapter 1 Introduction

## 1.1 Overview of Colon Cancer

Cancer that develops in the colon and rectum is called colon cancer or colorectal cancer. Colon cancer is a common type of malignancy, which has uncontrolled growth of the cells that line inside the colon or rectum. The colon is primarily responsible for the absorption of water and mineral nutrients from solid wastes before they are eliminated from the body. Fig. 1.1 shows the anatomy of the colon that is a muscular tube and has 4 sections: ascending colon (the vertical segment located on the right side of the abdomen), transverse colon (extending across the abdomen), descending colon (leading vertically down the left side of the abdomen) and sigmoid colon (extending to the rectum) [1].

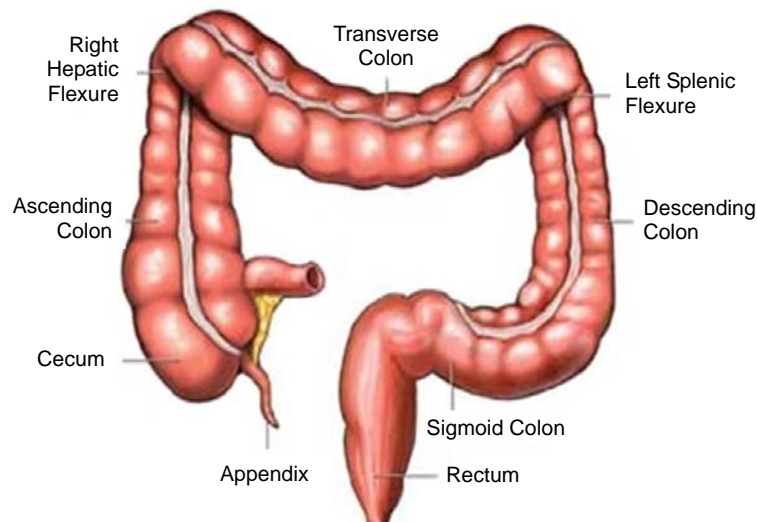


**Fig. 1.1** Anatomy of the colon [2].

Colon cancer arises from a series of genomic alterations that result in transformation of a normal epithelial cell into an adenocarcinoma cell. The biology of colon cancer is complex and involves concepts such as genomic alterations,

multistage carcinogenesis, oncogene activation, expansion of clones of neoplastic cell, homeostatic control of cell growth, and cell invasion [3]. The development of colon cancer is characterized by a progressively disordered genome and perturbed biology [4]. Fig. 1.2 shows the proliferation and growth of cancer cells invading through the basement membrane. The traditional understanding of developing colon cancer is based on the concept of the adenoma-carcinoma sequence [5-6]. According to this theory, benign precancerous colon lesions (e.g. adenomatous polyps) gradually transform to invasive cancer over time, and thus, early detection and removal of these precancerous polyps has been widely accepted to effectively prevent colon cancer development and decrease the associated mortality rate [7].

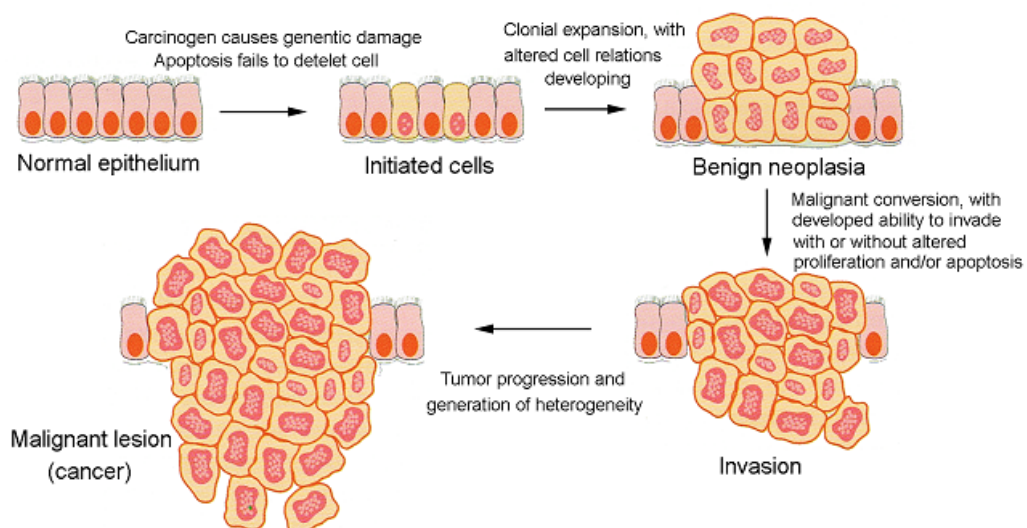


**Fig. 1.2** Conceptualization of morphologic progression through oncogenesis, incorporating altered cell relationships, and invasion through the basement membrane [8].

Colon cancer has become the third leading cause of cancer-related death, accounting for approximately 655,000 annual deaths worldwide [9]. The incidence of colon cancer varies with the economic development of individual countries, including the level of affluence and westernization of lifestyle [10]. For example, the highest incidence rates are found in Australia and North America, whereas the

lowest rates are found in Africa and South-central Asia [11]. In Singapore, the incidence of colon cancer has increased dramatically over the past three decades; colon cancer has become the most common malignancy for males and the second most common for females [12]. A number of factors appear to increase an individual's risk for colon cancer, including older age, male gender, diet and exercise habits, a history of inflammatory bowel disease, certain genetic syndromes, and a family history of colon cancer or adenomatous polyps [13].

Currently, both the incidence and mortality rates for colon cancer have been stable and even declining in some developed countries [9, 11]. The declining mortality and incidence rates might reflect the improving preventive methods for the early detection and treatment of adenomatous polyps and non-invasive cancers before they advance to metastatic carcinomas. According to the American Joint Committee on Cancer (AJCC) staging of colon cancer [14], if the colon cancer is diagnosed while it is still localized or confined to the primary site (stage I/IIa), the survival rate is 90% at 5 years; if the cancer has spread to regional lymph nodes (stage III) or directly beyond the primary site (stage IIIb), the corresponding 5-year survival rate is 67%; if the cancer has already metastasized to distant sites (stage IV), the 5-year survival rate is only 10% [15]. Thus, the disease stage directly affects mortality rate in colon cancer. However, only 39% of colon cancer is detected at an early stage (stage I/IIa) [8]. Hence, it is of imperative clinical value to develop sensitive diagnostic techniques to detect colon cancer at an early stage. In the remaining part of this Chapter, the screening methods for colon cancer are briefly reviewed and the challenges for conventional screening tests are discussed.

## **1.2 Screening Tests for Colon Cancer**

Patients with colon cancer may present symptoms such as occult or symptomatic anemia, bright red blood per rectum, abdominal pain, change in bowel habits, anorexia, weight loss, nausea, vomiting, or fatigue. Although the symptoms of colon cancer are not inherently unique, the biology of colon cancer provides opportunities for preventive strategies to detect at an early stage. The progression from premalignant lesions to colon cancer consists of multiple steps, such as development of polyps and occult bleeding, which are clinically recognizable. For instance, during the colonoscopic examination, the polyps can be found and removed before they turn into cancer. Thus, the screening test is a key element for increasing the chance of detecting a curable neoplastic lesion and decreasing colon cancer morbidity or mortality [16]. In the past 20 years, there are drastic progresses in the development of new screening methods for colon cancer [17]. In the next two sections, the conventional screening methods and novel techniques will be reviewed, including fecal occult blood testing, computed tomography (CT) colonography, endoscopic screening, and novel colonoscopes integrated with advanced optical techniques.

### **1.2.1 Conventional colon cancer screening methods**

#### **Fecal occult blood testing (FOBT)**

FOBTs aim to detect subtle blood loss in the gastrointestinal tract and are often done as the part of a routine examination. The cancerous tissue is more likely to bleed than normal tissue in the colon due to inflammatory bowel disease, adenomas polyps, or benign or cancerous tumors. Thus, microscopic bleeding provides the basis for

screening early colon cancer using FOBT. There are two main FOBT technologies: guaiac-FOBT (G-FOBT) and fecal immunochemical testing (FIT). G-FOBT is dependent on the detection of peroxidase activity of heme, while FIT is based on antibodies to detect globin [18]. Since globin does not survive in the passage through the upper gastrointestinal tract, the FIT's detection of globin is specific for occult bleeding from the large bowel. Therefore, FIT is more sensitive and specific for detection of cancerous and pre-cancerous lesions than the G-FOBT. Moreover, FIT does not require dietary or drug restriction prior to testing [19].

FOBT can be simple and easy to perform in the convenience and privacy at home. These advantages for easily undergoing the test could lead to higher rates of screening participation. However, the biology of bleeding is complex. Positive tests could result from either upper gastrointestinal bleeding or lower gastrointestinal bleeding, thus they warrant further investigation for colon cancer or gastric cancer. The sensitivity of FOBT is difficult to estimate, but studies of interval cancers suggest that only 50% of cancers will be picked up in population screening and the specificity is much higher at around 98% [20]. In other words, if the test result is negative, no further investigation is needed and the participant is recalled for testing in two years. Otherwise, colonoscopy is offered for further investigation [16].

### **Computed tomography (CT) colonography**

CT colonography, which is also referred to as 'virtual colonoscopy', is a CT scan x-ray test to provide a three dimensional radiologic assessment of the colon for large colon polyps and cancers. This test has been recommended to people without symptoms to screen for colon polyps and cancers. The main advantages of CT colonography are considered to have the ability to visualize the whole bowel and

localize any lesions with less invasion than conventional colonoscopy [21].

The sensitivity for the CT colonography depends on the lesion size. For the detection of a 1 cm diameter polyp or even larger size, CT colonography can achieve sensitivity around 90%. For polyps less than 1 cm, the sensitivity decrease rapidly; the sensitivity is only about 50% for detection of the flat or small lesions (<1 cm) [22-23]. Consequently, radiologists are advised not to attempt to interpret polyps with 5mm or smaller diameter that are found by CT colonography. Moreover, there are additional challenges for the utilization of CT colonography for screening colon cancer. First, it is not therapeutic and full bowel cleaning is also necessary. Second, the radiologic equipment and imaging software are not widely available. Finally, the evaluation of images is time-consuming. Hence, more studies are needed before this technique becomes established as a standard screening method.

### **Endoscopic screening**

In 1963, the first endoscopy for the colon was introduced by Turell; and since then flexible sigmoidoscopy has been used for colon examination in the clinic [24]. Currently, endoscopy has become the primary diagnostic and therapeutic method for the evaluation and treatment of colonic disease. Sigmoidoscopy and colonoscopy are the most common screening procedures.

A sigmoidoscopy allows an examination of the final 2 feet of the colon, reaching 30-60 cm into the colon from the rectum through sigmoid. This examination can be conducted without sedation and only with enema preparation. The whole procedure for the sigmoidoscopy takes 10 to 20 minutes, and the patient does not need recovery facilities. There are two types of sigmoidoscopy: rigid and flexible sigmoidoscopy. Flexible sigmoidoscopy is generally the preferred procedure.

This is because the flexible sigmoidoscope with its 60cm length flexible probe allows more comfortable insertion and manipulation around the rectosigmoid junction and sigmoid colon compared to the rigid sigmoidoscope. Approximately 75% of colon cancer occurs in the rectum or sigmoid colon, thus flexible sigmoidoscopy has been reported to have 60% to 70% sensitivity for the detection of advanced neoplasms and a 60% to 80% reduction in mortality of colon cancer [25-26]. However, due to the limited probe length, flexible sigmoidoscopy is not sufficient to detect polyps or cancer in the ascending or transverse colon. Moreover, sigmoidoscopy is less sensitive for adenomas than colonoscopy even in the distal colon [27].

Colonoscopy, which is the most complete methods for examining the colon, has been accepted as the gold standard for the diagnosis of colon cancer. The first complete colonoscopy was reported by Wolf in 1971 [28]. With the development of light source, flexible shaft, fiber optic, angulation control, and charge coupled devices (CCDs), video colonoscope was invented in the 1980s [29]. Currently, the conventional white-light reflectance (WLR) colonoscope transmits light to the lumen via fiber optics cables from a separate light source, and then retrieves images digitally using a CCD chip at the tip with a 140° field of view [30]. Under visual guidance, the colonoscopic examination can be used to look for inflamed tissue, ulcers, and abnormal growths in the colon and assist doctors in detecting early signs of colon cancer. Integrated with the ability to take biopsies and intervene therapeutically, colonoscopy is the ideal diagnostic tool for colon cancer. Although the sensitivity for the colonoscopy is strongly associated with the operator's skill, the quality of the colon preparation, and the withdrawal time that it takes to examine

the entire colon, colonoscopy is more sensitive than sigmoidoscopy for adenoma detection. Less than 6% of advanced adenomas (at least 1 cm in diameter) are reported to be missed on colonoscopy [31]. A 50% reduction in mortality colon cancer was observed in a case control study of colonoscopy in the US veteran population [27]. In addition, colonoscopy also showed clear mortality benefit in a population of people with hereditary colon cancer [32].

Colonoscopy has become the established routine procedure for colon disease screening. However, there are several limitations that hamper colonoscopy from being the primary screening tool for colon cancer, such as the bowel preparation, cardiovascular events during sedation, perforation and bleeding, longer time for employment, relatively high cost, and the need for trained personnel. Thus, some advanced techniques have been developed to complement conventional colonoscopy for the non-invasive *in vivo* detection and diagnosis of colon cancer during colonoscopic examination.

### **1.2.2 New colonoscopy techniques**

As introduced in the previous section, applying different screening methods for early detection of colon cancer is effective to reduce related mortality. FOBT as the first step screening has showed a 15-38% reduction on an intention-to-screen basis at the population level, while colonoscopy as the second step further provides comprehensive adenoma detection. Currently, it is recommended that screening for colon cancer begins at 50 years age with annual or biennial FOBT screening and every 5 years flexible sigmoidoscopy or colonoscopy. However, the limitations for these conventional screening methods, as discussed above, render a demand for new colon cancer detection and diagnosis techniques. Here, four representative novel

colonoscopy screening methods were selected to demonstrate the improvements in the diagnosis of precancer and cancer in the colon.

### **Chromoendoscopy**

Chromoendoscopy takes advantage of stains or pigments to enhance mucosal details to improve tissue localization, characterization, and diagnosis of colon cancer [33]. During colonoscopy screening, the stains can be sprayed using specially designed catheters through the instrument channel. Then the effect of these stains on the subtle mucosal irregularities can be visualized under a white light colonoscope or fluorescence endoscope. The major absorptive dye is methylene blue and contrast agent is indigo carmine [34]. Saitoh *et al.* reported the successful application of chromoendoscopy using 0.08% indigo carmine to improve the diagnosis of flat and depressed lesions by 65% [35]. Chromoendoscopy has been shown to be a very simplistic method to enhance mucosal detail by spraying of stains, thus it has been widely applied in a variety of clinical settings and throughout all gastrointestinal tract segments (including the colon) by the endoscope in the past 10 years [36]. Chromoendoscopy is perceived to be a safe procedure, and the stains are considered to be nontoxic at the concentrations used [37]. However, because of the usage of the chemical dyes, the side effect of these chemical stains warrants further investigation.

### **Confocal microendoscopy**

Confocal microscopy is a powerful tool to perform high-resolution non-invasive imaging of a thin plane or section within a thick turbid biologic tissue [38]. It enables the optical sectioning capability for *in vivo* imaging of tissue with depth selectivity and realizes real-time microscopic visualization of tissue at the cellular level. As a result, the confocal microendoscope can improve the selection of tissue

for biopsy and increase the accuracy of diagnosis. Moreover, it may even replace tissue extraction biopsy and realize real-time non-invasive optical biopsy [39]. A miniaturized confocal microscopy has been developed by OptiScan and Pentax Corporation to incorporate into the distal tip of conventional colonoscopy for simultaneous white light endoscopy and confocal microscopy [40]. Based on the *in vivo* subsurface analysis of colonic cellular structures, Kiesslich *et al.* reported a high accuracy (sensitivity 97.4%, specificity 99.4%, and accuracy 99.2%) for detecting neoplastic changes during confocal microendoscopy in the colon [40]. The successful applications of confocal microendoscopy have demonstrated the potential for a non-destructive optical biopsy for performing instantaneous mucosal histopathology without the risk of bleeding [41]. Despite the promise of confocal microendoscopy technologies, continual technical advances are needed to further explore the full potential of confocal microendoscopy for colon cancer detection and diagnosis, such as sectioning at greater depths, contrast agents for specific disease, and increased frame rates for reducing scanning time.

### **Capsule endoscopy**

Capsule endoscopy was developed to examine parts of the gastrointestinal tract that cannot be seen with other types of endoscopy. After a patient swallows the capsule that contains a tiny camera, images are captured and sent back to a computer for construction inside luminal view of entire gastrointestinal tract [42]. Currently, it has been successfully used to visualize the upper gastrointestinal tract and small bowel [17]. But a few applications have been reported in the colon due to the limited battery life. Van Gossum *et al.* have reported that 73% of advanced adenoma and 74% of cancer cases are correctly detected by capsule endoscopy compared with

conventional colonoscopy [43]. However, capsule endoscopy has not been widely explored for detection of colonic lesions. This is due to the impact of gastrointestinal motility on the visualization and accuracy of image capture. The slow motility could result in slow progress and battery failure before completion of the whole exam, while the rapid motility could result in inadequate imaging and poor image quality. Moreover, it still lacks the ability to biopsy the detected lesions during the screening procedure. Until upon resolution of these issues, capsule endoscopy could provide a major advance in the diagnosis of colonic disease.

### **Autofluorescence imaging and spectroscopy**

Laser-induced fluorescence spectroscopy and imaging take advantage of endogenous fluorophores to improve the detection of microscopic lesions at the molecular level during endoscopic examination. Since endogenous fluorophores are associated with the structural matrix of tissues or involved in cellular metabolic processes, autofluorescence (AF) techniques have been developed to interrogate the colonic epithelial surfaces to reveal subtle lesions not seen by conventional WLR endoscopy. When the colonic tissues are illuminated by low-power laser, the emitted fluorescence light with longer wavelength than the illumination light is the tissue AF arising from endogenous fluorophores. Different excitation wavelengths induce different groups of fluorophores, each of which emits at a range of different wavelengths.

Fluorescence emission from tissue is not only affected by constitutions of fluorophores, but also influenced by tissue architecture, light absorption properties, biochemical environment, and metabolic status of the tissue [44]. When cancer occurs, the invasion of the cancer cells results in the alteration of tissue

morphological structure and biochemical composition. As a result, the tissue AF emission changes accordingly. Thus, AF techniques have been explored to interrogate cancer in various organs by comparing the differences of AF spectra or images between normal and cancer tissues. AF bronchoscopy has become one of the well developed techniques for detecting early lung cancer [45]. AF technique has also been integrated with conventional WLR colonoscopy for detecting premalignant lesion in the colon [46]. A clinical study has reported the successful application for differentiating benign hyperplastic polyps from adenomatous polyps with a sensitivity of 90% and a specificity of 95% [47]. To date, tissue fluorescence was one of the best developed methods to enhance the conventional endoscopic diagnosis of gastrointestinal lesions [48]. In Chapter 2, the principle of tissue fluorescence will be further introduced, together with the application of fluorescence imaging and spectroscopy for detection of precancer and cancer in the colon.

### **1.3 Challenges for Colonoscopy Screening**

To date, colonoscopy is the accepted gold standard for the screening and surveillance of colon cancer. In general, the diagnosis of colon cancer is based on conventional WLR colonoscopic inspections followed by the histopathological examination of biopsied tissues. However, the conventional WLR colonoscopy heavily relies on the observation of gross morphological changes of tissues. As a result, the flat and depressed neoplastic lesions, which have strong potential to develop early submucosal invasion, are difficult to identify due to the lack of obvious morphological changes. A recent study reported a 4.0% miss rate during colonoscopy for detecting cancer in usual clinical practice and further highlighted the fact that colonoscopy techniques require further refinement [49]. Hence, it is

highly desirable to develop advanced diagnostic techniques to complement WLR endoscopy for improving the non-invasive *in vivo* detection and diagnosis of colon cancer. As introduced in the previous section, combining different technologies and integrating them into a multifunctional endoscope would offer new optical features in colonoscopy and improvement for cancer diagnosis.

This thesis focuses on developing a near-infrared (NIR) AF spectroscopy and imaging system to complement conventional white light colonoscopy. We develop a novel polarized NIR AF and diffuse reflectance (DR) imaging system to improve the early detection of colon cancer. Moreover, we explore an endoscope-based NIR AF spectroscopy system to realize real-time *in vivo* NIR AF spectra measurements during clinical colonoscopic examination.

## **1.4 Thesis Organization**

This thesis is organized as follows. Chapter 2 first reviews the theory of fluorescence imaging and spectroscopy techniques and then introduces the clinical applications of fluorescence imaging and spectroscopy for detection and diagnosis of cancers in different organs. It also presents the research motivations and objectives.

Chapter 3 elaborates on the development of a novel polarized NIR AF imaging system for tissue measurements. Specifically, it presents the application of the integrated polarized NIR AF imaging system combined with NIR DR imaging for colon cancer detections.

Chapter 4 explores the endoscope-based NIR AF spectroscopy system for real-time *in vivo* identification of colonic polyps during colonoscopic screening. Multivariate statistical techniques (principal components analysis (PCA) combined

with linear discriminate analysis (LDA)) are employed for classification of subtypes of colonic polyps.

Chapter 5 investigates the origins of endogenous fluorophores for NIR AF from colonic tissue by using a non-negativity-constrained least squares minimization (NNCLSM) biochemical model.

Chapter 6 implements the integrated visible (VIS) and NIR DR spectroscopy for improving colon cancer diagnosis.

Finally, conclusion and discussion on future directions are presented in Chapter 7.

## **Chapter 2 Fluorescence Imaging and Spectroscopy**

This Chapter serves to introduce the research motivations and objectives of the thesis. The necessary principal knowledge and concepts for developing fluorescence technique to detect precancer and cancer in the colon are presented first. As some related works are also the rudimentary elements of the proposed researches, this Chapter reviews the development of fluorescence spectroscopy and imaging in clinical diagnosis.

### **2.1 The Basis of Fluorescence**

#### **2.1.1 Interaction of light with a molecule**

Fig. 2.1 shows that light is a form of electromagnetic radiation, consisting of an oscillating electric field with an oscillating magnetic field perpendicular to it [50]. When a molecule is placed in an oscillating electric field like light, it will experience a pushing and pulling force. At the same time, the molecule could oscillate at specific resonant frequencies that are related to its states. Each state of the molecule is associated with the energy level, which can be demonstrated by a diagrammatic way called the Perrin-Jablonsk diagram [51]. If the molecule oscillates in synchrony with the oscillating field, the molecule can absorb energy from the field. Since the energy of the light is proportional to its frequency, a given molecule will absorb a specific set of wavelengths of light. The range of wavelength absorbed by valence electrons varies from about 1000 nm (near infrared) through the visible (VIS) and ultraviolet (UV) down to about 100 nm (far UV).

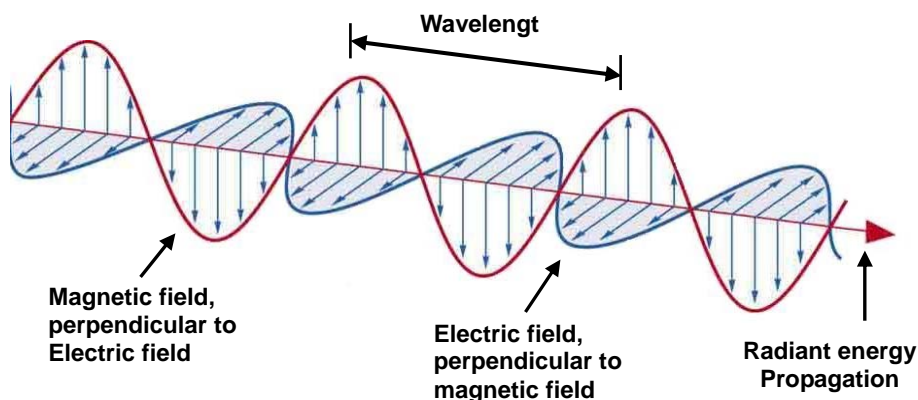


**Fig. 2.1** Electromagnetic waves with the electric field in a vertical plane and the magnetic field in a horizontal plane [52].

When a molecule absorbs the energy from the oscillating field, the electron cloud of the molecule would redistribute, and then cause the changes of dipole moment and shape of the molecule. Since electronic absorption is often accompanied by vibrational motion as the atoms move to their new positions, the molecule bonds alter. Consequently, the energy state of the molecule could move into the excited states from the ground states. However, the excited states of molecules are unstable and they relax (lose their energy) by a number of mechanisms, such as collisions with other molecules or reactions with other species. The excited molecule may also relax by emitting a photon of light to return to a lower state, though not always the same lower state from which it came. The emitted photon will have an energy corresponding to the difference in energy between the initial and final states of the molecule. The emission of a photon is known as fluorescence or in some cases phosphorescence.

Fig. 2.2 illustrates the Perrin-Jablonski diagram describing the transitions responsible for absorption, fluorescence, and phosphorescence interactions. Molecules are always in their ground state ( $S_0$ ) at room temperature. When a molecule absorbs a photon of light and the energy of the incident radiation exactly

matches one of the available energy-level transitions, the molecule would move into a higher energy state, such as the excited singlet state ( $S_1$ ) and the lowest excited triplet state ( $T_1$ ). Fluorescence occurs when the molecules return to  $S_0$ , from the excited singlet state such as  $S_1$ , by emission of a photon. The process happens readily and quickly with the result that excited electronic states survive only for a very short period of time, typically a few nanoseconds, before emitting. A molecule in  $T_1$  could also lose by emission of a photon to return to  $S_0$  and then we have phosphorescence. Molecules are continuously interacting with their surroundings to transfer vibrational energy to the surrounding molecules. This vibrational energy transfer process is named the vibrational relaxation (VR) or thermalization. It occurs in both the ground and excited electronic states. Vibrational relaxation can lead reaction of cold molecules or de-excitation of hot molecules, until both of them reach thermal equilibrium. Thus, the measurements of tissue absorption, fluorescence, and phosphorescence could provide biochemical information associated with changes in electronic energy states [53].

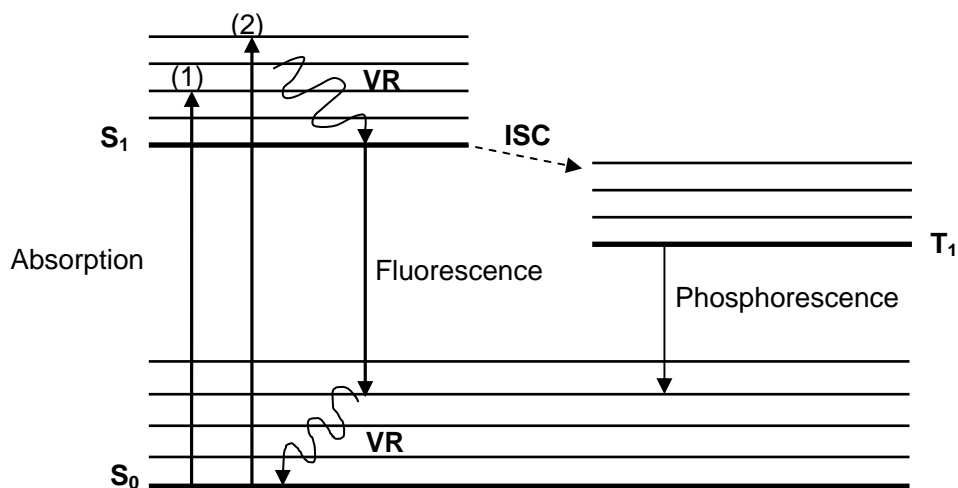
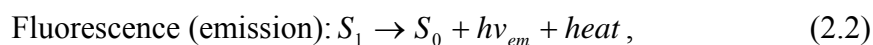


**Fig. 2.2** Simplified Perrin-Jablonski diagram showing three electronic states, several vibrational states, absorption of electromagnetic radiation, and emission of fluorescence or phosphorescence [54].

### 2.1.2 Properties of fluorescence

Fluorescence is defined as the radiative transition between two electronic states of the same spin multiplicity [55]. It is a luminescence in which the molecular absorbs a photon and triggers the emission of another photon with a longer wavelength [56]. Fluorescence occurs when an orbital electron of a molecule relaxes to its ground state by emitting a photon of light after being excited to a higher quantum state by some type of energy [57], expressed as



where  $hv$  is a generic term for photon energy:  $h$  is the Planck's constant and  $\nu$  is the frequency of light,  $S_0$  is the ground state of the fluorescent molecule and  $S_1$  is its first excited state. Besides fluorescence, the excited molecule can also relax by various competing pathways. For example, the excitation energy can be dissipated as heat (vibrations) to the solvent by non-radiative relaxation or converted to a triplet state which may subsequently relax via phosphorescence.

### 2.1.3 Fluorescence polarization [56, 58-59]

Fluorescence polarization was first described by Perrin in 1926 [60] and then greatly developed for the application in biological systems. It is based on the observation of the molecular orientation and mobility using polarized light. If excited with polarized light, the fluorescence emission from samples is also polarized. Polarization is a general property of fluorescent molecules.

When excitation light is polarized, the absorption of the fluorophores will depend on the orientation of its dipole in the ground state compared to the polarized

excitation light. Fluorophores with dipoles, which are perpendicular to excitation light, cannot absorb the energy of polarized excitation light; fluorophores with dipoles that are parallel to excitation light will absorb the most. Thus, polarized excitation will induce the photon selection for the fluorophore absorption. The emitted fluorescence is measured with an analyzer. When the emission is parallel to the excitation, the measured intensity is called  $I_{\parallel}$ , while when the emission is perpendicular to the excitation light, the measured intensity is  $I_{\perp}$ . Fluorescence polarization is defined by the following equation:

$$P = \frac{I_{\parallel} - I_{\perp}}{I_{\parallel} + I_{\perp}} \quad (2.3)$$

Since the presence of the analyzer induces photon selection, the global fluorescence intensity that is recorded in the presence of the analyzer is lower than that obtained in its absence. This is a consequence of the decrease in the number of absorbing and emitting fluorophores. The polarization unit is a dimensionless entity. According to Equation (2.3), the value of  $P$  does not depend on the intensity of emitted light and the fluorophore concentration. But the reality is quite different. The values of  $P$  occur between -1 ( $I_{\parallel}=0$ ) and 1 ( $I_{\perp}=0$ ). Natural or unpolarized light, where  $I_{\parallel}=I_{\perp}$ , yields a  $P$  value of 0. These two extreme values of  $P$  are observed when the polarized absorption transition moment and that of the emission are perpendicular ( $I_{\parallel}=0$ ) or colinear ( $I_{\perp}=0$ ).

Fluorescence polarization is a technique specially applied to study molecular interactions. The use of polarized light measurements has been well developed to characterize cells and tissues in medicine and biology [61-62]. The interactions of polarized light and tissue, such as scattering, offer a mechanism of gating or

selecting the photons. The back reflectance light from the initial tissue layer, which scatters back out of the tissue by one or two single scattering events, retains the linear polarization to the incident light. The remaining incident light continues to penetrate into the deeper layer and the orientation of polarization becomes randomized due to the multiple scattering events. At last, approximately half of this deeply penetrating light is absorbed and another half of this randomly polarized light is backscattered to the surface. Thus, the fluorescence polarization has the ability to selectively probe the emitted photon that arises from different depth of the tissue.

#### **2.1.4 Fundamentals for fluorescence detection**

The basic measurement of fluorescence requires a light source that matches the absorption spectrum of the molecule and a detector to monitor the emitted fluorescence. A fluorescence emission spectrum is a plot of the magnitude of the emitted fluorescence as a function of its wavelength. In biology and medicine application, fluorescence emission generally occurs from organic molecules, which are called fluorophores. Fluorophores can be used as a natural indicator to study the structure, dynamics, and metabolism of living cells. Each fluorophore has its own specific fluorescence properties that are dependent on its structure and the surrounding environment (e.g., temperature, pH, polarity, and oxidation state). As such, these characteristics make fluorescence techniques ideal tools in the measurement of tissue for clinical diagnosis.

Biological tissues are optically turbid. At a microscopic level, tissue can be considered as a scattering and absorbing center with random distribution [63]. Scattering and absorption affect both the excitation light fluence rate in tissue and the amount of excitation or fluorescence light that leaves the tissue [64]. The

scattering is usually assumed to be caused by tissue constituents with different refractive index. When light propagates through the tissue, these scatterers would introduce small changes in the direction of the light. Although the scattering is highly forward directed and the direction changes are small, multiple scatter events will produce significant effects on the light distribution in the tissue [65]. Both exogenous and endogenous chromophores can absorb the energy of the incident light and re-emit fluorescence at longer wavelengths. Hence, based on the measured the fluorescence light emitted from the tissue, we can interrogate the interactions between the excitation light and the tissue.

Fig. 2.3 depicts the light-tissue interaction that takes place when the fluorescence emission is measured. Monochromatic light is incident on the tissue surface. This light scatters within the tissue, where it can either be absorbed or diffusely reflected from the tissue surface. The remaining lights propagate into the tissue media. Some will go out after multiple scattering in tissue and some will be absorbed. The absorbed light can be converted to fluorescence. This fluorescent light continues to scatter in the tissue, where it can either be reabsorbed or emitted from the tissue surface. As a result, the emitted fluorescence contains contributions not only from tissue fluorophores, but also from absorbers and scatters. In addition to interaction with these tissue constituents, reflection and refraction may also take place at the interface between the tissue and the exterior medium due to differences in refractive index [66]. All of these chromophores can have wavelength-dependent signatures that affect the measured fluorescence spectrum. Thus, to understand the changes in tissue fluorescence spectra that are associated with certain disease, we must examine changes in all types of chromophores.

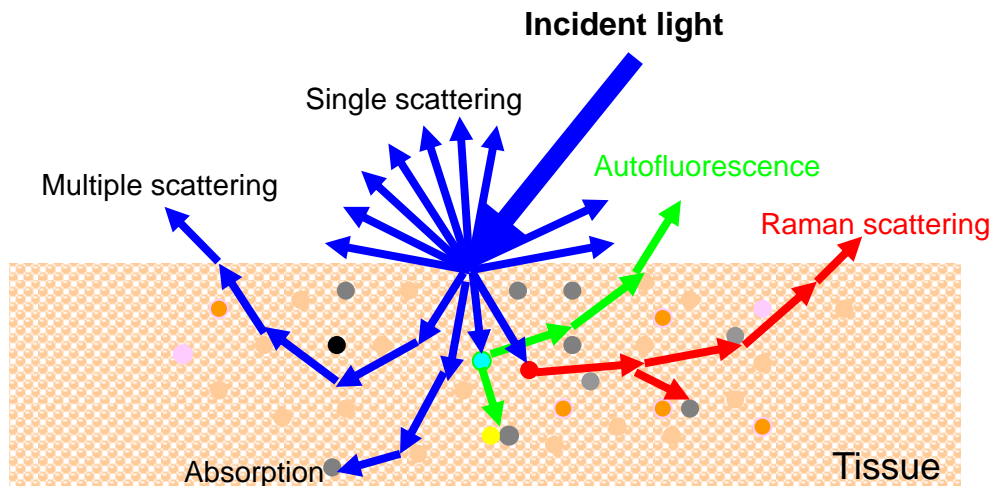


**Fig. 2.3** Interactions between tissue and light.

There are three important types of chemical groups that interact with light in tissue: fluorophores (chemical groups that can convert absorbed light to fluorescence), absorbers (chemical groups that absorb light but do not produce fluorescence), and scatterers (structures that change the incident photon direction but conserve its energy) [57]. The optical properties of each type of chromophore may depend on both wavelengths and tissue types.

### **Fluorophores**

Fluorophores are a functional group of molecules that will absorb energy of a specific wavelength and emit energy at different wavelengths, such as connective matrix (collagen, elastin), cellular metabolic coenzymes (reduced nicotinamide adenine dinucleotide (NADH), flavin adenine dinucleotide (FAD), and flavin mononucleotide (FMN)), aromatic amino acids (tryptophan, tyrosine, and phenylalanine), byproducts of the heme biosynthetic pathway (porphyrins), and lipopigments (lipofuscin, ceroids) [34]. Each group of fluorophores is characterized by its distinct excitation and emission wavelength ranges (as shown in appendix 2).

## Absorbers

Absorbers also affect fluorescence spectra measured in tissue since the emitted fluorescence can be reabsorbed while exiting the tissue. Fig. 2.4 shows examples of primary absorption spectra of some biological tissues. In the UV and VIS regions of the spectrum, the absorption increases with shorter wavelength mainly due to proteins and hemoglobin. In the red to near-infrared (NIR) regions, absorption is minimal. Thus, this region suits for diagnosis and therapy. In the infrared region, the absorption increases with longer wavelengths due to tissue water content.

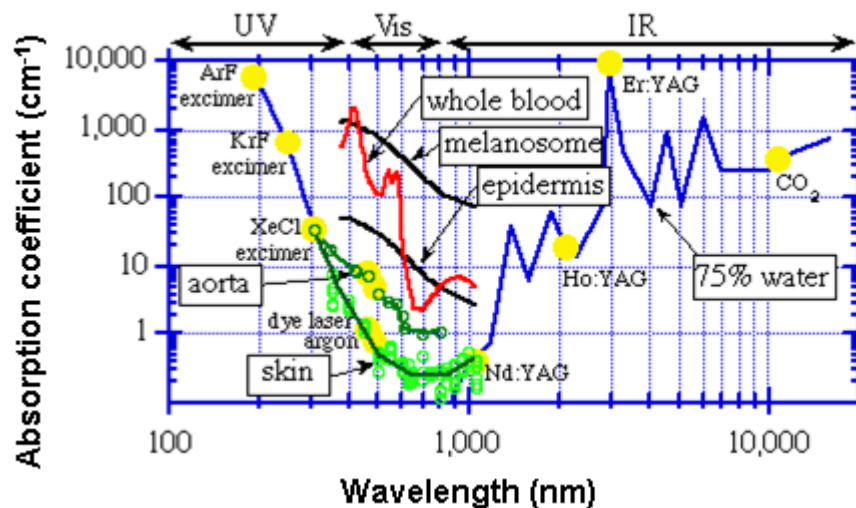


**Fig. 2.4** Absorption spectrum for some tissues (aorta, skin) and tissue components (whole blood, melanosome, epidermis, and water) [67].

## Scatters

Due to the intense scattering of tissue, light can propagate into tissue, enabling one to extract information noninvasively from this volume of tissue [65]. The elastic tissue scattering arises from the microscopic heterogeneities of refractive indices for cells with complex structure. The laser penetration depth depends on the wavelength; the longer the light wavelength scatters less and penetrates deeper into the tissue. The exceptions are laser wavelengths above 1300 nm, which hardly penetrate into

the tissue due to the high absorption by the tissue water. VIS light can propagate from 0.5 to 1.0 mm, while the red and infrared laser light have the highest penetration depth from up to 3 mm [55].

## **2.2 Application of Fluorescence in Clinical Diagnosis**

An increasing number of fluorescence technologies are available for the detection and diagnosis of diseases, such as fluorescence microscopy, autofluorescence (AF) endoscopy, and exogenous fluorescent contrast agents [68-71]. There are several advantages of fluorescence measurements for clinical diagnosis [72]. First, fluorescence is characterized by high sensitivity allowing concentrations of biomolecules to be measured down to as low as  $10^{-18}$  M (attomole); the measurements are also fast. Second, fluorescence is affected by different types of fluorophores, absorbers, and scatters. Hence it is capable of investigating subtle changes of disease progression, such as concentration of metabolites, tissue structure, cellular orientation, and distances between molecules. Moreover, fluorescence is also sensitive to the chemistry of the environment (e.g. pH, ionic strength, and fluidity), and thus, it can also be applied for studies where the disease changes the chemistry of the environment. At last the products of fluorescence and fluorescence itself are safe for tissue diagnosis; there is little or no alteration in sample structure. Hence, fluorescence measurements are ideal for *in vivo* studies and studies of living tissues.

Currently, there are two major approaches of fluorescence-based techniques: exogenous contrast agents and AF. The first approach relies on the presence of exogenous contrast agents. For the exogenous fluorophores, both organic and inorganic fluorescence contrast agents are now available for chemical conjugation to

target molecules. In contrast, AF technique relies on endogenous molecules within the tissue. Based on the subtle changes in the tissue composition and morphology associated with disease transformation, tissue AF can be used for the detection of diseased tissues.

### **2.2.1 Exogenous fluorescent contrast agents**

To date, the exogenous fluorescence contrast agents have been largely exploited to selectively localize the suspicious lesions with photosensitizers for photodynamic therapy. With drug-induced fluorescence, the signal is much stronger than tissue AF. Thus, the contrast between tumor and surrounding normal tissue could be highly enhanced. Nonspecific fluorochromes are often used as contrast agents, such as indocyanine green (ICG, cardiogreen). ICG has been approved for the use in indicator-dilution studies in humans since 1958 [73]. It is one of the least toxic agents ever administered to human. ICG absorbs NIR light and emits fluorescent light at a wavelength of 780 nm and 830 nm [74]. It has been widely used in clinic and experimental studies, such as vascular mapping, angiograms of the eye, and adenocarcinoma detection in different organs [75]. However, the conventional organic exogenous contrast agents suffer from significant limitations[76]. First, it is difficult to control excitation wavelengths, which are dependent on chemical structure. Tuning a conventional fluorophore to precise wavelengths needs highly complicated chemistry and the molecules are potentially unstable. Second, it suffers from lower quantum yield. The quantum yield for the organic contrast agents is usually less than 15% in aqueous environment [75]. Moreover, the conventional contrast agents are highly susceptible to photobleaching, which limits the fluence rate for sample and further affects the sensitivity for detection.

In contrast, inorganic fluorescent semiconductor nanocrystals, also called quantum dots (QDs), have the potential to solve problems that limit the application of organic contrast agents. QDs are synthesized in organic solvents and typically comprise an inorganic core and inorganic shell of metal. Due to such special structure properties, the fluorescence emission for QDs can be tuned to specific peaks of discrete wavelength [75]. Moreover, QDs can be excited with a single wavelength and emit at several different wavelengths. Thus, they are suitable for multiplex detection of multiple targets in a single experiment. With the unique optical properties, QDs have been explored for *in vivo* fluorescence imaging to provide direct visual guidance for minimizing incision and dissection inaccuracies and realize real-time confirmation of complete resection [77-78]. However, because of the multi-layered structure, QDs are typically large in diameter and difficult to clear from the circulation. The *in vivo* toxicity of QDs remains unknown. Hence, the studies of QDs still focus on the animal's models. Currently, the medical usage of gold nanoparticles in the human body has been approved by the Food and Drug Administration (FDA) [79].

### **2.2.2 Autofluorescence**

The second type of fluorescence-based diagnostic technique is AF, which relies on subtle changes in the tissue composition and morphology to help localize diseased tissue without using any exogenous contrast agents [80]. In diagnostic applications, AF techniques exhibit both advantages and disadvantages. AF is characterized by signal amplitude and a lower spectral selectivity than those of exogenous fluorescence induced by contrast agents. It has relatively low quantum efficiency and suffers from the overlapping of both the excitation and emission spectra of

several endogenous fluorophores that coexist in the tissue. On the other hand, AF provides real information of the biological substrate since it is directly related to the biomolecules in their natural environment without any perturbation of exogenous substances. Thus, AF has the great advantage of real-time monitoring the changes of the endogenous fluorophores in different physiological pathological or experimental conditions. In 1938, AF was first investigated by microscopy [81]. With the advancements in the fields of excitation sources, light delivery systems and sensitive detection devices, as well as a better knowledge of the endogenous fluorophores, AF has been applied in characterization of biology tissues. Over the past two decades, AF technology has been integrated into endoscopy to probe the biochemistry of epithelial surfaces, revealing the presence of disease not seen by conventional white-light endoscopy [82].

The AF of biological tissues arises from endogenous molecules within the tissue. These biomolecules are called fluorophores, which are responsible for the tissue's morphological structure or involved in the metabolic and functional processes of cells. For instance, collagen and elastin are the representative of structural proteins in the extracellular matrix of connective tissue; reduced nicotinamide adenine dinucleotide (NADH), flavin adenine dinucleotide (FAD), and flavin mononucleotide (FMN) are the enzymes, which are typically involved in metabolism; aromatic amino acids (tryptophan, tyrosine, and phenylalanine) are used to synthesize the protein in the human body; porphyrins are the by-products of heme biosynthesis [34]. When cells are in disease states, they often undergo different metabolism rates or have different structures compared to those in normal conditions. These changes in the morphological and biochemical properties of cells

and tissues could alter the concentration and distribution of the endogenous fluorophores and further affect the autofluorescence properties. Hence, AF can provide a significant amount of information about the morphological structure and metabolic processes associated with the disease progression. The endogenous fluorophores have been used as a specific marker for biological processes and AF has become an intrinsic biological parameter to track disease development.

In general, the fluorescence emission bands are often broad, relatively featureless, and overlap with one another. This is because a single excitation wavelength could excite many fluorophores. Consequently, the emission signals may overlap many fluorophores since the absorption and emission bandwidths of these molecules can be broad. Tissues have a mixture of several fluorophores that occur in different concentrations and at different depths. The overall AF emission of a tissue is strictly dependent on at least one of the following parameters [56]: the fluorophore concentration, spatial distribution throughout the tissue local microenvironment, and the particular tissue architecture. In addition, the fluorescence characteristics of a biological tissue also depend on the tissue optical properties. The concentration and distribution of non-fluorescent absorbers and scatterers within the tissue will affect the propagation of the light (both excitation and emission), influencing the signal amplitude and the spectral shape of the AF spectrum.

To date, AF technique has been widely applied for diagnosis in oncology. During the progression of cancer, AF properties of tissues will be affected by the alterations of both morphological structure and metabolic activity [83]. For colon cancer, the proliferation of neoplastic cells causes the thickening of the mucosa layer, and this histological alteration results in a strong decrease or loss of the contribution

of brightly fluorescing collagen and elastin from the normal submucosa [84]. As a result, colonic cancer tissue has a reduction of fluorescence emission compared to the normal tissue [84]. Therefore, the difference of tissue AF can be used to identify the early colon cancers or premalignant lesions from normal tissues.

AF spectroscopy and imaging have been intensively studied to improve the detection and localization of early cancer in different organs, including the cervix, bladder, lung, breast, esophagus, stomach, uterus, skin, and colon [85-89]. Tissue AF has also shown promise in other clinical applications such as the diagnosis of atherosclerosis [90] and Alzheimer's disease [91]. AF bronchoscopy is one of the successfully developed techniques that significantly improve the sensitivity for detection of early lung cancer. It is performed and evaluated as an adjunct to the white light bronchoscopy for detection of lung cancer. When the bronchial surface is illuminated by violet or blue light, normal tissue emits strong fluorescence in the green, while dysplasia, carcinoma *in situ*, and invasive cancer have decreased AF emissions [92]. A number of commercial AF bronchoscopy devices have been developed to improve conventional white light bronchoscopy [93]. The relative sensitivity of AF bronchoscope versus white-light examination alone is found to increase by an average of two-fold in detecting high-grade dysplasia and carcinoma *in situ* [94]. As the latest advancement in this field, an integrated endoscopy system for simultaneous imaging and spectroscopy (OmniScope) has been developed to improve the specificity of AF bronchoscope while maintaining high sensitivity [95].

### **2.2.3 Near-infrared autofluorescence**

*In vivo* fluorescence measurement of tissues is significantly wavelength dependent and the used excitation and emission wavelengths determine the dominant

fluorophores that are involved. This is because the different excitation wavelengths can activate different groups of fluorophores, each of which emits at a range of different wavelength. Currently, most tissue spectroscopy studies center on the use of UV or VIS wavelength (250-550 nm) as excitation light for cancer detection in various organs including the colon [87, 96]. When using excitation light with UV or VIS wavelength, the light will be highly absorbed by endogenous chromophores in tissue and the transport of light is exponentially attenuated according to the Beer-Lambert law [55]. Due to their shorter excitation wavelengths, the laser light can only penetrate limited depth and extract information from superficial tissue layers. Unlike the UV and VIS light, NIR light (700-1000nm) is able to penetrate deeper in the tissue due to less absorption and scattering from the water and tissue. Moreover, NIR light is non-carcinogenic and it is safe for tissue diagnosis. Thus, NIR AF technique has the promising potential for the non-invasive *in vivo* detection of lesions located deeper inside the tissue. With the development of highly sensitive detectors, monochromatic light sources (lasers) with safe levels of power per wavelength, and the study of fluorophores in the NIR region, NIR AF technique has been applied for detection and diagnosis of cancer [97-100].

Demos *et al.* utilized long-wavelength laser excitation in the green and red spectral region to study various types of normal and malignant human tissues including breast, liver, kidney, pancreas, prostate, and bladder tissues [101]. The experimental results indicated that the AF intensity of cancer tissues were considerably different from those of normal tissues. The differences of NIR AF intensity between normal and cancer tissue can be attributed to the concentration changes of endogenous fluorophores, such as porphyrin productions. Porphyrins,

which exhibit absorption in the red spectral region and emit in the NIR and far-red region, are assumed to be responsible for the NIR AF emissions in tissues [102]. But the origins of the other endogenous fluorophores are still not well understood, which warrant further investigations.

Besides the cancer detection, NIR AF has also been applied to detect brain diseases [91, 103-104]. Hanlon *et al.* demonstrated the investigation of NIR fluorescence spectroscopy for the detection of Alzheimer's disease in vitro [91]. Both the excitation light used and the resulting tissue AF were at NIR wavelengths, which can propagate through the skull and overlying tissue. Thus, NIR AF technique has the clinical potential to realize non-invasive diagnosis of Alzheimer's disease in living patients. Moreover, NIR light has also been used for the functional mapping of the cerebral cortex, and further explored to develop a novel and non-invasive NIR imaging brain-computer interface system [104].

However, to date, there are few studies on applying NIR AF technique for the early detection of colon cancer. Based on the theory of fluorescence and successful application of NIR AF technique, we extend the previous UV/VIS work to the NIR domain for the early detection of precancer and cancer in the colon.

## **2.3 Motivations**

The motivations for this thesis are summarized as follow:

- 1) The endoscopy combined with biopsy is accepted as the gold standard for cancer detection and diagnosis. However, conventional white light colonoscopy heavily relies on the gross morphological tissue changes, and thus, it suffers from low sensitivity of detection for subtle changes in the colonic mucosa epithelium. Moreover, biopsy is invasive and has the risk for

serious complications. Hence, it is necessary to develop advanced optical diagnostic techniques to complement conventional endoscopy for improving the diagnosis of precancer and cancer non-invasively.

- 2) AF technique, which is capable of probing the changes of both tissue morphological structures and concentration of endogenous fluorophores, has been widely applied for the diagnosis of cancer in different organs. However, the majority of these studies are using the UV or VIS wavelength light for excitation, which limits the penetration depth for detecting the suspicious lesion located in the deep layer of the tissue. Compared to UV and VIS, NIR light is non-carcinogenic and safe for tissue diagnosis, and both the excitation light used and the resulting tissue are at NIR wavelengths that can penetrate deeper into the tissue up to 1 mm. Hence, it is highly desirable to develop robust NIR AF spectroscopy and imaging system for the clinical detection and diagnosis precancer and cancer.
- 3) Polarized light would be a good tool to study different types of molecule rotations. The molecular global rotation and local dynamics are dependent on the tissues structure, surrounding environment, and metabolic function of the system. As a result, these motions differ from the normal tissue to diseased tissues due to the changes of morphology and biochemical composition. If a molecule is illuminated with polarized light, the fluorescence emission will also become polarized. Consequently, the polarized AF emission has capability for cancer diagnosis and characterization. However, because of the comprehensive mechanism, the potential of polarized NIR AF techniques for clinical cancer detection has not been fully explored.

- 4) The early diagnosis and removal of premalignancies (e.g., adenomatous polyps) have been widely accepted for effective prevention colon cancer development and decreasing the associated mortality rate. However, the subtle macroscopic differences among subtypes of colonic polyps may not be apparent under WLR endoscopic imaging. Hence, all polyps found during colonoscopy are routinely resected and sent for histopathological examinations. The removal of polyps without malignancy potential (i.e., hyperplastic polyps) could incur additional time, costs, and risks. Therefore, there is an urgent need to develop non-invasive, sensitive, and advanced optical diagnostic techniques that improve the differentiation of adenomatous polyps from hyperplastic polyps.
- 5) NIR AF clinical applications have been limited not only by the difficulty in capturing inherently weak tissue NIR AF signals, but also by relatively less knowledge of possible endogenous fluorophores responsible for tissue NIR AF emission. The investigation of these endogenous fluorophores, which are associated with the structural matrix of tissues or cellular metabolic processes, could be advantageously helpful to understand the origins of the tissue AF in the NIR region and interpret the changes of AF emission at molecular level.
- 6) DR spectroscopy in the VIS range has been widely investigated in several applications related to diagnosis, prognosis, and assessing treatment response of cancers in different organs. The integrated VIS and NIR DR spectroscopy, which contain both hemoglobin and water signatures, has not be well studied for improving the diagnosis of colon cancer.

## 2.4 Research Objectives

The main aims of this research are summarized as follows:

- We develop the polarized NIR AF imaging system for improving the detection and diagnosis of colon cancer.
- We explore endoscopy-based NIR AF spectroscopy to realize *in vivo* differentiation of colonic adenomatous polyps during clinical colonoscopic examination.
- We investigate the endogenous fluorophores for tissue NIR AF emission by using the non-negativity-constrained least squares minimization (NNCLSM) biochemical modeling.
- We implement the integrated the VIS/NIR DR spectroscopy for improving the detection and diagnosis of colon cancer.

The specific objectives of this research are itemized as below:

- 1) We develop a novel integrated NIR AF and NIR diffuse reflectance (DR) imaging system for the detection of colon cancer. The experimental results demonstrate the potential of NIR AF imaging technique for improving cancer detection compared to conventional white light reflectance imaging method.
- 2) We also propose the polarized NIR AF imaging technique to further improve the capability of NIR AF imaging for cancer diagnosis and characterization. The polarization technique is employed to selectively probe the AF light photons that arise from the subsurface or deep areas of tissue. Moreover, the depolarization imaging (i.e., the ratio of the difference between parallel-polarization image ( $I_{\text{pal}}$ ) and perpendicular-polarization image ( $I_{\text{per}}$ ) to the sum of  $I_{\text{pal}}$  and  $I_{\text{per}}$ ) is explored to improve the contrast between normal and

cancer tissue.

- 3) We further apply the ratio imaging of white light images to AF images under different polarization conditions to eliminate the geometric effect of imaging measurements for achieving the best diagnostic accuracy.
- 4) We couple a novel bifurcated flexible fiber-probe into our endoscopy-based fluorescence spectroscopy to realize *in vivo* NIR AF tissue measurement at colonoscopy.
- 5) We evaluate the diagnostic efficacy of NIR AF spectroscopy in conjunction with multivariate statistical technique (i.e., principal components analysis (PCA) and linear discriminate analysis (LDA)) for the rapid and non-invasive *in vivo* identification of precancer in clinical colonoscopic examination.
- 6) We investigate the endogenous fluorophores in the NIR range by utilizing NNCSLM biochemical modeling. We reconstruct fitting spectra by using basis reference spectra from the representative biochemicals (i.e., collagen I, elastin,  $\beta$ -NADH, FAD, L-tryptophan, hematoporphyrin, 4-pyridoxic acid, pyridoxal 5'-phosphate, and water) to compare the *in vivo* spectra acquired from colonic tissues and study the biochemical changes associated with the cancer progression.
- 7) We explore the integrated VIS-NIR DR spectroscopy for colonic tissue measurements and compare the diagnostic performance of VIS, NIR, and the integrated VIS-NIR DR spectra.

# Chapter 3 Autofluorescence Imaging of Colonic Tissues

## 3.1 Introduction

At present, screening of high-risk populations remains the most pragmatic approach for control the development and progression of colon cancer. In general, the diagnosis of colon cancer is based on conventional white-light colonoscopic inspections followed by the histopathological examinations of biopsied tissues. However, the conventional white light reflectance (WLR) colonoscopy, which is accepted as the gold standard method for screening and surveillance of colon cancer, heavily relies on the observation of gross morphological changes of tissues. The new colonoscopy techniques, which have been introduced in the section 1.2.2, have shown the potential to complement conventional WLR colonoscopy to improve the non-invasive *in vivo* detection and diagnosis of early cancer in the colon.

Among these techniques, autofluorescence (AF) is the promising approaches that is capable of probing the changes of tissue morphological structures and intrinsic fluorophores, such as collagen, nicotinamide adnine dinucleotide (NADH), and flavin adenine dinucleotide (FAD) in the tissue [30, 80, 92, 105-107]. Thus, AF technique has been developed to complement conventional endoscope and the light-induced AF endoscopic imaging can be used to reveal subtle lesions which cannot be detect by WLR endoscope. In the past two decades AF imaging has been comprehensively investigated for improving the diagnostic sensitivity of malignant lesions in various organs, including the colon [46, 80, 92, 96, 106-110]. The video

endoscopy system combining with the AF technique has been developed for screening in the upper gastrointestinal tract [46, 111].

But to date, most of AF studies focus on the utilization of ultraviolet (UV) or short visible (VIS) wavelengths as excitation light and suffer from a limited penetration depth. Unlike UV excitation light, the near-infrared (NIR) light is non-carcinogenic, and it is safe for tissue diagnosis [91, 112-114]. Both the excitation light used and the resulting tissue AF are at NIR wavelengths that can penetrate deeper into the tissue up to 1 mm [112-113]. Hence, NIR AF could potentially be useful for the non-invasive *in vivo* detection of lesions located deeper inside the tissue. In this chapter, we extend the previous UV/VIS AF work [46, 96, 109-110, 115] to the NIR domain for ex vivo colonic tissue diagnosis and characterization. We examine if colonic tissue exhibits observable NIR AF under the 785 nm laser excitation. Moreover, polarization technique is integrated into NIR AF imaging system to evaluate that if the integrated NIR AF imaging and NIR diffuse reflectance (DR) imaging with polarization technique can be used for improving colon cancer detection and diagnosis. The ratio imaging of NIR DR image to NIR AF image is used to eliminate the geometric effect of the imaging measurement and the depolarization imaging is expected to improve the contrast between normal and cancer tissues.

## **3.2 Experiments**

### **3.2.1 Near-infrared autofluorescence imaging system**

Fig. 3.1 shows a schematic diagram of the integrated NIR AF and DR imaging system developed for ex vivo measurements of colonic tissues. A 785 nm excitation

light from a diode laser (maximum output: 300 mW, B&W Tec Inc, Newark, DE) is coupled into a 200  $\mu\text{m}$  fiber and delivered into a collimator (F220SMA-B, Thorlabs, Newton, NJ) for excitation. The laser beam passes through a narrow band-pass (BP) filter (LL01-785-12.5, Semrock Inc. Rochester, NY) to remove interference of fiber background fluorescence and laser noise. Then the filtered laser light is reflected by a dichroic mirror (Reflection: 450-800 nm, Transmission: 800-1400 nm; Semrock Inc., Rochester, NY) and shine onto the tissue specimen. The induced AF emission from tissue passes through the dichroic mirror and a 850 nm long-pass filter (FEL0850, Thorlabs, Newton, NJ). Finally, the tissue AF signals are collected by an NIR-optimized back-illuminated, deep-depletion charge-coupled device (CCD) detector (Cascade II 512, Photometrics, Tuscon, AZ) within 8.2 $\times$ 8.2 mm image area. With the highest available quantum efficiency (>90% peak QE) of our back-illuminated EMCCD, the weak NIR AF images can be captured. For the NIR DR imaging, a tungsten halogen light (HL-2000, Ocean Optics Inc., Dunedin, FL) is coupled into a 200  $\mu\text{m}$  fiber and passes through a beam expander to illuminate the tissue directly. The NIR DR photons from the tissue are collected by the CCD after passing through the dichroic mirror and the 850 nm long-pass filter. To integrate polarization technique into the NIR AF imaging system, two linear polarizers (47-328, Newport Corporation, Irvine, CA) are placed along the AF and DR illumination light paths, and the parallel and perpendicular polarized AF/DR images can be acquired in tandem by rotating the analyzer positioned in front of the camera lens in the NIR AF/DR imaging system. To our knowledge, our integrated NIR AF and DR imaging system firstly combined polarization technique to acquire polarized AF and DR images from colonic tissues.

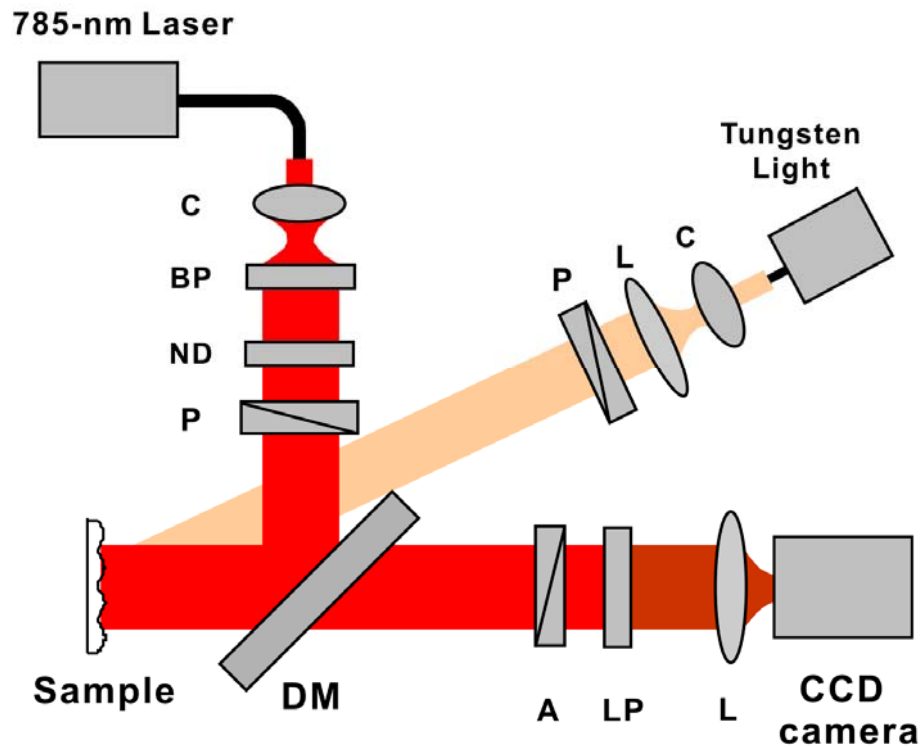


**Fig. 3.1** Schematic diagram of the integrated NIR AF and NIR DR imaging system with polarization developed for tissue measurements: collimator (C); band pass filter (BP); neutral density filter (ND); dichroic mirror (DM); long pass filter (LP); polarizer (P); analyzer (A); lens (L).

With this integrated NIR AF/DR imaging system combined with polarization technique, a set of six images can be acquired for colonic tissues in tandem, i.e., NIR AF image and the corresponding NIR DR image under three different excitation light polarization conditions (i.e., non-polarization; parallel and perpendicular polarization). The system fluorescence signal has been recorded as background images and subtracted automatically. The system acquires NIR AF images and DR images within the spectral bandwidth of 850-1100 nm, and each NIR AF image was acquired within 5 s with the 785 nm laser light irradiance of  $0.15 \text{ W/cm}^2$ , which is less than the American National Standards Institute (ANSI) maximum permissible skin exposure limit set out for a 785-nm laser beam ( $1.63 \text{ W/cm}^2$ ) [118], while each NIR DR image was acquired within 0.01 s with the tungsten light and the incident

optical power on sample surface is  $0.002 \text{ W/cm}^2$ .

To explore the feasibility of our developed NIR AF imaging system, a chicken muscle-melanin sandwich model is developed to estimate the penetration depth of NIR AF imaging system. The sandwich model consists of chicken breast muscle tissue and melanin powder. Melanin, which is able to emit strong AF signal in the NIR region, is selected as an inclusion to embed in the chicken muscle sandwich. The bottom chicken muscle layer is 2 mm thick and the upper layers are several very thin chicken muscle layers with approximate thickness of 0.1 mm. Fig. 3.2 (a) shows the AF image of solid melanin powder ( $\sim 1 \text{ mm}$  in diameter) on the center of the chicken muscle bottom layer without any upper layers. Under the excitation of 785 nm laser, the melanin powder emits strong NIR AF signal, which shows the bright point in the center of the images compared to surrounding chicken tissues. The Fig. 3.2 (b) is the intensity profile along the line in the Fig. 3.2 (a). We can roughly calculate the intensity ratio of melanin to chicken muscle by dividing the maximum intensity to the minimum one.

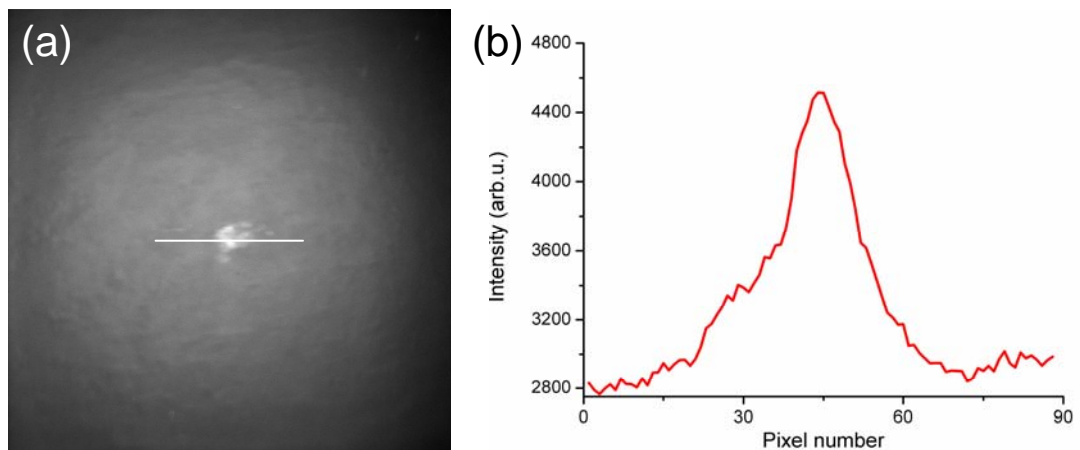


**Fig. 3.2** (a) NIR AF image of chicken muscle with melanin powder and (b) intensity profile along the line as indicated on the image (a).

In order to measure the change of the AF intensity from the melanin with the increment of thickness of the upper chicken muscle layer, the chicken muscle layers are placed on the top of chicken muscle base one by one. A series of NIR AF images are recorded after adding each chicken muscle layer and the ratio intensities of melanin to chicken muscle are calculated accordingly. The experiment repeats six times for the statistic analysis. Fig. 3.3 shows the mean NIR AF ratio of the melanin over the chicken muscle  $\pm$  standard error (SE). The curve increases first till reaching the maximum at 0.2 mm and then decreases. The maximum value is not at the initial point and this could be attributed to the increasing of AF emission from melanin power. Due to the AF emission of first two chicken muscle layers, the melanin powder might be further excited and induce more AF emission. It also may be attributed to the nonuniformity of the excitation light distribution inside the tissue that may have a subsurface maximum. With the increment of the upper chicken muscle layer, the excitation light was significantly attenuated and the AF emission from melanin was also obscured. Thus, the ratio intensity of melanin to surrounding chicken muscle keeps decreasing with the increment of thickness of upper chicken muscle layer. Based on the test of chicken muscle-melanin sandwich model, our NIR AF imaging system shows that our excitation light and resulting AF can penetrate up to 2.5 mm into chicken muscle tissues, approximately.

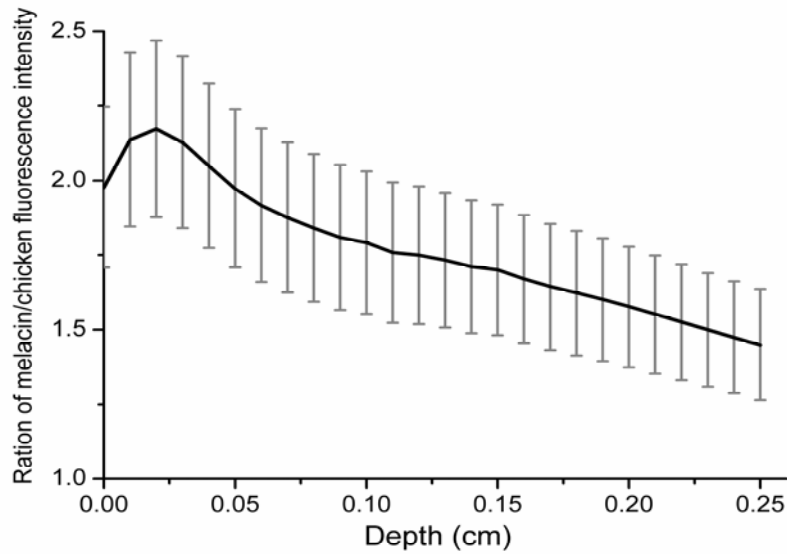


**Fig. 3.3** The mean NIR AF intensity ratio of the melanin over the chicken muscle  $\pm 1$  standard error (SE) with the increasement of depth.

To explore the fluorecence polarization technique for the detection and diagnosis of colon cancer, we acquired polarized NIR AF and DR images under every 20 degree for a total rotation of 360° and perpendicular polarized AF and DR images under 90° and 270°. For each image, a homogenous area (~2 x 2 mm<sup>2</sup>) on both normal and cancer tissue is selected respectively to estimate the average intensity. Fig. 3.4 is the polar diagrams to illustrate the change of NIR AF and DR signals as a function of polarization for a total rotation of 360°.

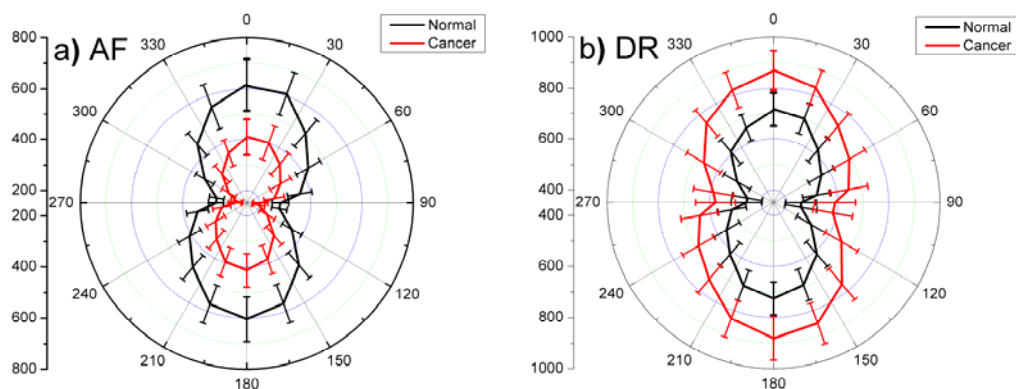


**Fig. 3.4** Polar diagrams displayed for a full sample rotation of every 20 degree for six paired colonic tissues, (a) NIR AF imaging, (b) NIR DR imaging. The error bars stand for the standard errors (SE).

The trend in intensity changes of AF and DR intensities are consistent in all six paired colonic tissues (normal *vs.* cancer). The maximum intensity is under the parallel-polarized condition (0° and 180°) while the minimum intensity is under the perpendicular-polarized condition (90° and 270°). The parallel-polarized images have the higher intensity than the perpendicular-polarized images for both NIR AF and DR imaging modes. This is because the parallel-polarized images mainly contain the information of structures on the surface or subsurface of the tissue while the perpendicular-polarized images predominantly contain information from deep areas of the tissue [116]. The observation of the intensity differences between parallel- and perpendicular polarization condition is in agreement with the literature [62]. As such, the polarized NIR AF imaging technique has the ability to selectively probe the AF light photons that arise from the subsurface or deep areas of tissue. We also calculated the polarization ratio value ( $\text{ratio} = (I_{\text{par}} - I_{\text{per}}) / (I_{\text{par}} + I_{\text{per}})$ ) for both normal and cancer tissues in NIR AF images to investigate the change of fluorescence polarization properties associated with the malignant transformation. The mean polarization ratio value of colonic cancer tissues is  $0.34 \pm 0.04$ , while the mean polarization ratio value of normal tissue is  $0.38 \pm 0.04$ . The lower polarization ratio value of cancer tissues could be attributed to the more multiple light scatterings that occur in deeper regions of tissue due to the disorganized structures of tissue in colonic adenocarcinoma as compared to the normal tissue. Multiple scattering is caused by the high density of tissue scattering centers, originating from the random fluctuation of the local refractive index in the tissue microstructure, such as inside the cell and in the extra-cellular matrix. Due to hyperproliferation of cancerous cells, there might be an increase in the disorder of collagen network, such as the

breakdown of the crosslinkages between microfibrils and the deformation in the oriented collagen structure (collagen fibers are shortened and more disconnected). The organized fibrous structures such as collagen, which are the structural protein in the extracellular matrix of the colonic wall and the dominant fluorophore in the submucosa of colon tissues of colon tissues [115], are the main contribution to the retardance and diattenuation of the tissue due to its birefringent nature. Because of its hierarchical structure and fibril alignment, the optical anisotropy properties of collagen can be used to reflect the change of birefringent properties associated with structural or cellular metabolic progression in colonic precancer and cancer [117]. Since the structural and functional properties of these fibers change as a result of tissue abnormalities, the colonic cancer tissues suffered stronger depolarization compared to the normal tissues. As such, the polarization measurements may also be used as a sensitive probe for assessing tissue status.

### **3.2.2 Tissue preparation**

A total of 48 paired (i.e., normal vs. cancer) colonic tissue specimens (average size of  $\sim 4 \times 4 \times 2 \text{ mm}^3$ ) were collected from 48 patients (20 men and 28 women with a mean age of 62) who underwent partial colectomy or surgical resections with clinically suspicious lesions or histopathologically proven malignancies in the colon. All patients preoperatively signed an informed consent permitting the investigative use of the tissue, and this study was approved by the Institutional Review Board (IRB) of the National Healthcare Group (NHG) of Singapore.

Immediately after surgical resections, the tissue specimens are immersed in physiological saline solution and sent to the laboratory for NIR AF/DR imaging measurements. The paired tissue specimens from each patient were placed on a

standard glass slide ( $26 \times 76 \times 1.2 \text{ mm}^3$ ) covered by aluminum foil which has very small fluorescence background. The cancer tissue was placed at the upper part of the slide while the normal one was placed at bottom part of the slide for NIR imaging measurements. After the NIR imaging acquisitions, the tissue specimens were fixed in 10% formalin solution and then submitted back to the hospital for histopathological examinations. The histopathological examinations confirmed that 48 tissue specimens were normal, and 48 tissue specimens were cancer (moderately differentiated adenocarcinoma).

### **3.3 Results and Discussion**

#### **3.3.1 NIR autofluorescence and reflectance diffuse imaging**

Using the integrated NIR AF/DR imaging system combined with the polarization technique, we have successfully acquired NIR AF/DR images of 48 paired colonic tissues under the three excitation light polarization conditions (i.e., non-polarization, parallel and perpendicular polarization). Fig. 3.5 shows the representative NIR DR images and AF images of one pair of colonic tissue (normal ( $9 \times 6 \text{ mm}^2$ ) vs. cancer ( $6 \times 3.5 \text{ mm}^2$ ) confirmed by histological examinations): (a) NIR DR image without polarization; (b) NIR DR image with parallel polarization, and (c) NIR DR image with perpendicular polarization; (d) NIR AF image without polarization; (e) NIR AF image with parallel polarization, and (f) NIR AF image with perpendicular polarization. Cancer tissue was located at the upper frame of images while the normal one was located at bottom frame of images.

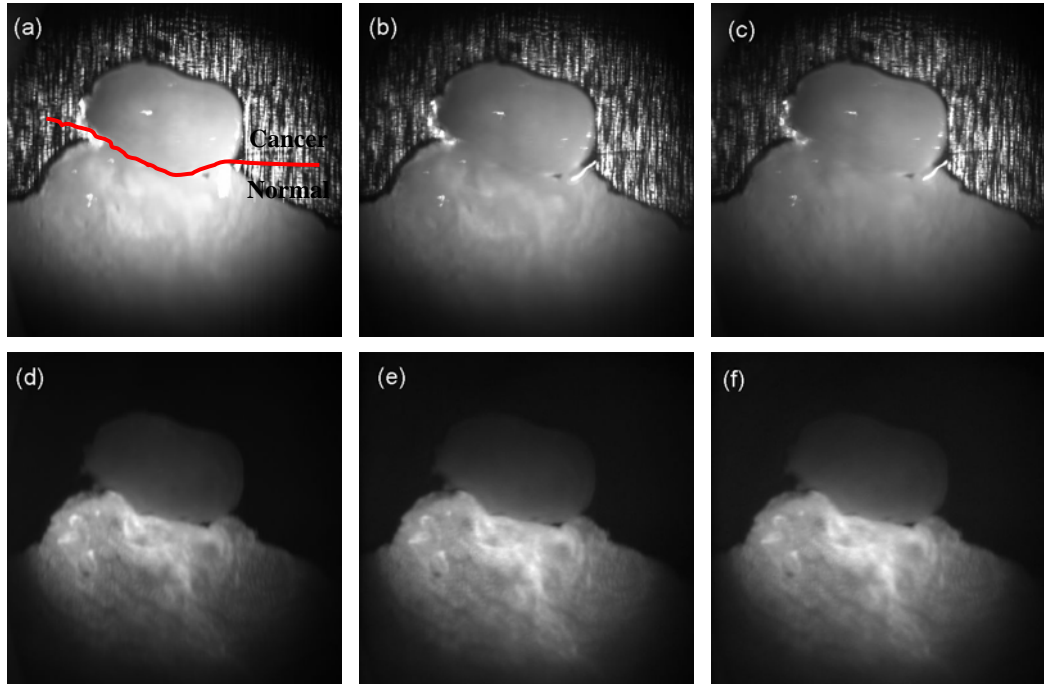


**Fig. 3.5** Representative NIR DR and AF images of colonic tissues acquired using tungsten halogen light illumination and 785 nm laser excitation under different polarization conditions: (a) DR with non-polarization, (b) DR with parallel polarization, (c) DR with perpendicular polarization, (d) AF with non-polarization, (e) AF with parallel polarization, (f) AF with perpendicular polarization.

NIR DR images as shown in Fig. 3.5 (a-c) can not distinguish the difference between cancer and normal tissues by naked eyes. By contrast, the AF images under three different polarization conditions (Fig. 3.5 (d-f)) show that the cancer tissue, which is with the feature of lower intensity, can be easily distinguished from normal tissue. In order to further quantitative analysis the intensity difference between colonic normal and cancer tissue, we calculate the intensity ratio between the normal and cancer colonic tissue. As shown in Fig. 3.6, a homogenous area ( $\sim 2 \times 2 \text{ mm}^2$ ) is selected to estimate the average intensity of both normal and cancer tissue respectively. Due to the size variation of colonic tissues from different patients, the size and the location of the homogenous area for calculating the average intensity are different individually. Fig. 3.6 shows the average intensity for both normal and cancer tissue in the NIR DR and NIR AF images. The intensity ratio of cancer to

normal tissue is 1.19 for the NIR DR image in Fig. 3.6 (a) and 2.7 for the NIR AF image in Fig. 3.6 (b). The experimental results demonstrate that 37 colon cancer tissues have lower AF intensity than the corresponding normal tissues. In other word, for 77.1% of paired colonic tissue, the intensity ratio of normal to cancer tissues is higher than 1. The mean value of the intensity ratios from all NIR AF imaging results is 1.2 ( $p=3.5E-4$ ). Whereas, the mean intensity ratio for all NIR DR images is 0.98 and not statistical significant for classification the cancer from normal colonic tissues.

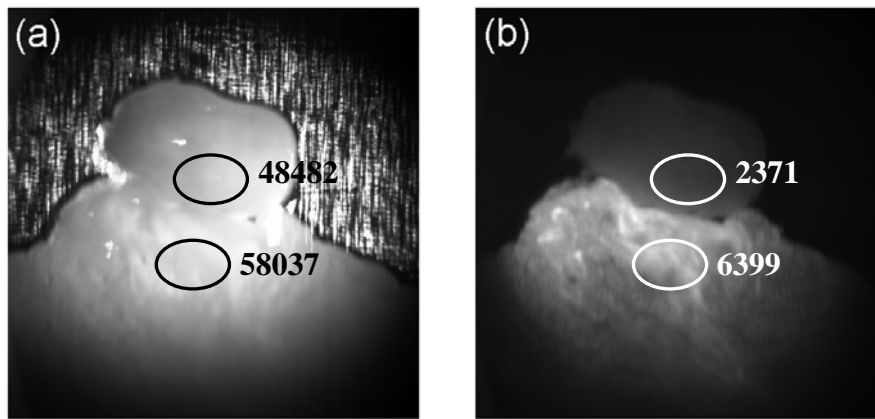


**Fig. 3.6** The average AF intensity for the normal and cancer colonic tissues based on the selected region on (a) NIR DR image and (b) NIR AF images.

Our integrated NIR AF imaging system successfully acquired NIR AF images of colonic normal and cancer tissues. Our results demonstrated that the colon cancer tissue can be identified from normal tissues with significant lower AF intensity in NIR AF images under different polarization conditions. This is because AF imaging takes advantage of the intrinsic fluorophores, which are associated with the structural matrix of tissues or involved in cellular metabolic processes, to assess both the structural and the biochemical progression of colon cancer. The differences of fluorescence intensity between normal and cancer tissue could be attributed to the changes of tissue optical properties of cancer tissue in the colon [84]. For example,

the proliferation of neoplastic cells caused the thickening of mucosal tissue in cancer tissue [84, 115], which could significantly attenuate the excitation light penetration and also obscure the tissue AF emission from the tissue, resulting in an overall decrease of NIR AF intensity from cancer tissue as compared to normal colonic tissue. In addition, the changes in concentrations of endogenous fluorophores such as NADH, collagen, flavins, porphyrin, etc., in tissue associated with malignant transformation [84, 115, 119] may also attribute to the differences in the NIR AF emission between normal and cancer colonic tissue. But the origins of the specific endogenous fluorophores responsible for NIR AF emission in colonic tissue are still not well understood, which warrant further investigations, such as high-performance liquid chromatography (HPLC) can be used to identify, quantify and purify the individual components of the mixture actually. In Chapter 5, we developed the non-negativity-constrained least squares minimization (NNCLSM) biochemical modeling to quantitative investigate the endogenous fluorophores which are responsible for the NIR AF differences between normal and cancer tissues.

### **3.3.2 Polarization autofluorescence imaging**

In our NIR AF imaging system, we integrated the polarization technique into NIR AF imaging system to explore the diagnostic ability of polarization fluorescence imaging. Fig. 3.7 (a-c) shows the representative NIR AF images of the paired colonic specimens under the different polarization conditions in pseudo-color: (a) NIR AF image without polarization; (b) NIR AF image with parallel polarization, and (c) NIR AF image with perpendicular polarization. Fig. 3.7 (d) shows the intensity profiles along the lines as indicated on NIR AF images in Fig. 3.7(a-c), respectively, illustrating that the cancer tissue shows a relatively lower NIR AF

intensity than the normal tissue. Since the heterogeneous structure of tissue, the line was drawn to cross the homogenous area which located at the center of field of view. Then the ratio of average intensity of last 20 points to the first 20 points in intensity profile was calculated. For instance, NIR AF emission arising from cancer tissue reduces by 2.0-, 2.2-, and 2.4- fold, respectively, in intensity as compared to the normal tissue under the non-polarization, parallel and perpendicular polarization conditions. The contrast of NIR AF emission between normal and cancer colonic tissue has been enhanced in the parallel- and perpendicular polarization condition compared to the non-polarization condition.

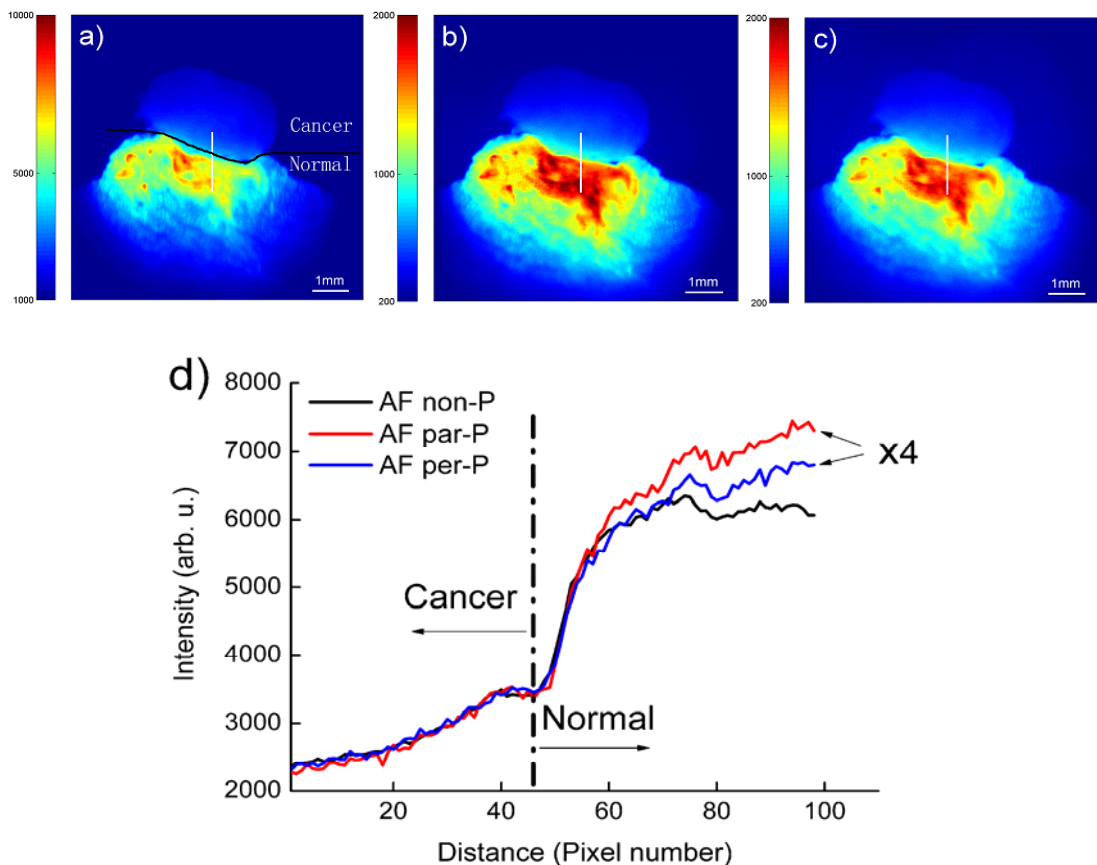


**Fig. 3.7** Representative pseudocolor NIR AF images of colonic tissues acquired using 785 nm excitation under different polarization conditions: (a) non-polarization, (b) parallel polarization, and (c) perpendicular polarization. (d) Intensity profiles along the lines as indicated on the NIR AF images in (a-c). Note that the AF intensity profiles under the parallel and perpendicular polarizations have been magnified by 4 times in Fig. 3.7(d) for better visualization.

To compare the diagnostic performance of NIR AF imaging under different polarization conditions, NIR AF intensities are as calculated from the homogenous area on the normal and cancer NIR AF images, respectively (Fig. 3.6). Fig. 3.8 (a-c) shows the pair-wise comparison of NIR AF intensities of all 48 paired (normal vs cancer) colonic tissues under the three polarization conditions (i.e., (a) non-polarization, (b) parallel and (c) perpendicular polarization). NIR AF intensities of cancer tissue are significantly lower than those of normal tissue with the  $p$ -values of  $3.5E-4$ ,  $3.2E-8$  and  $5.8E-9$ , respectively, under the non-polarization, parallel and perpendicular polarization light excitation conditions (paired 2-sided Student's  $t$ -test,  $n=48$ ). Based on the intensity ratio of normal to cancer tissue ( $I_{\text{normal}}/I_{\text{cancer}}$ ), the diagnostic accuracies of 79.2% (38/48), 91.7% (44/48) and 93.8% (45/48), respectively, can be achieved by using the NIR AF imaging under the non-polarization, parallel and perpendicular polarization light excitation. Hence, the polarized NIR AF imaging was able to enhance the contrast between normal and cancer colonic tissue with a higher diagnostic accuracy (of  $\sim 92$ -94%) compared to the non-polarized AF imaging (accuracy of  $\sim 79\%$ ).

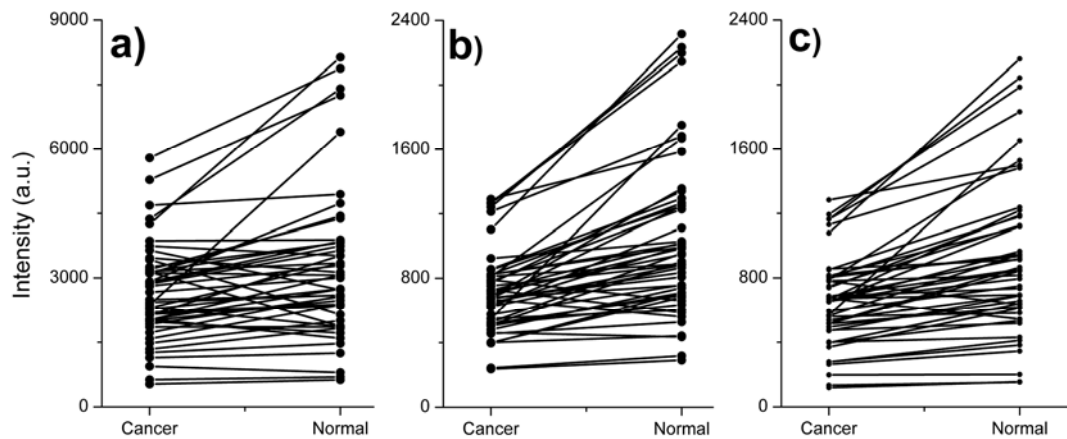


**Fig. 3.8** Pair-wise comparison of NIR AF intensities of all 48 paired (normal vs. cancer) colonic tissues under the three different polarization conditions: (a) non-polarization, (b) parallel polarization, and (c) perpendicular polarization.

To explore the possible reason that the polarized NIR AF imaging performs better than the non-polarized NIR AF imaging technique for detection of colon cancer, we have also studied NIR AF polarization properties of normal and cancer colonic tissue by calculating the polarization ratio values ( $\text{Ratio}=(I_{\text{par}}-I_{\text{per}})/(I_{\text{par}}+I_{\text{per}})$ ) in NIR AF images (Fig. 3.9 (a)). It is observed that the polarization ratio values of cancer colonic tissue are in the range of 0.0001 to 0.01, while the polarization ratio values of normal tissue are much higher, ranging from 0.012 to 0.075 as shown in Fig. 3.9 (b). Similar to the polarized reflectance imaging [62], the parallel-polarized NIR AF imaging contains the information mainly from the surface or subsurface of the tissue, whereas the perpendicular-polarized NIR AF imaging reveals the information predominantly from deep areas of the tissue [62, 120]. A strong linear polarization of cancer tissue reflects that much more multiple light scatterings may occur in deeper regions of tissue due to the disorganized structures of tissue in colonic adenocarcinoma, resulting in a larger perpendicular polarized light component as compared to the normal tissue. As such, the polarized NIR AF imaging technique has the ability to selectively probe the AF light photons that arise from the subsurface or deep areas of tissue for improving cancer diagnosis and characterization.

### **3.3.3 Ratio imaging of NIR DR/NIR AF**

The acquired Tissue NIR A F image not only depends on the tissue status (e.g., tissue surface structures, physiology or histopathology status, etc.), but also the measurement conditions (e.g., light excitation-tissue-collection configurations with respect to the tissue surface, illumination light power variation, etc.) [121]. To eliminate the geometrical effects on NIR AF measurements such as the variations of

the light source-tissue distance, the varying angles for the incident light and tissue fluorescence collections, and the irregularities of the tissue surface which are naturally encountered in practical tissue fluorescence imaging, we have also measured the NIR DR images from normal and cancer tissue serving as background image to normalize the NIR AF image for correcting the artifacts of NIR AF image non-uniformity. Fig. 3.10 (a-c) shows the NIR DR images of normal and cancer colonic tissue acquired under the three polarization conditions, which give no significance differences in NIR DR intensities between normal and cancer tissue ( $p$ -values of 0.20, 0.28 and 0.17, respectively for the non-polarization, parallel and perpendicular polarization conditions, paired 2-sided Student's  $t$ -test,  $n=48$ ).

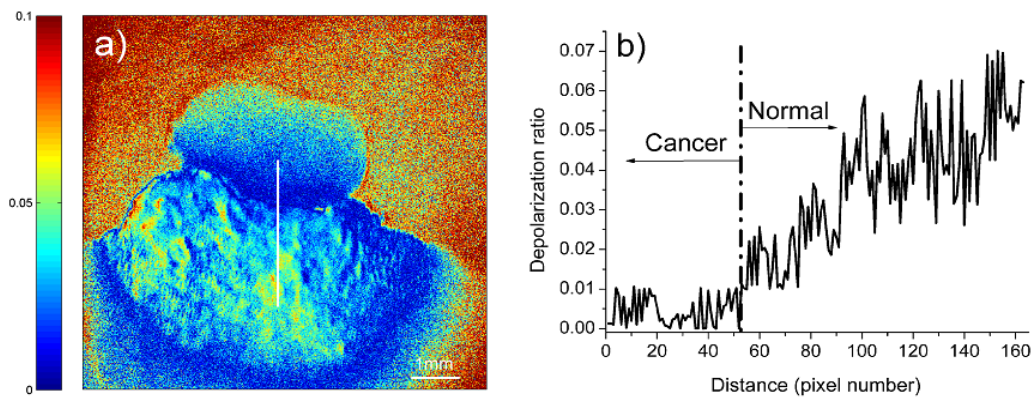


**Fig. 3.9** (a) The processed polarization ratio image  $((I_{par}-I_{per})/(I_{par}+I_{per}))$ , where  $I_{par}$  and  $I_{per}$  are the NIR AF intensities under the parallel and perpendicular polarization conditions) of normal and cancer tissue. (b) Polarized ratio values along the line across normal and cancer colonic tissue as indicated on the polarization ratio image in Fig.3.9 (a).

When normalize the NIR DR images (Figs. 3.10 (a-c)) to the corresponding NIR AF images (Figs. 3.7 (a-c)), much enhanced differences in NIR ratio imaging between normal and cancer tissue can be observed clearly in Figs. 3.11 (a-c) (with the  $p$ -values of  $5.0E-5$ ,  $2.5E-9$  and  $7.8E-10$ , respectively under the non-polarization, parallel and perpendicular polarization conditions (paired 2-sided Student's  $t$ -test,

n=48)), and the NIR DR/NIR AF ratio values of cancer tissue can be  $\sim 2.8$ -fold larger than those of normal tissue (Fig. 3.8 (d)). The diagnostic accuracies of 83.3% (40/48), 93.8% (45/48) and 95.8% (46/48), respectively, can also be achieved by using the NIR DR/NIR AF ratio imaging under the non-polarization, parallel and perpendicular polarization conditions.

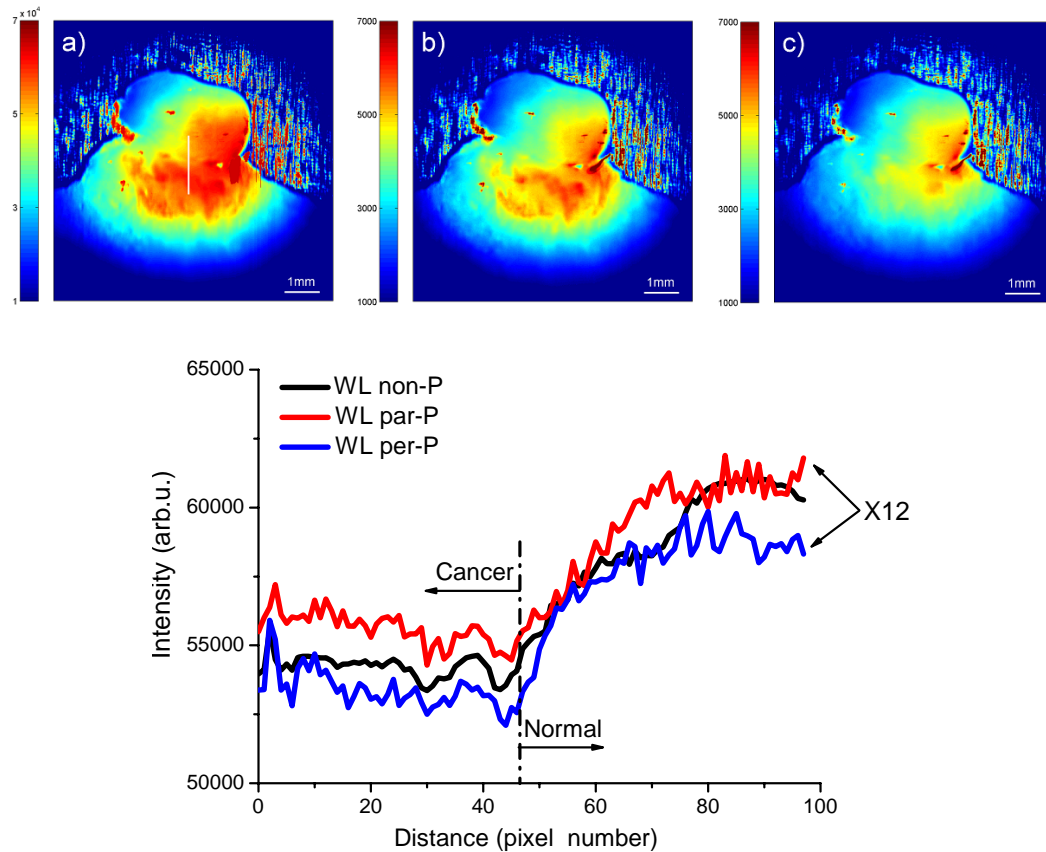


**Fig. 3.10** NIR DR images of colonic tissues acquired using a broadband light source under different polarization illumination: (a) non-polarization, (b) parallel polarization, (c) perpendicular polarization, and (d) intensity profiles along the lines as indicated on the NIR DR images in (a-c). Note that the AF intensity profiles under the parallel and perpendicular polarizations have been magnified by 12 times in Fig. 3.7 d for better visualization.

Therefore, with the ability of correcting the geometrical effects on NIR AF measurements, the NIR DR/NIR AF ratio imaging technique can further improve the diagnostic accuracy (of  $\sim 94$  to  $96\%$ ) for colon cancer detection. Since the white light source was shined on the tissue with an angle, we can observe the intensity gradient

from left to right (Fig. 3.10 and Fig. 3.11). With optimized the system, the non-uniform illumination in DR image might be corrected if the white light could be coupled into the same light path as laser excitation. After integrating into conventional colonoscopy system, the NIR DR/NIR AF ratio imaging technique may have the potential for delineating the margins of tumors for surgical operation.

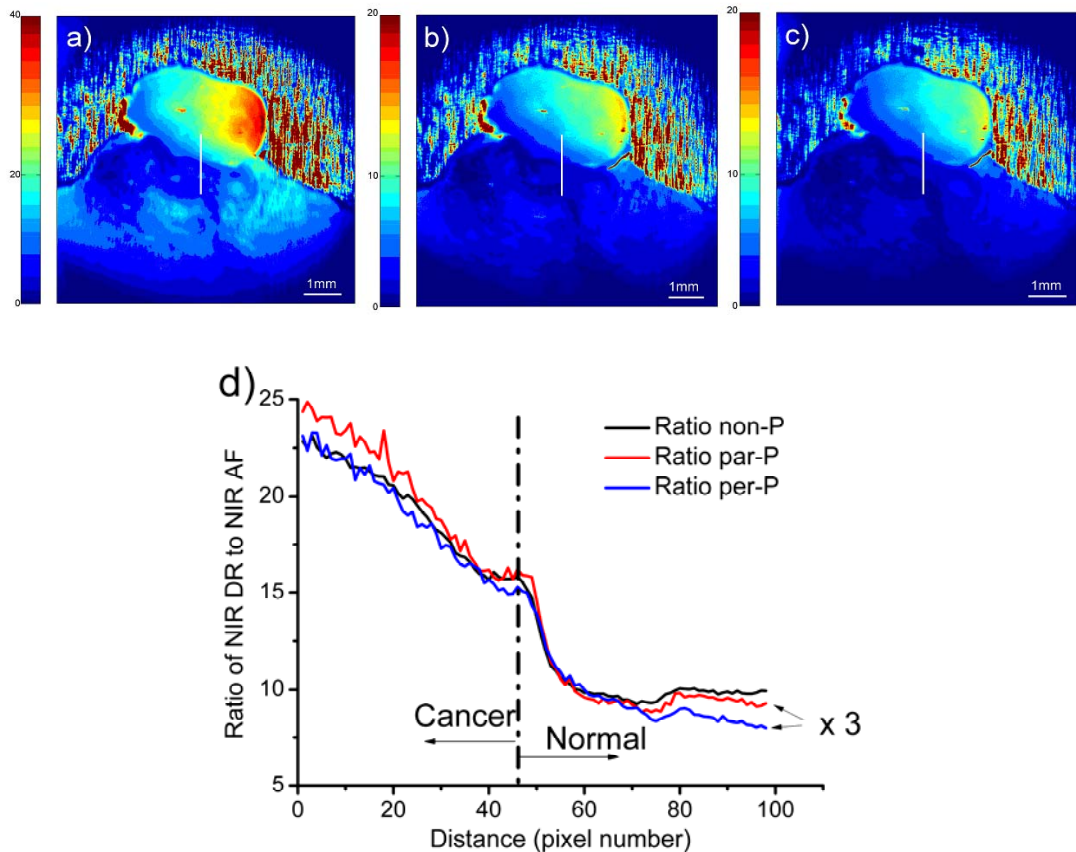


**Fig. 3.11** Ratio imaging of the NIR DR image to the NIR AF image under different polarization conditions: (a) non-polarization, (b) parallel polarization, (c) perpendicular polarization. (d) Comparison of ratio intensity profiles along the lines as indicated on the ratio images in (a-c). Note that the ratio intensity profiles under parallel and perpendicular polarization have been magnified by 3 times in Fig. 3.11 d for better visualization.

### 3.4 Conclusion

The diagnostic accuracies and p-values for classification normal and cancer tissue using different NIR imaging methods have been summarized in Table 1. We evaluate

the diagnostic ability of integrated NIR AF imaging system, in total nine imaging methods: NIR AF and the NIR DR images under non-, parallel- and perpendicular polarization conditions and corresponding ratio image NIR DR/NIR AF.

**Table 3.1** Comparison of diagnostic accuracy and p-value (paired 2-sided Student's t-test) of different NIR imaging modalities (i.e., NIR AF imaging and NIR DR image under non-, parallel- and perpendicular polarization, and the ratio imaging of NIR DR to NIR AF for detection of colon cancer.

| Imaging modalities                | Non-polarization                  | Parallel polarization              | Perpendicular polarization         |
|-----------------------------------|-----------------------------------|------------------------------------|------------------------------------|
| NIR DR                            | 35.4%(17/48)<br><i>p</i> =0.20    | 43.8%(21/48)<br><i>p</i> =0.28     | 31.2%(15/48)<br><i>p</i> =0.07     |
| NIR AFI                           | 77.1%(37/48)<br><i>p</i> =3.5E-4  | 91.6%(44/48)<br><i>p</i> =5.8E-09  | 93.8%(45/48)<br><i>p</i> =3.2E-08  |
| Ratio imaging of NIR DR to NIR AF | 83.3% (40/48)<br><i>p</i> =5.0E-4 | 93.8% (45/48)<br><i>p</i> =1.3E-08 | 95.8% (46/48)<br><i>p</i> =6.2E-08 |

First, the NIR AF imaging takes the advantage of endogenous fluorophores and structure to investigate the differences of NIR AF emission between colonic normal and cancer tissue without using any chemical dyes. The distinctive difference of intensity in NIR AF images between normal and cancer tissue was employed to identify the cancer from normal colonic tissues. Second, the polarization fluorescence technique with the ability to select the fluorescence light that backscatters from the superficial tissues or deeper region of the tissue was developed to improve the diagnostic ability of NIR AF imaging. When the lesions invaded into different layer of the tissue, the polarization NIR AF imaging can yield images whose contrast is in the region of interest. As a result, the NIR AF imaging under polarized conditions gives a higher diagnostic accuracy (~92-94%) than the non-polarized AF imaging (~79%), while the NIR DR imaging did not reach significance on statistical testing ( $P=0.20$ ,  $0.28$  and  $0.07$ ). Finally, the NIR DR/NIR AF ratio

imaging further improves the diagnostic accuracy and achieved the best diagnostic accuracy (~96%) under perpendicular-polarization condition due to correction of the geometrical effects.

In summary, we found that under the 785 nm laser excitation, NIR AF emission from colonic tissue can be detected and imaged by the sensitive NIR imaging system. Significant differences in AF intensity are observed between colonic normal and cancer tissue, indicating the feasibility of NIR AF imaging technique for detection of colon cancer. Then we combined the polarization technique with NIR AF imaging and the polarized NIR AF images yielded better diagnostic accuracy than the non-polarized images. Finally, the NIR DR/NIR AF ratio imaging under polarization condition further improves the colon cancer diagnosis and characterization. We anticipate that with further miniaturization of the current NIR excitation and imaging system coupled with an endoscope to realize the *in vivo* detection in different organs and it can be extended to the test any type of samples with contrast agents or without. The integrated NIR AF and NIR DR imaging with polarization excitation technique developed in this work may have the potential to be a clinically useful tool for *in vivo* diagnosis and detection of colon cancer during colonoscopic examination.

# **Chapter 4 Endoscopy Based Spectroscopy for *in vivo***

## **Diagnosis of Colonic Polyps**

### **4.1 Introduction**

Available scientific data and considerable clinical experience have indicated that 95% of colon cancers arise from benign adenomatous polyps [7]. In the past three decades, the concept of colon cancer development via benign neoplasms (e.g., adenomatous polyps) has progressively gained creditability. Fig. 4.1 shows a discontinuous process for the development of colon cancer, from normal mucosa, to an increased cellular proliferation, to early simple benign adenoma, to adenoma with advanced histological features, and finally to invasive carcinoma and metastases [122]. There is a close association between adenomas and carcinomas [123]. For instance, 30% of patients with colon cancer have at least one synchronous adenoma, and in patients with two or more synchronous cancers, 50-85% has synchronous adenoma [10]. Thus, the interruption of this adenoma-carcinoma sequence by finding and resecting precancerous polyps can effectively prevent colon cancer.

Colonoscopy is the gold standard to detect and treat polyps in the colon. However, identification of adenomatous polyp can be difficult during routine colonoscopic examination. Since the conventional white light reflectance (WLR) colonoscopy heavily relied on the gross morphological tissue changes, investigations have demonstrated that 22% of polyps may be missed on the first colonoscopy [124]. Furthermore, subtle macroscopic differentiation between adenomatous and hyperplastic polyps may not be apparent under WLR endoscopic imaging, limiting diagnostic accuracy. Therefore, all polyps that were founded at colonoscopy are

routinely resected and send for histopathological examinations. But, the removal of hyperplastic polyps with no malignancy potential could incur additional time, costs, and risks. For diagnostic colonoscopy, serious complications of perforation and bleeding occur only in 0.1% to 0.2% of patients, whereas after applying polypectomy the incidence of serious complications of perforation or bleeding may be as high as 10% [105]. Moreover, there are increased time for colonoscopy procedure and additional cost of forceps and pathologies. Hence, it is of imperative clinic value to develop non-invasive and sensitive advanced optical diagnostic techniques for identification of adenomatous polyp during colonoscopy examinations. It would be a useful tool in the clinical to assist the endoscopists for the targeted biopsies to reduce unnecessary biopsy and associated risks and pathology costs.

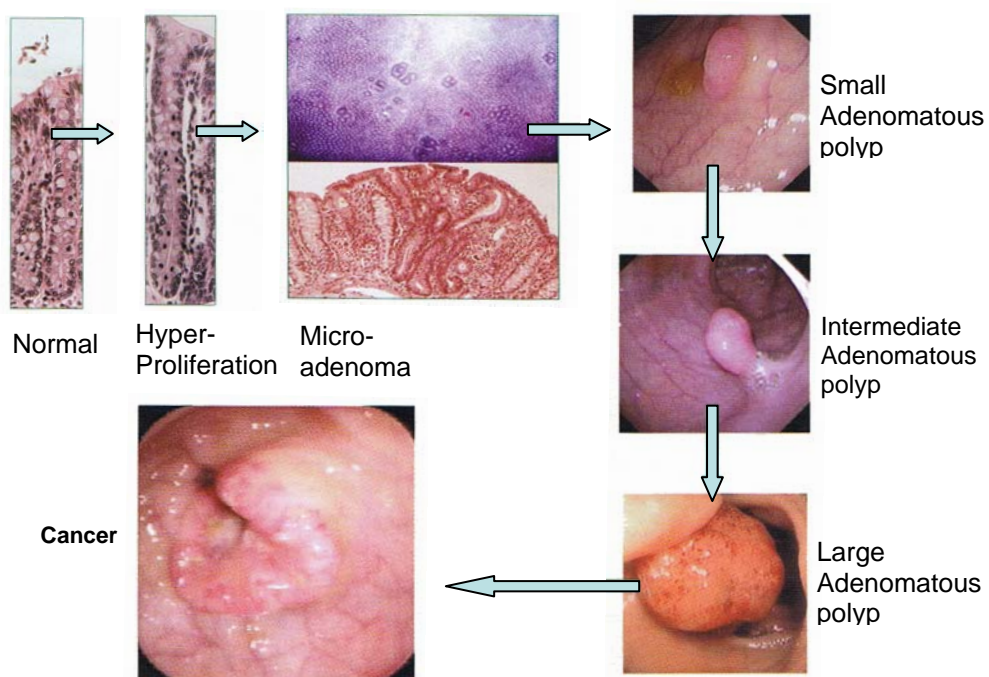


**Fig. 4.1** Phenotypic stages in the adenoma-carcinoma sequence [8].

In recent years, advanced optical spectroscopy and imaging techniques, which characterize tissue both at the microstructure and molecular level, have been investigated to complement the standard white light endoscopy for improving the non-invasive *in vivo* diagnosis of early cancer in the colon [125-127]. Chromoendoscopy takes advantage of chemical contrast agents to identify small and flat polyps that might be missed on conventional WLR colonoscopy and ensure complete removal of neoplastic region during polypectomy [128]. Narrow band imaging (NBI), which uses of band-width filters to increase the blue spectrum intensity of the light, enhance the visualization of superficial capillaries. The neoplastic tissue can be identified from normal mucosa in NBI modality due to the prominent vascular network [129]. With the development of high-sensitivity near infrared (NIR) detectors and fiber-optic probes, NIR Raman spectroscopy has been applied for clinical differentiating adenomatous from hyperplastic polyps at the molecular level [130].

In addition, laser-induced autofluorescence (AF) spectroscopy and imaging are capable of probing changes of tissue morphological structures and concentrations of endogenous fluorophores in the tissue. Alterations in the concentration and distribution of endogenous fluorophores, which are associated with neoplastic transformation, lead to differences in AF emission spectra among normal tissues, hyperplastic and adenomatous polyps. Therefore, the AF technique has shown the promise for distinguishing adenomatous polyps from normal tissue and hyperplastic polyps during colonoscopy [47, 105, 110, 131-134]. The commercial WavSTAT optical biopsy system with UV light excitation has been developed to provide accurate information to the gastroenterologist and assist in

classification of hyperplastic and adenomatous polyps [132]. But to date, few NIR AF applications have been developed for early cancer and cancer detection in the colon. In this work, we develop a NIR AF spectroscopy system to realize *in vivo* NIR AF measurements on the colonic polyp tissue under the guidance of wide-field endoscopic imaging. We employ the novel bifurcated flexible fiber-probe that can pass down the instrument channel of medical endoscopes for effective excitation light delivery and NIR AF and Raman signal collections [126]. The main aim of this study is to evaluate the diagnostic efficacy of the NIR AF spectroscopy for *in vivo* differentiation of colonic adenomatous polyps during colonoscopic examination.

## **4.2 Experiments**

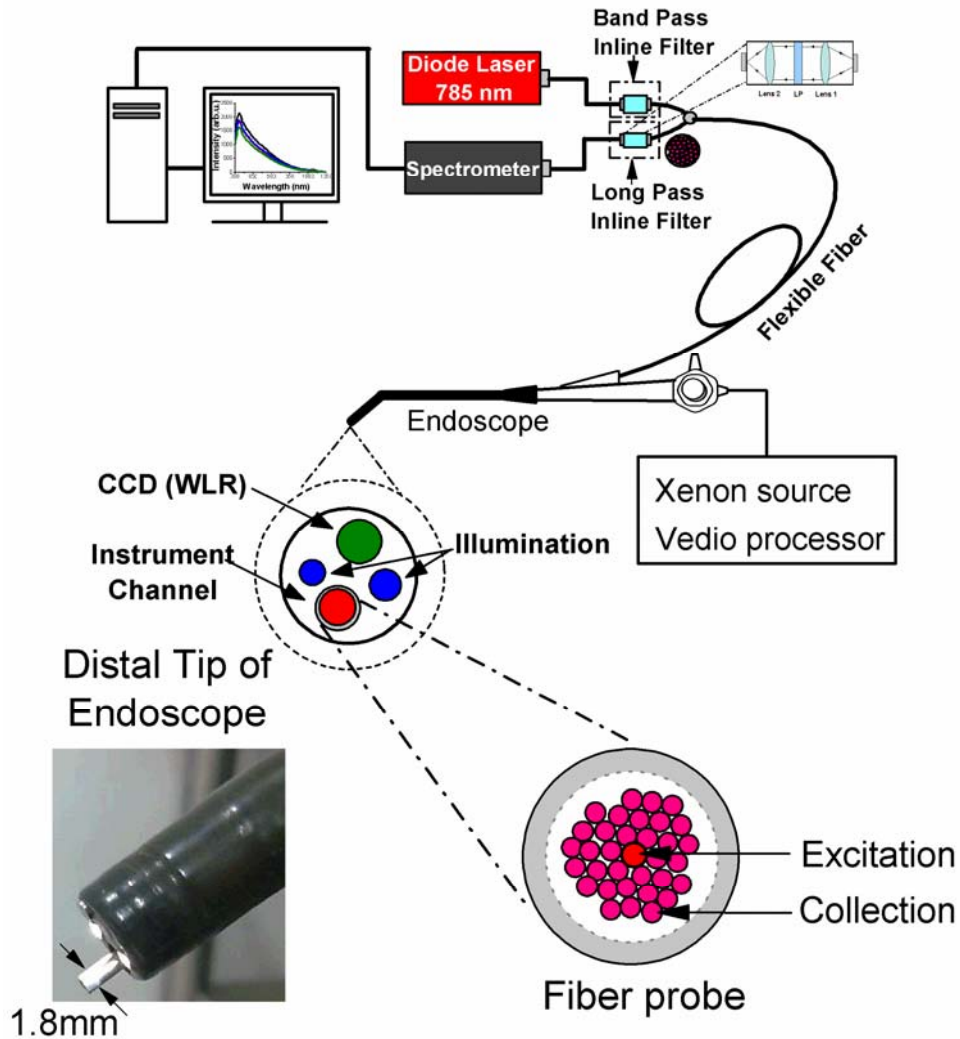
### **4.2.1 Integrated NIR AF spectroscopy system**

Fig. 4.2 shows the schematic diagram of the integrated fluorescence spectroscopy and wide-field endoscopic imaging system developed for *in vivo* tissue AF measurement at colonoscopy. The endoscopy-based fluorescence spectroscopy system consists of a spectrum-stabilized 785 nm diode laser (maximum output: 300mW, B&W TEK Inc., Newark, DE); a scientific-grade spectrometer QE65000-FL (FWHM=6nm, Ocean Optics, Dunedin, FL); and a specially designed endoscopic fiber probe (1.8mm in diameter, 2.5 m in length) for both laser light delivery and *in vivo* AF spectrum collection. The endoscopic fiber probe was composed of 32 collection fibers surrounding the central light delivery fiber (core diameter of 200  $\mu\text{m}$ , N.A.=0.22) with two stages of optical filtering incorporated at the proximal and distal ends of the probe [126]. The distal end of the fiber probe is coated with two different types of filters; the central excitation fiber is coated with a

narrow bandpass filter (centered at 785 nm, FWHM=  $\pm 2.5$ nm), whereas the surrounding collection fibers are coated with edge long-pass filters (cut off at 800 nm). The bandpass filter reduces most of the fused-silica noise generated in the excitation fiber of the fiber probe before the excitation beam hits the tissue, and the edge long-pass filters of the collection fibers reinforce the reflected excitation light to be blocked yet allow the scattered tissue signal to pass back to the detector. At the proximal ends of the fiber probe, the excitation and emission fibers were coupled into two separate in-line filter modules: one integrated with a narrow bandpass filter (LL01-785, Semrock, Inc.) for suppressing laser noise, fluorescence, and Raman emissions from the 200  $\mu$ m core diameter fiber that connects the 785 nm laser to the in-line filter for tissue excitation, and one integrated with an edge long-pass filter (LP02-785RU, Semrock, Inc.) for further reduction of the laser light while permitting the scattered-tissue fluorescence signals to pass through toward the AF spectrometer. In the in-line filter modules, besides the filters, there are two lenses for effectively coupling the light into the fiber for laser excitation and AF signal collection.

A personal computer controls the system using a custom-designed program that triggered data acquisition and background spectrum subtraction. The system acquired *in vivo* tissue AF spectra in the wavelength range of 810-1050 nm from colonic tissue within 1 second using 785 nm excitation power of 1 W/cm<sup>2</sup>, which is less than the ANSI maximum permissible skin exposure limit set out for a 785-nm laser beam [118]. The wide-field colonoscopy imaging system primarily comprises a 300W dedicated short-arc xenon light source, a video colonoscopy (CF-Q160AL, Olympus), and a video system processor (CV-160, Olympus) for WLR imaging.

With this unique NIR AF endoscopic spectroscopy system, wide-field endoscopic images and the corresponding real-time *in vivo* AF spectra of colonic polyp imaged can be simultaneously acquired, displayed, and recorded in the video system and the PC, respectively.



**Fig. 4.2** Schematic diagram of the integrated autofluorescence spectroscopy and wide-field endoscopic imaging system for *in vivo* tissue AF measurement at colonoscopy.

#### 4.2.2 Patients and procedure

This study was approved by the IRB of the NHG of Singapore. All patients preoperatively signed an informed consent permitting the *in vivo* AF endoscopic

spectroscopy measurements during colonoscopy. Fig. 4.3 (a-c) show the white-light reflectance (WLR) images of different types of colonic tissues during clinical colonoscopy. Under the guidance of wide-field WLR endoscopic imaging, the 1.8-mm fiber probe was passed through the instrument channel of the colonoscope to gently contact on the tissue surface for acquiring in vivo tissue NIR AF spectra in real-time. Following the acquisitions of NIR AF spectra from suspicious colonic polyps, the surrounding normal colonic mucosal tissue (approximately 2 cm in distance away from the polyps) was also measured by NIR AF technique serving as a control. A total of 198 colonic tissue sites (116 normal tissue, 48 hyperplastic, and 34 adenomatous polyps) were acquired from 96 patients (55 male and 41 female, with a median age of 50 years) undergoing colonoscopic screening. Immediately after NIR AF spectra acquisitions, all the tissue sites measured were biopsied or resected (e.g., polyps) and fixed in formalin for routine histopathologic examinations.

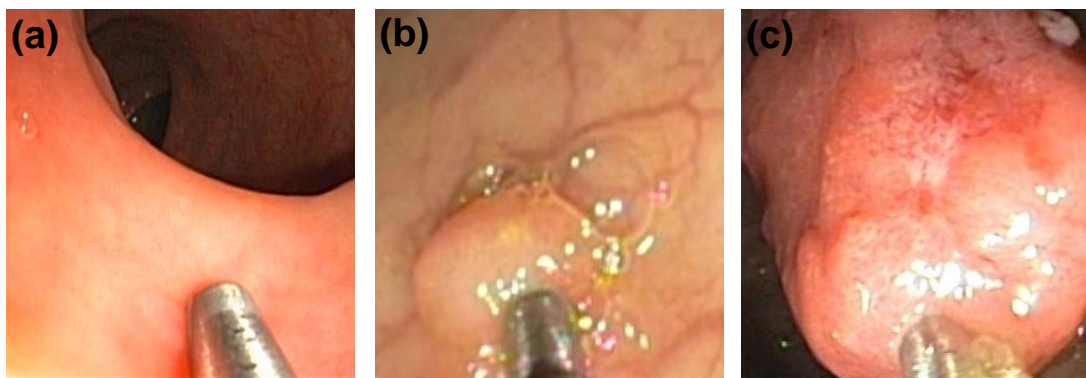


**Fig. 4.3** White-light reflectance (WLR) images of colonic tissues during clinical colonoscopy (a) normal, (b) polyp, and (c) cancer.

#### **4.2.3 Multivariate analysis**

AF spectroscopy can probe great wealth information of intrinsic fluorophores, such as collagen, elastin, and porphyrin. But the AF spectrum usually contains many overlapping bands and the data interpretation can not be easily based on simple

visual inspection for subtle change in tissues. Hence, different statistical techniques would be needed to analysis AF spectrum for tissue diagnosis and classification. The AF spectrum data usually consists of many different variables (i.e., intensity, spectral shape and wavelength) for different cases (i.e., normal tissue, hyperplastic polyp, and adenomatous polyp). Each of these variables could be considered to represent a different dimension. Given  $n$  variables, each of the cases may be regarded to be located in a unique position in an  $n$ -dimensional hyperspace that is difficult to visualize. Therefore, various statistical algorithms have been explored to reduce this massive dimensional space to an interpretable dimensional space [135].

### **Principal component analysis (PCA)**

PCA is a mathematical procedure that uses an orthogonal transformation to convert a set of observations variables, which are possibly correlated with each other, into a set of values of uncorrelated variables called principal components (PCs). PCA decomposes the spectroscopic data matrix  $S$  into scores  $T$  and loading  $P$ , according to the relation,

$$S = T \cdot P \quad (4.1)$$

With this equation, PCA transforms a number of correlated variables into a number of uncorrelated variables (PCs) which describe the greatest variance of the spectral data. The number of PCs is less than or equal to the number of original variables. It is usually employed as a method for variable or data reduction by retaining the first few principal components. The first principal component accounts for as much of the variability in the data, and each succeeding component has the highest variance possible in turn. Each component is orthogonal to the preceding components. In addition, inspection of the plots generated by scores provides a mean to assess the

relationship between samples, since it helps to identify some clusters related to a certain feature and detect potential outliers.

### **Linear discriminant analysis (LDA)**

LDA is used for pattern recognition and machine learning to find linear combination of the measurements variables that separate the objects from different classes as much as possible. The distance (e.g. euclidean distances) between groups and the compactness of each group are used to determine the separability of classes. Then LDA follows the rule that the ratio of the between-to-within variability of the transformed training data vectors (i.e. spectra) should be maximized.

$$S_{MAX} = \{Variance_{between} / Variance_{within}\} \quad (4.2)$$

In other word, the aim of LDA is to find a discriminant function line that maximized the variance in the data between groups and minimizes the variance between members of the same group. LDA is closely related to PCA and both methods look for linear combinations of variables that best explain the data. LDA explicitly attempts to model the difference between the classes of data, while PCA does not take into account any difference in class.

In this study, we applied PCA-LDA for multivariate analysis. The high dimension of fluorescence spectral space (each fluorescence spectrum ranging from 810-1050 nm with a set of 325 intensities) will result in computational complexity and inefficiency in optimization and implementation of the LDA algorithms. As such, PCA was first performed on tissue fluorescence data set to reduce the dimension of fluorescence spectral space while retaining the most diagnostically significant information for tissue classification. To eliminate the influence of intersubject and/or intrasubject spectral variability on PCA, all spectra were standardized so that the

mean of the spectra was zero. Mean centering ensures that the PCs from an orthogonal basis [136]. Standardized AF data sets were assembled into data matrices with wavelength columns and individual case rows. The PCA was performed on the standardized spectral data matrices to generate PCs comprising a reduced number of orthogonal variables that accounted for most of the total variance in original spectra. Each loading vector is related to the original spectrum by a variable called PC score, which represents the weight of that particular component against the basis spectrum. PC scores reflect the differences between different classes. One-way analysis of variance (ANOVA) [135] was then used to identify the most diagnostically significant PCs ( $p < 0.05$ ) for separation of three different tissue classes. These significant PC scores were selected as input for the development of LDA algorithms for multiclass classification. LDA determines the discriminate function that maximizes the variances in the data between groups while minimizing the variances between members of the same group. The performance of the diagnostic algorithms rendered by the LDA models for correctly predicting the tissue groups was estimated in an unbiased manner using the leave-one-sample-out, cross-validation method on all model spectra. In this method, one sample (one spectrum) was held out from the data set, and the entire algorithm including PCA and LDA was redeveloped using the remaining tissue spectra. The algorithm was then used to classify the withheld spectrum. This process was repeated until all withheld spectra were classified. For the assessment of diagnostic sensitivity and specificity of NIR AF spectroscopy technique, histopathologic examination results serve as the gold standard. Multivariate statistical analysis was performed in the STATISTICA version 7 (Statsoft Inc., Tulsa, Oklahoma, USA).

### 4.3 Results and Discussion

We successfully employ the novel NIR AF spectroscopy system to acquire 198 *in vivo* NIR AF spectra under the guidance of colonoscopic WLR image from different types of colonic tissues, including normal ( $n=116$ ), hyperplastic polyp ( $n=48$ ), and adenomatous polyp ( $n=34$ ) colonic tissues. Based on spectral characters among these different types of colonic tissues, we apply PCA-LDA to run three group classifications among normal, hyperplastic polyp, and adenomatous polyp for distinguishing the subtypes of colonic polyps. Good classification results demonstrate the diagnostic potential of integrated NIR AF spectroscopy to be a clinical complement to conventional WLR endoscopy for the rapid, non-invasive, *in vivo* differentiation of precancer (adenomatous polyps) and cancer in clinical colonoscopy procedures.

Fig. 4.4 shows the *in vivo* mean NIR AF spectra  $\pm 1$  standard errors (SE) of normal ( $n=116$ ), hyperplastic ( $n=48$ ), and adenomatous polyps ( $n=34$ ) in the colon. On average, the NIR AF intensities of normal tissue in the entire spectral region of 810-1050 nm are significantly higher than those of hyperplastic and adenomatous colonic polyps ( $p<0.001$ , one-way analysis of variance (ANOVA)); and NIR AF signals from adenomatous polyps are significantly lower than hyperplastic colonic polyps ( $p<0.001$ ). The NIR AF spectral shapes from different types of colonic tissues show different decreasing trends with the increased wavelengths ranging from 810 to 1050 nm. In addition, the weak tissue Raman scatterings superimposed on the intense NIR AF spectra of different colonic tissues are also observed, which include the prominent Raman bands such as  $875\text{ cm}^{-1}$  ( $\nu(\text{C-C})$  hydroxyproline),  $936\text{ cm}^{-1}$  ( $\nu(\text{C-C})$  of proline and valine),  $1078\text{ cm}^{-1}$  ( $\nu(\text{C-C})$  of phospholipids),  $1265\text{ cm}^{-1}$

(amide III  $\nu(\text{CN})$  and  $\delta(\text{NH})$  of proteins),  $1302\text{ cm}^{-1}$  ( $\text{CH}_3\text{CH}_2$  twisting of proteins and nucleic acids),  $1335\text{ cm}^{-1}$  ( $\text{CH}_3\text{CH}_2$  wagging of proteins and nucleic acids),  $1445\text{ cm}^{-1}$  ( $\delta(\text{CH}_2)$  of proteins and lipids),  $1665\text{ cm}^{-1}$  (amide I  $\nu(\text{C}=\text{O})$  of proteins) and  $1745\text{ cm}^{-1}$  ( $\nu(\text{C}=\text{O})$  of phospholipids), as well as the strong Raman peaks appearing at  $2885\text{ cm}^{-1}$  ( $\text{CH}_2$  stretching of lipids) and  $2940\text{ cm}^{-1}$  ( $\text{CH}_3$  stretching of proteins) [115, 137-151].

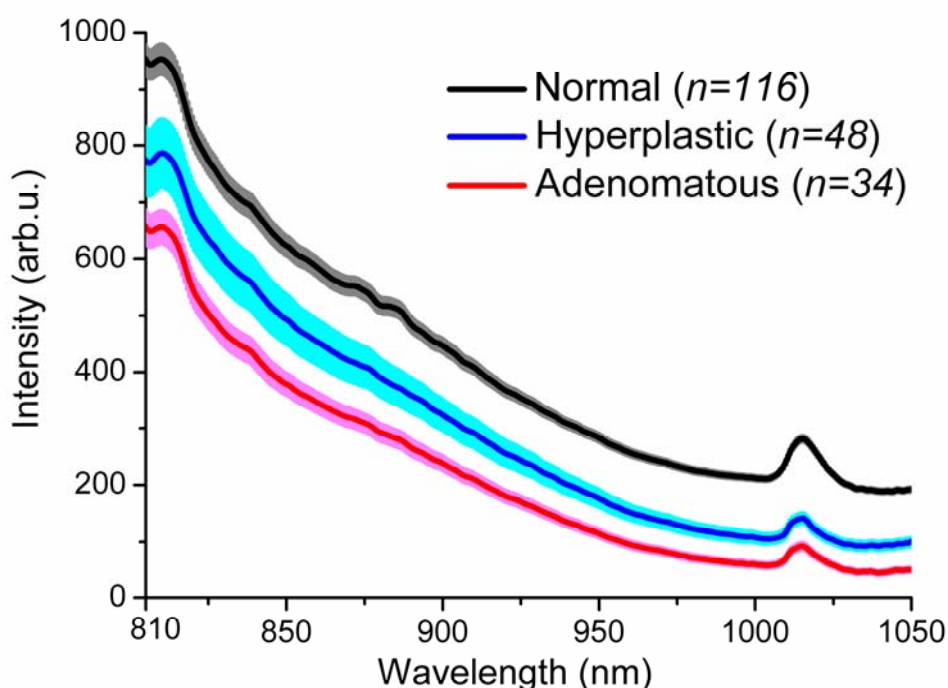


**Fig. 4.4** *In vivo* mean NIR AF spectra  $\pm 1$  SE of normal ( $n=116$ ), hyperplastic ( $n=48$ ) and adenomatous polyps ( $n=34$ ) colonic tissue. Note that *in vivo* NIR AF spectra of normal colonic tissue are vertically shifted for better visualization. The shaded areas in tissue AF spectra stand for the respective standard error.

The spectral shape differences from 810 to 1050 nm are apparent for NIR AF spectra among the three different colonic tissue types (i.e., normal, hyperplastic and adenomatous polyps). The ratios of NIR AF spectra of normal to hyperplastic and adenomatous polyps are not flat horizontal lines but increase from 810 to 1005 nm and then decrease until close to 1015 nm and finally increase again till 1050 nm (data not shown). Although no distinctive differences in Raman peak positions are

observed between normal, hyperplastic and adenomatous polyps tissues, by normalizing the colonic tissue Raman spectra [143], changes in Raman spectral lineshapes and relative intensities between normal and colonic polyps tissues are also revealed (data not shown). Hence, the NIR AF differences in both the spectral intensities and lineshapes of different colonic tissues observed in this study confirm the potential role of NIR AF spectroscopy technique for in vivo diagnosis of hyperplastic and adenomatous polyps in the colon.

In attempt to determine the most diagnostically significant AF features for identifying adenomatous polyp tissue from normal tissue and hyperplastic polyp colonic tissue, we have employed the multivariate statistical technique (PCA) together with the one-way ANOVA test to identify the significant principal components (PCs) of in vivo NIR AF spectra for differentiation among normal, hyperplastic and adenomatous colonic polyps. The first eight PCs (PC1- PC8) scores (Fig. 4.5) accounting for ~99% of the total variance are found to contain the diagnostically significant NIR AF/Raman features ( $p < 0.05$ ) for classification of different colonic tissues types. One notes that the first PC accounts for the largest variance (~80.50% of the total variance), and the successive PCs contribute progressively smaller variances (PC2~10.08%, PC3~4.05%, PC4~2.52%, PC5~0.79%, PC6~0.42%, PC7~0.12%, and PC8~0.09%). Some PC features, such as spectral line shapes, troughs, and peaks, are similar to tissue NIR AF spectra and Raman spectra of colonic tissues (Fig. 4.4).

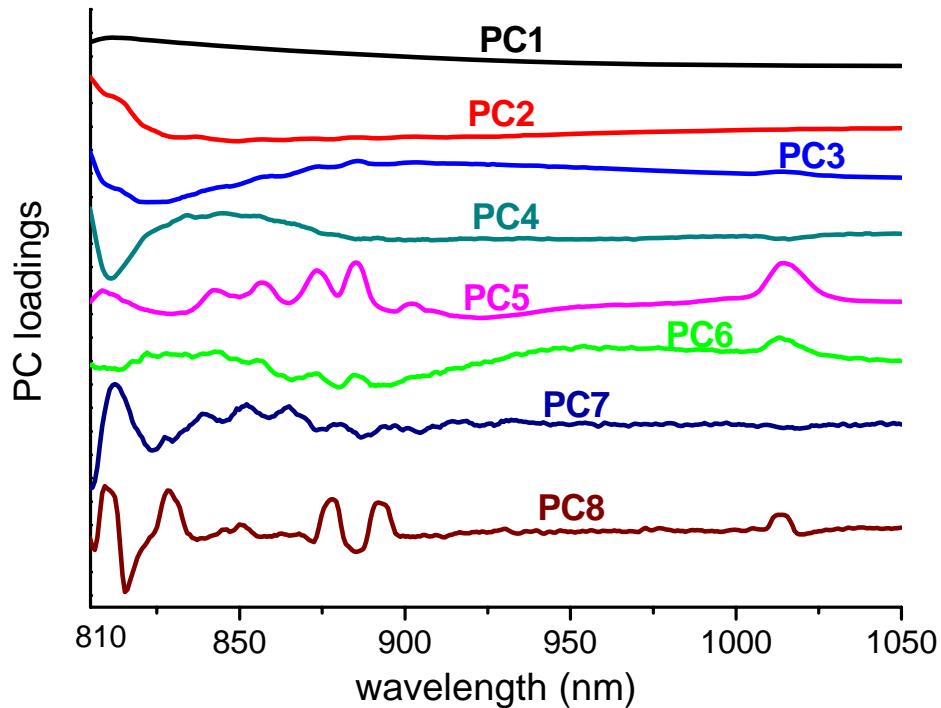


**Fig. 4.5** The first eight significant principal components (PCs) (PC1~80.50%, PC2~10.08 %, PC3~4.05%, PC4~2.52%, PC5~0.79%, PC6~0.42%, PC7~0.12%, and PC8~0.09%) accounting for ~99% of the total variance calculated from in vivo NIR AF spectra.

Fig. 4.6 shows the relationship between the diagnostically significant difference colonic tissue types. Fisher's least significant difference tests showed the different PC scores were largely associated with different degrees of diagnostic utility for classification of different colonic tissue types (normal tissue, hyperplastic polyp and adenomatous polyp). For instance, PC1 can be used for differentiating hyperplastic polyp from normal tissue and adenomatous polyp; PC2 is optimal in discriminating normal tissue from hyperplastic and adenomatous polyp; PC3 and PC7 can be used to distinguish adenomatous polyp from hyperplastic polyp and normal tissue; PC4 and PC6 can be used to separate adenomatous polyp from normal tissue; PC5 show efficacy in classification of the three different colonic tissue types; PC8 can be used to separate hyperplastic polyp from normal tissue.

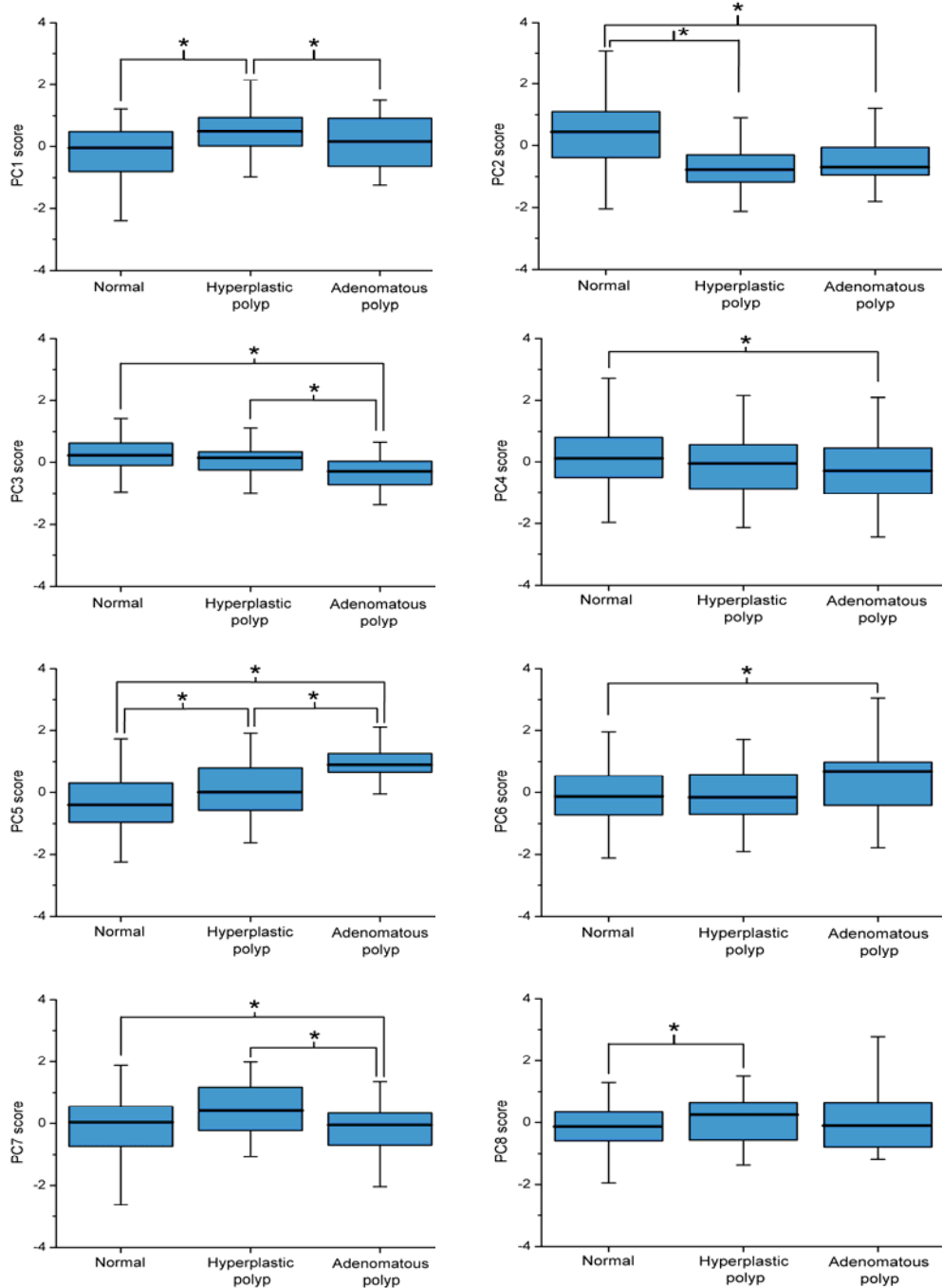


**Fig. 4.6** Box charts of the eight significant principal component (PC) scores for the three colonic types (normal, hyperplastic polyp and adenomatous polyp): a PC1, b PC2, c PC3, d PC4, e PC5, f PC6, g PC7, and h PC8. The line within each notch box represents the median, and the lower and upper boundaries of the box indicate first (25 percent percentile) and third (75 percent percentile) quartiles respectively. Error bars (whiskers) represent the 1.5-fold interquartile range. \* $P < 0.05$  (pairwise comparison of tissue types with *post hoc* multiple comparison tests (Fisher's least significant differences)).

All the significant eight PCs are then fed into the LDA model together with leave-one tissue-out cross validation to develop effective diagnostic algorithms for classification of different colonic tissues. Fig. 4.7 shows the ternary plot of depicting probabilistic outcomes in association with NIR AF data from normal, hyperplastic, and adenomatous polyp tissues, respectively. The final diagnostic category of each NIR AF data is determined by the nearest proximity of data to the diagnostic category related to the vertex of the ternary plot. The vertices in Fig. 4.7 represent the 100% posterior probabilities belonging to normal, hyperplastic, and adenomatous polyps, respectively. Table 1 summarized the classification results of *in vivo* NIR AF spectra of different colonic tissues. The diagnostic sensitivities of 83.6%, 77.1%, and 88.2%; specificities of 96.3%, 88.0%, and 92.1%; and accuracies of 88.9%, 85.4%, and 91.4%, respectively, are achieved using NIR AF spectroscopy for differentiation of normal, hyperplastic, and adenomatous colonic polyps.

In this study, we investigate the *in vivo* NIR AF spectral properties of normal, hyperplastic, and adenomatous colonic polyps, and explore the potential of translating the wealthy information of tissue morphological structure and endogenous fluorophores within the NIR AF spectra into clinically diagnostic algorithms to realize *in vivo* endoscopic identification of hyperplastic and adenomatous polyps in the colon. To understand and interpret the spectral differences among normal, hyperplastic, and adenomatous colonic polyps, it is important to know the origins of NIR AF spectral signals in the colonic tissues. To date, there are only a very limited number of tissue AF studies conducted at longer red to NIR wavelengths, which were mostly centered for examining tissue porphyrin-related fluorescence [101]. Porphyrins, which exhibits significant

absorption in the red/NIR spectral region accompanied by emission in the far-red and NIR regions [152], has been assumed as the major endogenous fluorophores responsible for NIR AF emission in tissues and the accumulation of porphyrins in various types of cancer has been discovered [153]. One should notice the possibility that NIR AF may also arise from biomolecules other than porphyrins, which may also be unevenly distributed between normal and tumor tissue and thus the origins of the specific endogenous fluorophores responsible for NIR AF emission in colonic tissue are still not well understood.

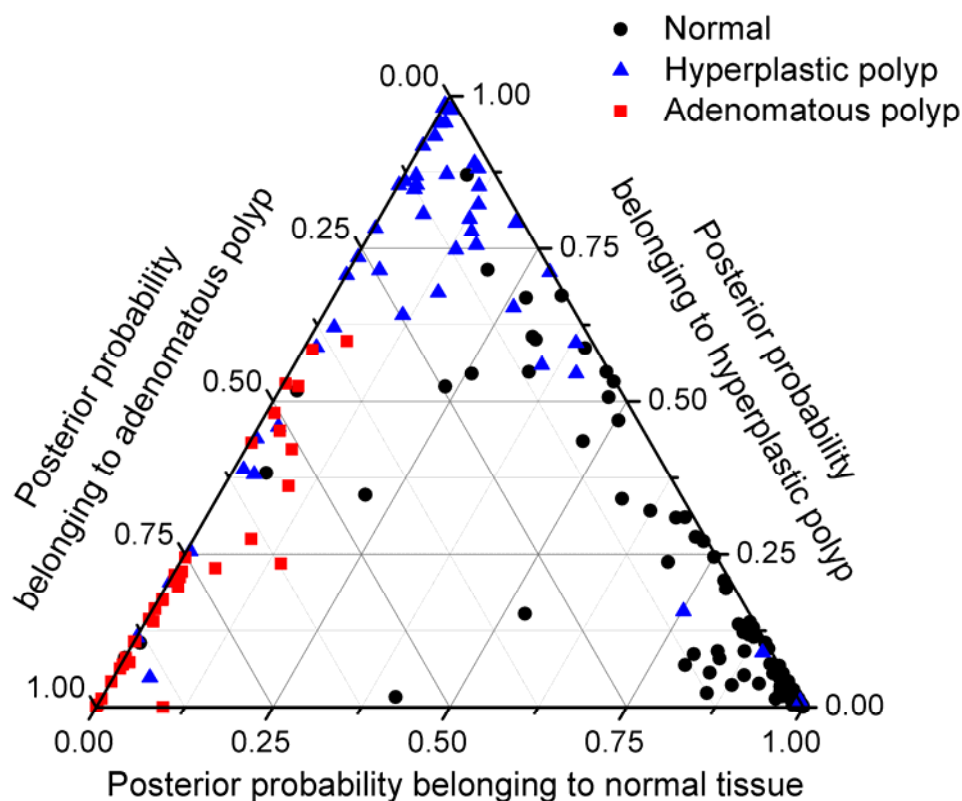


**Fig. 4.7** Two-dimensional ternary plot of the posterior probability belonging to normal tissue, hyperplastic and adenomatous polyp, illustrating the good clusterings of the three different colonic tissue types achieved by PCA-LDA algorithms, together with the leave-one tissue site-out, cross validation method.

**Table 4.1** Classification results of *in vivo* NIR AF spectra prediction for the three colonic tissue groups using PCA-LDA algorithms, together with the leave-one tissue site-out, cross validation method.

| Autofluorescence prediction |        |                    |                   |       |
|-----------------------------|--------|--------------------|-------------------|-------|
|                             | Normal | Hyperplastic polyp | Adenomatous polyp | Total |
| Normal                      | 97     | 14                 | 5                 | 116   |
| Hyperplastic polyp          | 3      | 37                 | 8                 | 48    |
| Adenomatous polyp           | 0      | 4                  | 30                | 34    |
| Sensitivity (%)             | 83.6   | 77.1               | 88.2              |       |
| Specificity (%)             | 96.3   | 88                 | 92.1              |       |
| Accuracy (%)                | 88.9   | 85.4               | 91.4              |       |

To investigate the endogenous fluorophores which are also responsible for the differences of NIR AF emission among normal, hyperplastic and adenomatous colonic polyps, we have developed the non-negativity-constrained least squares minimization (NNCLSM) biochemical modeling to analysis the biochemical compositions of colonic tissue [154]. Our modeling results showing the increased contents of hematoporphyrin for the adenomatous polyps than hyperplastic polyps and normal tissue were in agreement with previous reports [101]. The modeling results also shows that, adenomatous colonic polyps show lower contents belonging to collagen I, flavin adenine dinucleotide (FAD),  $\beta$ -nicotinamide adenine dinucleotide ( $\beta$ -NADH), L-tryptophan, and pyridoxal 5'-phosphate, while higher fit coefficients belonging to 4-pyridoxic acid, and water as compared to normal and hyperplastic polyps. We believe that the significant differences in both the spectral intensities and lineshapes of different colonic tissues (Fig. 4.4) could be attributed to the changes in concentrations and distribution changes of these endogenous fluorophores associated with structural or cellular metabolic progression in colonic

precancer and cancer. In addition, the alterations of tissue optical properties associated with adeno-carcinomatous progression could also cause the decreased NIR AF intensity of hyperplastic and adenomatous polyps compared to normal colonic tissue [84]. Due to cellular hyperproliferation, the thickening of the mucosa layer could significantly attenuate the excitation light penetration and also obscure the tissue AF emission from submucosa layer in the polyp tissue compared to normal colonic tissue [115]. For the adenomatous polyp, the growth of these crypt cells displace the lamina propria and further reduce the collagen AF emission from the lamina propria [84]. However there are many complicated biochemical processes to influence progression of polyp to colonic cancer associated with the structural matrix or cellular metabolism, resulting the differences of AF emission from different types of colonic tissues, and thus further investigation is required.

The good discriminant results obtained by employing the NIR AF spectra, which contain both NIR AF and Raman signatures, might be explained as follows. Tissue comprises various fluorophores (e.g., collagen, elastin, proteins, lipids, etc.) and each fluorophore has a different autofluorescence spectral pattern at specific excitation wavelengths [114]. In general, fluorescence spectroscopy is very sensitive to tissue biochemical and morphological changes but it is inaccurate in determining the types of specific changes occurring in tissue due to its very broad spectral line shapes. In contrast, Raman spectroscopy gives fingerprinting-type narrow spectral features that are very specific for different types of tissue biochemical changes. For instance, the prominent Raman signals at  $1302\text{ cm}^{-1}$ ,  $1445\text{ cm}^{-1}$ , and  $2885\text{ cm}^{-1}$  with its own sharp spectral features can be attributed to proteins, lipids, and DNA that are involved in the metabolic activities [137, 144, 146, 155]. During development and

progression of colonic polyp to cancer, epithelial cells undergo transformations that result in increased metabolic activity (e.g., increased mitotic activities that include enzymes, hormones, etc.) and the increased hyperchromatism and the nucleic acids-to-cytoplasm ratio of dysplastic cells [127, 130]. As such, the inherently weak Raman signals from tissues, which can probe biomolecular structures and conformations of tissue, have been applied for the early detection of precancer and cancer in different organs [143, 146, 156]. The raw spectral data containing both Raman and AF signatures offers an opportunity to examine both the biomolecular structure and composition of the tissue (Raman) as well as the endogenous fluorophores and morphological structures in tissue (AF), thereby providing more diagnostic information for tissue diagnosis and characterization. Therefore, Raman and AF are complementary optical techniques that provide different information about tissue under investigation. The combination of NIR AF spectra with the Raman signals using PCA-LDA can be a powerful tool for elucidating the biochemical structure and composition of tissue and thus may provide better diagnostic capability for tissue diagnosis.

#### **4.4 Conclusions**

We have acquired for first time *in vivo* NIR AF spectra from colonic tissues at 785 nm excitation during clinical colonoscopic examinations. We extend the previous UV/VIS AF work [105, 132, 134] to the NIR domain for colonic adenomatous polyp differentiation and characterization. Significant differences in both spectral shapes and intensities of *in vivo* NIR AF spectra among normal, hyperplastic, and adenomatous colonic polyps are observed. As biological tissue is very complex,

there are many factors related to morphological and biomolecular changes taking part in a myriad of biochemical processes to influence disease concurrently. Multivariate statistical techniques (e.g., PCA-LDA) can fully use the entire tissue spectra and elucidate diagnostic information for classification of multiple pathologies for cancer diagnosis and detection [127, 130, 136, 156]. In this study, Good classification between different colonic tissue types can be achieved using PCA-LDA modeling, suggesting the clinical potential of NIR AF technique for the rapid *in vivo* diagnosis and detection of colonic precancer and cancer during clinical colonoscopic procedures.

# Chapter 5 Study of Origin of Endogenous Fluorophores for NIR Autofluorescence

## 5.1 Introduction of Endogenous Fluorophores

The application of autofluorescence (AF) imaging and spectroscopy has been well investigated for *in vivo* and *ex vivo* diagnosis of cancers in different organs for several decades [85-89]. AF technique, which takes advantage of endogenous fluorophores, has been explored to improve the accuracy for detection and diagnosis of precancer and cancer in the colon [46, 80, 92, 96, 106-110]. Chapter 3 and 4 have demonstrated the potential of NIR AF imaging and spectroscopy to complement conventional endoscopy to provide *in vivo*, real-time, and non-invasive detection and diagnosis of precancer and cancer in the colon. However, the biological basis for the differences of AF emission between normal and diseased tissue is still not well understood. Hence, a better understanding of the origin of tissue AF (*i.e.*, endogenous fluorophores) is needed for fully exploiting the potential of AF-based tissue diagnosis and better understanding its limitation [81].

In general, the biochemical species are structural and metabolic. When cells in various disease states, they undergo different rates of metabolism or have different structures. Consequently, alterations occur in the concentration of fluorophores, their spatial distribution, local microenvironment surrounding the fluorophores, and the particular tissue architecture. These alterations result in distinct differences of AF emission for the diseased tissues compared to the normal ones. Therefore, tissue AF can provide a significant amount of information of the endogenous fluorophores, which are responsible for the tissue's morphological structure or involved in the

metabolic and functional processes of cells. Here, we summarize some known endogenous fluorophores and their fluorescence properties in biological tissues.

### **Amino acids**

Proteins contain three aromatic amino acids residues (tryptophan, tyrosine and phenylalanine) that may contribute to their intrinsic fluorescence [157]. These three amino acids have different excitation and emission spectra and different quantum efficiencies. Tryptophan exhibits higher quantum efficiency than those of tyrosine and phenylalanine. It has an maximum emission at wavelength (345 nm), which is longer than those of tyrosine (303 nm) and phenylalanine (282 nm) with excited below 280 nm [158]. The composition of amino acid can influence the fluorescence emission of proteins. Typically, tryptophan accounts for the majority of protein fluorescence and its emission is sensitivity to the polarity of the environment.

### **Structural proteins**

Structural proteins show maximum absorption at 240-280 nm and emission at 280-350 nm regions, respectively. Collagen and elastin account for the connective tissue and exhibit a strong fluorescence emission shifted to longer wavelengths. Collagen is the major extracellular matrix component and there are at least 11 types of collagen according to the different composition of the monomeric chains and the degree of polymerization. The fluorescence of collagen has an excitation maximum at 330-340 nm and emission maximum at 400-410 nm. Elastin is the major component of the elastic fibers in most connective tissue along with collagen. The fluorescence of elastin has an excitation maximum at 350 nm and an emission maximum at 420 nm.

Collagen and elastin are important in the diagnostic application of AF since

they are highly fluorescent biochemicals. Their contributions to the overall AF depend on the histological organization of the tissue. In the submucosa layer, collagen and elastin are the most abundant fluorophores and they have been used for diagnosis of neoplasia of multilayered epithelial tissue, such as cervical, gastric, and colonic tissues [159]. For instance, in normal colon tissues, the detected AF is dominated by the submucosal tissue [115]. However, the invasiveness of tumor cells induces thickening of mucosal and replace the most fluorescent component lamina propria by lesser fluorescent neoplastic crypt cells [84]. Thus, the colonic cancer tissues can be identified from normal tissues based on the reduced fluorescence signals [84, 160-161].

### **Pyridine nucleotides and flavins**

The pyridine nucleotides and flavins have an important role in cellular energy metabolism [162]. They are mainly responsible for the fluorescence emission rising from the cytoplasm of single cells. Their cytoplasmic localization is related to their participation to most part of metabolic reactions, which lead to energy production or anabolic and catabolic functions in the cell [162]. Nicotinamide adenine dinucleotide (NADH) is mainly involved in reactions leading to energy production, while nicotinamide adenine dinucleotide (NADPH) is the major electron acceptor for reductive biosyntheses. NADH absorbs at about 340 nm and fluoresces in the 420-490 nm regions and its fluorescence properties are associated with the nicotinamide group in the reduced state. Flavin adenine dinucleotide (FAD) is the other major electron acceptor. The oxidized form, FAD is fluorescent with the absorption maximum at 445 nm and the emission maximum at 525 nm. Several investigators have reported that when excited in the near-ultraviolet (near-UV) region, the reduced

AF near 500 nm in tumor may be due to the decrease in the oxidized forms of flavins and the relative amount of NADH in malignant tissues compared to normal surrounding tissues [87, 163].

### **Porphyrins**

Porphyrins are a ubiquitous class of naturally occurring molecules that are involved in various biological processes, such as transport of oxygen, catalysis and pigmentation. In early 1924, red fluorescence of necrotic tumors was noted in the study of rat sarcomas [164]. In 1960, porphyrins, which have an excitation maximum near 410 nm and emission maxima at 630 and 690 nm, are confirmed as the source of the red fluorescence [165]. A pathological accumulation of porphyrins can be attributed to some specific enzyme defects in the biosynthesis of heme. At present, neoplastic lesions can be diagnosed by administering the precursor 5-aminolevulinic acid (ALA) to monitor the change in amount of protoporphyrin IX [166]. In addition, porphyrin derivatives have been explored for the photodynamic therapy of tumors due to their ability to activate photodynamic processes and lead to the production of reactive species [167].

### **Vitamins**

Only a few vitamins attract attention for the study of fluorophores due to their especially spectral properties and functional metabolic engagement in tissue, such as FAD precursor vitamin B<sub>2</sub> (riboflavin), Vitamins B<sub>6</sub> and A. Vitamins B<sub>6</sub> (pyridoxine) and its metabolites exhibit an appreciable AF signal. It participates in numerous reactions, such as metabolism of amino acids, and lipids [109]. Pyridoxal 5'-phosphate (PLP), which is the main circulation form of vitamin B<sub>6</sub>, exhibits an excitation maximum ranging from 330-390 nm and an emission varying from 400-

500 nm. It is important in one-carbon metabolism and is critical for DNA synthesis and methylation, both of which are potential involved in colorectal carcinogenesis [168].

Based on the understanding of these endogenous fluorophores, AF imaging and spectroscopy have been applied for diagnosis of precancerous (adenomatous polyp) and cancer with high-detection sensitivities, especially in the UV or short visible (VIS) regions in the past two decades [47, 110, 131-132, 134]. However, NIR AF clinical applications have been limited not only by the difficulty in capturing inherently weak tissue NIR AF signals, but also by relatively few studies of endogenous fluorophores in the NIR region. In this chapter, we develop a biochemical modeling (i.e., non-negativity constrained least squares minimization (NNCLSM)) to study the biochemical constituents of different types of colonic tissues in the NIR region.

## **5.2 Experiments**

### **5.2.1 The partial least square model**

Partial least-squares modeling is a powerful new multivariate statistical tool that has been successfully applied to the quantitative analysis near-infrared data [169]. In this study, we develop a semi-quantitative biochemical analysis algorithm based on a prior biochemical knowledge using a linear combination (i.e., NNCLSM) of representative basis reference spectra acquired from biochemicals in colonic tissues [170]. This can be used to provide a ‘best fit’ of the spectral components or basis spectra found within the measured spectrum. The contribution of each basis spectrum to the *in vivo* colonic AF spectra was calculated by normalizing the

NNCLSM fit coefficients. The differences between the original AF spectra and the least-square fitting spectra presumably arise from the contribution of other molecules that are not included in the modeling. This explained simply below:

$$\min_c E(c) = \|c \cdot S - d\|_2^2, \text{ where } c \geq 0. \quad (5.1)$$

Where  $c$  is the matrix of concentrations or contribution coefficients to be predicted,  $S$  is the matrix of spectral components of biochemicals, and  $d$  is the measured spectrum of different types of colonic tissues. This can be used to provide a ‘best fit’ of the spectral components or basis spectra found within the measured spectrum by minimizing the difference  $E$  between  $c \cdot S$  and  $d$ . The contribution of each basis spectrum to the *in vivo* colonic AF spectra was calculated by normalizing the NNCLSM fit coefficients. The residual variations between the original AF spectra and the least-square fitting spectra presumably mainly arise from the contributions of other molecules that are not included in the modeling. The one advantage of NNCLSM modeling is that it is applicable even when there other molecules that contribute to the *in vivo* colonic spectra than those included in the model [170].

### **5.2.2 Tissue specimens spectra**

Under the guidance of wide-field endoscopic WLR images, *in vivo* NIR AF spectra of colonic tissue sites were acquired from 100 patients (57 male and 43 female, with a median age of 51 years) who underwent colonoscopy screening. In total 263 *in vivo* NIR AF spectra were used to run the biochemical fitting model, in which 116 spectra were from normal, 48 spectra were from hyperplastic polyp, 34 spectra were from precancer (adenomatous polyps), and 65 spectra were from colonic cancer tissues.

For the *ex vivo* colonic tissues, a total of 17 paired (i.e., normal *vs.* cancer)

colonic tissue specimens were collected from 17 patients (6 men and 11 women with a mean age of 58) who underwent partial colectomy or surgical resections with clinically suspicious lesions or histopathologically proven malignancies in the colon. All patients preoperatively signed an informed consent permitting the investigative use of the tissue. In total, 100 NIR AF spectra of resected colonic tissues were included for biochemical analysis, in which 68 spectra were from normal and 32 were from colon cancer tissue.

### **5.2.3 Basis reference biochemicals**

Nine basis reference AF spectra are obtained from the following biochemicals (Sigma-Aldrich, St. Louis, MO, USA) for colonic tissue biochemical fitting, i.e., Collagen I (C9879), Elastin (E1625), FAD (F6625),  $\beta$ -NADH (N4505), L-tryptophan (T0254), Hematoporphyrin (H5518), 4-pyridoxic acid (P9630) and pyridoxal 5'-phosphate (82870). They represent the main biochemical components within colonic cells and tissues [109, 159-160, 168, 171-174]. For instance, collagen I and elastin are representative of structural proteins in the extracellular matrix of the colonic wall [159]; 4-pyridoxic acid and pyridoxal 5'-phosphate represents the active form of vitamin B<sub>6</sub> [175];  $\beta$ -NADH is the co-enzymes in oxidation-reduction reactions [176]; L-tryptophan represents amino acid that body use to synthesize the protein [177]; Hematoporphyrin is an endogenous porphyrin formed by the hydrolysis of hemoglobin [167]; FAD is the enzymes typically involve in metabolism [110]. Besides these biochemicals, the deionized water was also included for spectral modeling since water is one of the main components in the body and helps conversion of mechanical energy into chemical energy for cell processes [178].

The spectra of these nine biochemicals were measured directly on their original form without any further purification or preprocessing using the instrumentation previously described in the Chapter 4 for the *in vivo* measurements of colonic polyps. For the powder biochemicals, they will be placed in the center of the glass slide covered by the aluminum foil. The diameter of the powder is big enough to cover the laser spot and the depth is thick enough for preventing the reflectance from aluminum foil. For the water, it is sorted in the cap covered by the aluminum foil and the depth of the water is around 3 cm. The water spectrum acquired is without NIR AF background signal from aluminum foil.

## **5.3 Results and Discussion**

### **5.3.1 *In vivo* colonic tissues**

Fig. 5.1 shows the *in vivo* mean autofluorescence spectra  $\pm 1$  standard error (SE) of normal (n=116), hyperplastic polyp (n=48), adenomatous polyp (n=34), and cancer (n=65) colonic tissues. All the spectra were acquired under the guidance of WLR endoscopic images during clinical colonoscopic examination. The significant differences of AF intensity were observed among different types of colonic tissue. Cancer tissues show much lower intensity compared to other three types of colonic tissues (normal, hyperplastic polyp, and adenomatous polyp). The adenomatous polyps with lower AF intensity can be distinguished from hyperplastic polyps and normal tissue as shown in Fig. 5.1. The intensity differences between hyperplastic polyp and normal tissue are not obvious. This is because hyperplastic polyp is still a type of noncancerous growth in the colon. These differences of fluorescence intensity among normal, hyperplastic polyp, adenomatous polyp, and cancer tissue

could be attributed to the changes of tissue optical properties in the colon as we discussed in Chapter 4. Due to hyperproliferation, the thickening of mucosa layer significantly attenuates of the excitation light penetration and also obscures the tissue AF emission from the polyp tissue and cancer tissues [84, 115].

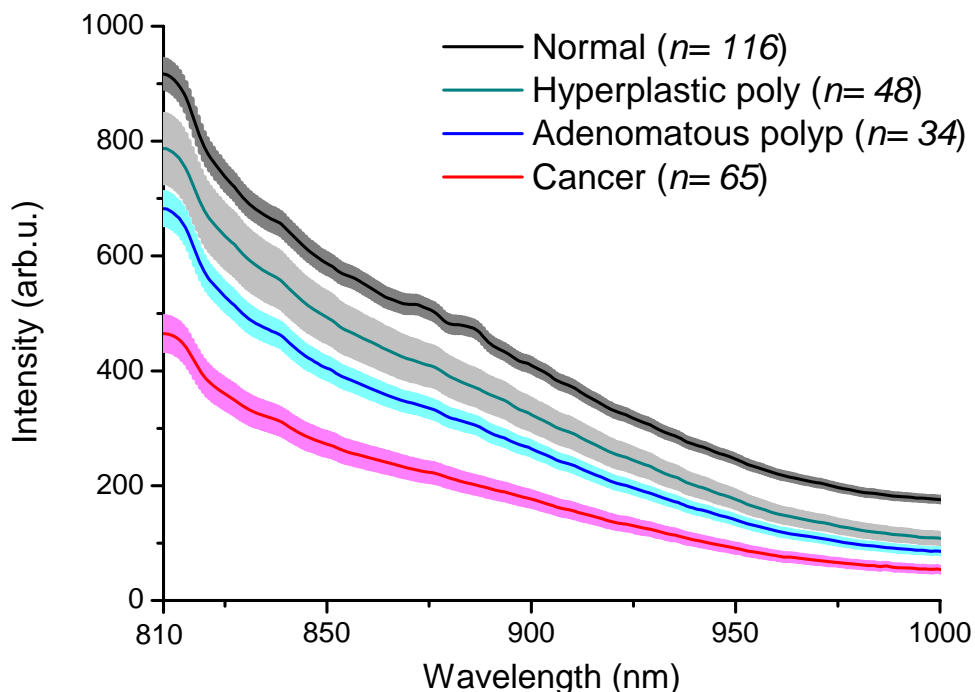


**Fig. 5.1** *In vivo* mean NIR AF spectra  $\pm 1$  standard error (SE) of normal ( $n=116$ ), hyperplastic polyps ( $n=48$ ), adenomatous polyps ( $n=34$ ), and cancer ( $n=65$ ) colonic tissue. The shaded areas in tissue AF spectra stand for the respective standard error. Note that *in vivo* NIR AF spectra of normal colonic tissue are vertically shifted for better visualization.

In addition, the changes in concentrations and distribution of endogenous fluorophores may also attribute to the differences in the NIR AF emission among different types of colonic tissues. However, the changes of endogenous fluorophores are complex and few studies have been done in the NIR region. Porphyrins are assumed as the major fluorophores to be responsible for the NIR AF in the tissues. We extend the previous study of endogenous fluorophores in the UV/VIS region [109] to NIR region and further explored the optical properties of endogenous fluorophores in the NIR region. By utilizing the NNCLSM model, the concentration

for endogenous fluorophores was calculated among different types of colonic tissues. The differences of concentration for different fluorophores among normal, hyperplastic polyp, adenomatous polyp, and cancer colonic tissues were investigated. To investigate the origin of tissue biochemicals, which are responsible for the differences among normal, hyperplastic polyp, adenomatous polyp, and cancer colonic tissue, we explore NNCSLM algorithm to reconstruct tissue AF spectrum of each type by a database of nine basis reference spectra. These nine biochemicals are the major tissue biochemical constituents present in the colon, including: collagen type I,  $\beta$ -NADH, FAD, L-tryptophan, Elastin, hematoporphyrin, 4-pyridoxic acid, pyridoxal 5'-phosphate and water. We measure the NIR spectra from these nine biochemicals with our integrated NIR AF spectroscopy system. Fig. 5.2 shows the NIR AF spectra of nine chemicals that are measured without any further processing. Because of special design of fiber probe, our integrated NIR AF spectroscopy can acquire both the AF and Raman signals. The prominent Raman peaks can be observed in our biochemical spectra, such as  $\beta$ -NADH, FAD, L-tryptophan. The spectra acquired from colonic tissue are also composite NIR AF and Raman spectra as we demonstrated in Chapter 4. Thus, these Raman peaks wouldn't induce artifacts for fitting.

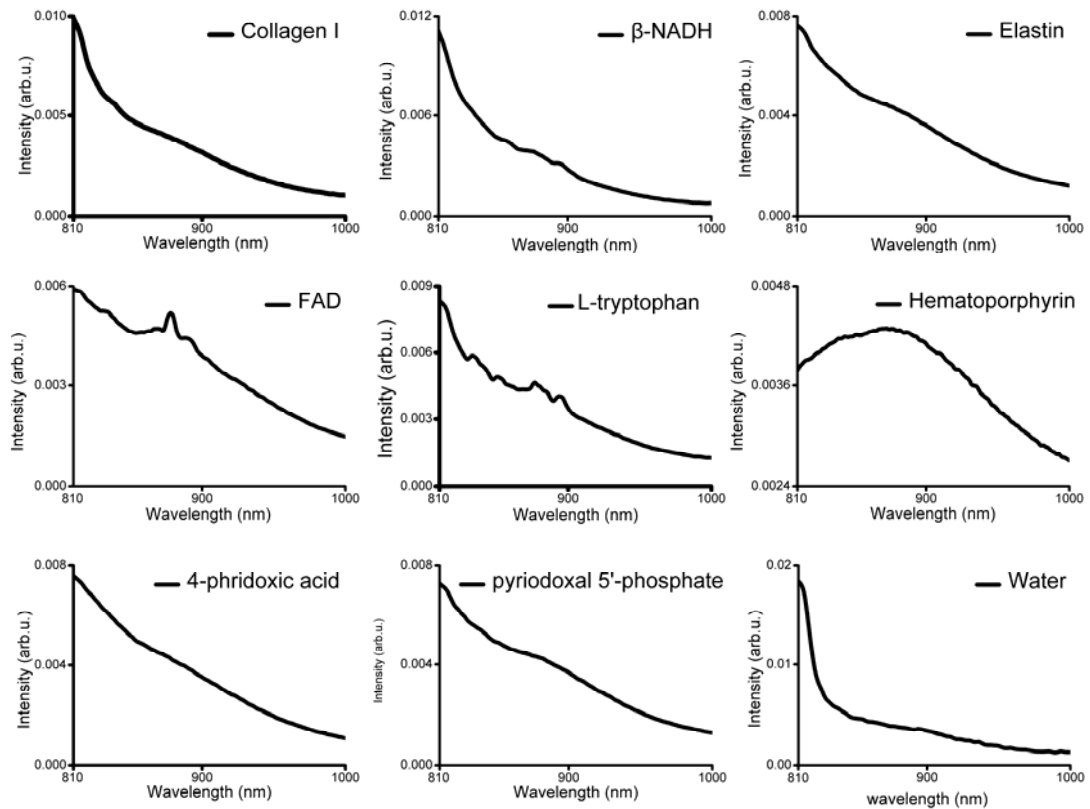


**Fig. 5.2** The nine basis reference AF spectra from collagen I, elastin,  $\beta$ -NADH, FAD, L-tryptophan, hematoporphyrin, 4-pyridoxic acid, pyridoxal 5'-phosphate and water are used for biochemical modeling of the colonic tissue.

Based on the equation 5.1, NIR AF spectra measured from nine biochemicals are used as basis reference to fit 263 colonic tissues spectra individually. Fig. 5.3 shows the representative comparison of the reconstructed spectra to the *in vivo* AF spectra measured from normal, hyperplastic polyp, adenomatous polyp, and cancer colonic tissue, respectively. It is evident that acceptable fit-residuals between the reconstructed AF spectra and the measured AF spectra can be achieved (residual variations: (a) normal:  $\pm 2.8E-4$ ; (b) hyperplastic polyp:  $\pm 3.07E-4$  (c) adenomatous polyp:  $\pm 2.9E-4$ ; (d) cancer:  $\pm 2.18E-4$ ), substantiating the implications of the chosen biochemicals in colonic tissue. The fit coefficients which are the relative concentration for nine reference biochemicals can be obtained for different types of colonic tissues.

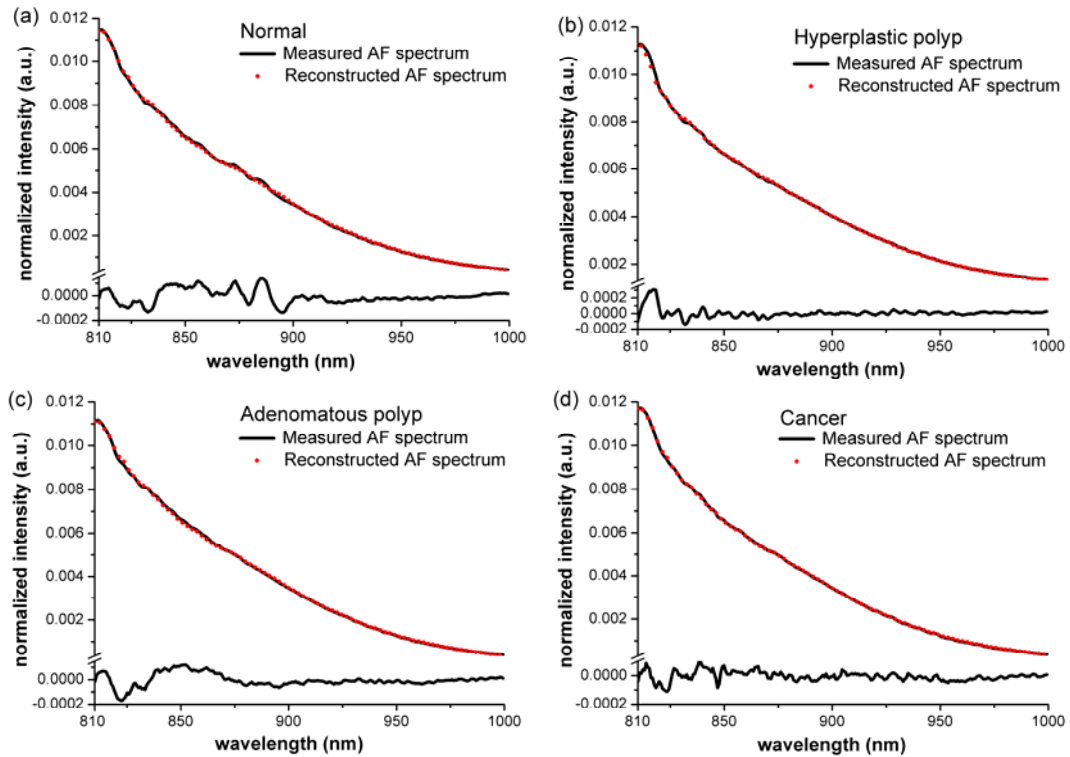


**Fig. 5.3** Comparison of *in vivo* colonic AF spectra measured with the reconstructed tissue AF spectra through the employment of the nine basis reference AF spectra: (a) normal, (b) hyperplastic polyp, (c) adenomatous polyp, and (d) cancer colonic tissues. Residuals (measured spectrum minus reconstructed spectrum) are also shown in each plot.

Fig. 5.4 shows the mean fit coefficients for each of the reference biochemicals in normal, hyperplastic polyp, adenomatous polyp, and cancer tissue. One-way ANOVA [135] illustrates that the adenomatous polyp and cancer colonic tissues are associated with lower fit coefficient belonging to collagen ( $p=7.33E-4$ ),  $\beta$ -NADH ( $p=5.44E-15$ ), FAD ( $p=7.88E-6$ ), L-tryptophan ( $p=5.207E-14$ ), elastin ( $p=1.62E-4$ ), pyridoxal 5'-phosphate ( $p=4.9E-2$ ), while higher fit coefficients belonging to hematophphrin ( $p=4.81E-4$ ), 4-pyridoxic acid ( $p=3.9E-4$ ) and water ( $p=4.46E-13$ ), as compared to the normal and hyperplastic polyp tissues. Overall, there are significant changes (i.e., increase or decrease) in nine tissue biochemical constituents related to collagen type I,  $\beta$ -NADH, FAD, L-tryphophan, elastin, hematoporphyrin, 4-pyridoxic acid, pyridoxal 5'-phosphate and water among

different types of colonic tissues. The above results demonstrate that AF spectroscopy is able to directly assess the biochemical changes of colonic tissue associated with cancer transformation in real-time.

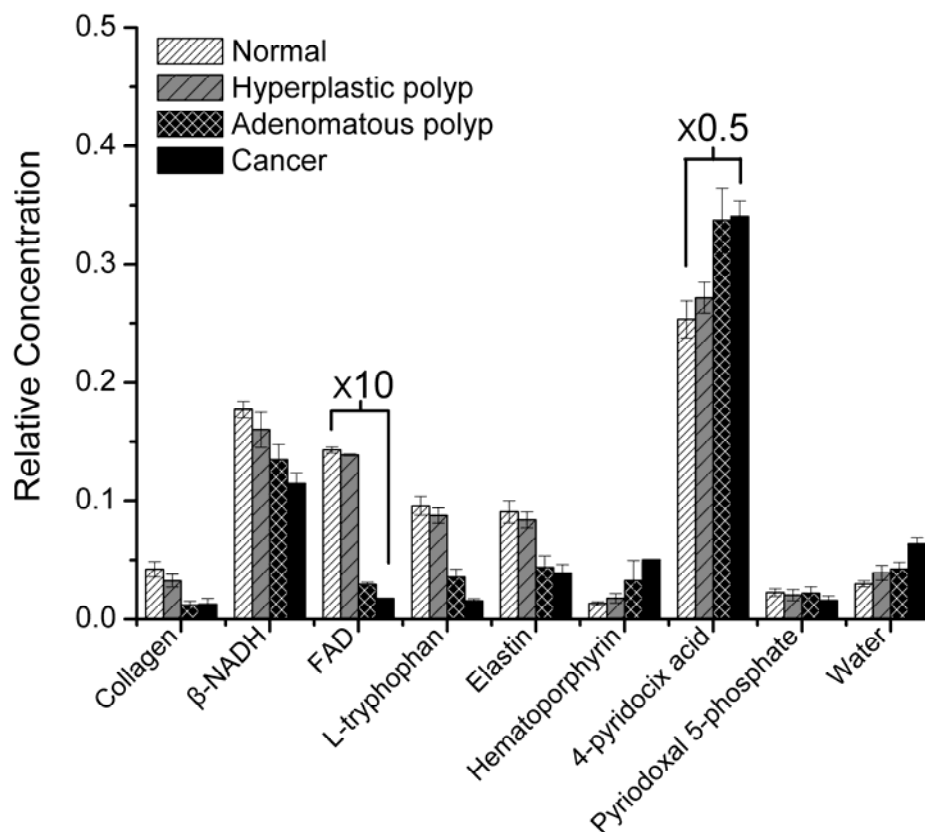


**Fig. 5.4** Histograms displaying the average compositions of the tissues diagnosed as normal, hyperplastic polyp, adenomatous polyp, and cancer. The one standard error (SE) confidence intervals as shown for each model component. All nine biochemicals are for discriminating four different type of colonic tissues ( $p < 0.05$ ); the relative concentration of 4-pyridoxic acid times 0.5 and FAD times 10.

The modeling showed that collagen and elastin AF signals, which represent the structural proteins in the extracellular matrix of the colonic wall, are significantly lower for precancer and cancer tissue compared to the normal tissue. This could be attributed to thickening mucosa layer or replacement of the submucosa by cancerous cells and a decrease in the fluorescence emission of submucosa collagen and elastin will ensue [159]. These findings are in agreement with collagenases studies which usually associate degrading the collagen cross links and decrease in collagen

fluorescence during significant tissue architectural changes [171]. Additionally, significant reduction in the  $\beta$ -NADH and FAD autofluorescence signal of precancer and cancer colonic tissue were also observed. This phenomenon strongly reflects changes in the metabolic rate in cancer changes since the nicotinamide adenine dinucleotide and flavins play an integral role in cellular metabolism. The ratio of the fluorescence of FAD to the sum of the fluorescences of FAD and NADH, which is described 'redox ratio', typically decreases in cancer, is sensitive to changes in the metabolic rate and vascular oxygen supply [179]. On the other hand, AF signals from hematoporphyrin which is an endogenous porphyrin formed by the acid hydrolysis of hemoglobin has been found to be higher for the precancer and cancer colonic tissue than normal tissue. The accumulation of hematoporphyrin in various types of cancer was discovered and exploited since 1950s [153] and it has been established for photodetection or photodynamic therapy of colon cancer since hematoporphyrin fluorescence was higher in cancer than in surrounding mucosa in specimens [172]. Significant reduction in the L-tryptophan AF signal of precancer and cancerous colonic tissue was also observed, suggesting that a mechanism by which cancer-related immune stimulation affected the tryptophan depletion [180]. On the top of these, vitamin B<sub>6</sub>, whose main circulation form is pyridoxal 5'-phosphate (PLP) and major excretion product is 4-pyridoxic acid, is important in one-carbon metabolism, which is critical for DNA synthesis and DNA methylation, both of which are potential involved in colorectal carcinogenesis [181]. Our observations that lower pyridoxal 5'-phosphate and higher 4-pyridoxic acid in precancer and cancerous colonic is agreement with vitamin B<sub>6</sub> deficiency study which usually associate risk for colon cancer and colon adenoma [160, 168, 182].

To investigate potential of fitting coefficients for generating diagnostic algorithms for effective classification of colonic normal, hyperplastic polyp, precancer (adenomatous polyp), and cancer, we employ linear discriminant analysis (LDA). LDA determines the discriminant function that maximizes the variances in the data between the groups while minimizing the variances between members of the same group. All nine significant biochemicals were loaded into a LDA model. Table 5.1 summarized the diagnostic indices for classifying the four different types of colonic tissues (normal, hyperplastic poly, adenomatous polyp, and cancer). Cancer can be 100% correctly classified from normal, hyperplastic polyp and adenomatous polyp. 88.8% of normal colonic tissue was identified based on the relative concentration of nine biochemicals, but 12 normal spectra were misclassified as hyperplastic polyp and 1 normal spectrum was misclassified as adenomatous polyps. For the adenomatous polyps, 73.4% spectra were correctly identified. However, the diagnostic sensitivity for the hyperplastic polyp was only 47.9%, 24 of 48 spectra were classified as normal. This result is not surprising. Since the hyperplastic polyps are noncancerous and treated as benign in clinic. Therefore, the biochemicals are not sufficient to distinguish the changes of endogenous fluorophores between normal and hyperplastic polyp in the colon. The biochemicals based diagnostic algorithm yielded overall accuracies of 84.4%, 84%, 95.8%, and 100% respectively, for classification of colonic normal, hyperplastic polyp, adenomatous polyps, and cancer tissues based on the concentration of nine biochemicals that are selected for the modeling.

**Table 5.1** Classification results of nine biochemicals for the four colonic tissue groups using LDA algorithms.

| Tissue type        | Biochemical prediction |                    |                   |        |       |
|--------------------|------------------------|--------------------|-------------------|--------|-------|
|                    | Normal                 | Hyperplastic polyp | Adenomatous polyp | Cancer | Total |
| Normal             | 103                    | 12                 | 1                 | 0      | 116   |
| Hyperplastic polyp | 24                     | 23                 | 1                 | 0      | 48    |
| Adenomatous polyp  | 4                      | 5                  | 25                | 0      | 34    |
| Cancer             | 0                      | 0                  | 0                 | 65     | 65    |
| Sensitivity        | 88.8%                  | 47.9%              | 73.4%             | 100%   |       |
| Specificity        | 81%                    | 92.1%              | 99.1%             | 100%   |       |
| Accuracy           | 84.4%                  | 84%                | 95.8%             | 100%   |       |

### 5.3.2 Ex vivo colonic paired specimens

Based on the successful application of biochemical model fitting on the *in vivo* colonic tissues, we further explore the biochemicals analysis on the resected colonic paired tissues (normal *vs.* cancer). We run the same NNCSLM modeling to estimate the concentration of nine reference biochemicals for the ex vivo colonic tissues and employ LDA algorithm to classify the cancer from normal colonic tissue. We compare the trends in biochemical changes between *in vivo* and ex vivo colonic tissues.

Fig. 5.5 is the mean AF spectra  $\pm 1$  standard error (SE) of normal (n=68) and cancer (n=32) colonic tissues. We acquired spectra from paired tissue after surgical resections without any chemical processing and frozen. The cancer tissue shows the significant lower intensity compared to normal ones. We cannot directly compare the intensity for these two different datasets (*i.e.*, *in vivo vs.* ex vivo) since the spectra

are not acquired from the same patients. But we find that the SE for the resected colonic tissues have larger variations for normal and cancer tissues than those of *in vivo* tissues, although ex vivo colonic tissues has smaller data size (100 spectra) than *in vivo* ones (263 spectra). This is because the molecular spectroscopic properties are highly dependent on environmental effects. After being resected from living environment, ex vivo specimens did undergo some changes and thus, the concentration and distribution of endogenous fluorophores are different from *in vivo* condition consequently. In this section, we employ the biochemical modeling to estimate the concentration of endogenous fluorophores for the ex vivo colonic tissues and compare the difference between *in vivo* and ex vivo colonic specimens.

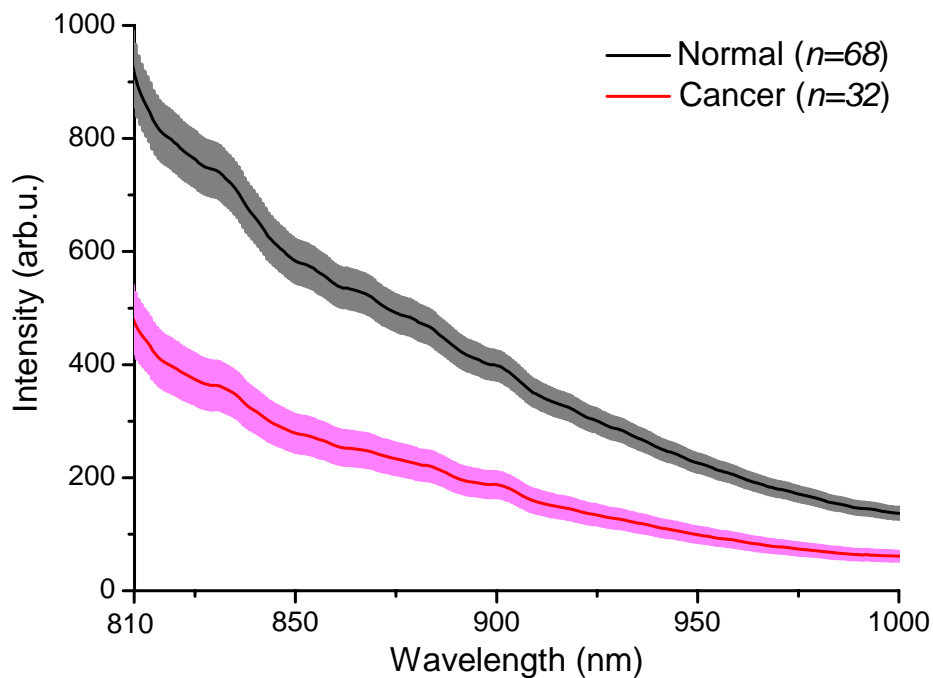


**Fig. 5.5** Ex vivo mean NIR AF spectra  $\pm 1$  standard error (SE) of normal ( $n=68$ ) and cancer ( $n=32$ ) colonic tissue. The shaded areas in tissue AF spectra stand for the respective standard error.

The same nine references biochemicals as shown in Fig. 5.2 (i.e., collagen type I,  $\beta$ -NADH, FAD, L-tryptophan, Elastin, hematoporphyrin, 4-pyridoxic acid, pyridoxal 5'-phosphate and water) were used to fit the measured spectra from

resected colonic tissues by using NNCSLM model individually and the relative concentration for nine reference biochemicals can be obtained. Fig. 5.6 shows the representative fitting results for normal and cancer tissue, respectively. Small fit-residuals (of <5%) between the reconstructed AF spectra and the measured AF spectra can be achieved.

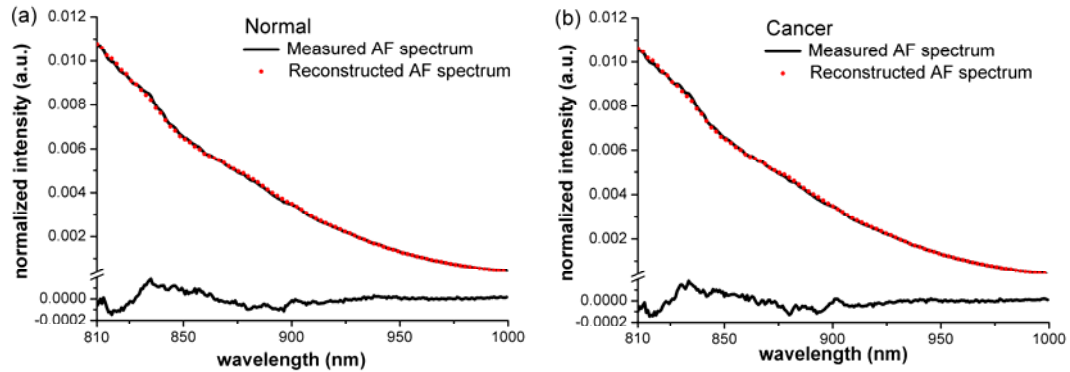


**Fig. 5.6** Comparison of ex vivo colonic AF spectra measured with the reconstructed tissue AF spectra through the employment of the nine basis reference AF spectra: (a) normal and (b) cancer colonic tissues. Residuals (measured spectrum minus reconstructed spectrum) are also shown in each plot.

Fig. 5.7 shows the mean fit coefficients for each of the reference biochemicals in ex vivo normal and cancer tissue. Student's *t*-test illustrates that cancer colonic tissues are associated with lower fit coefficient belonging to collagen ( $p=5.31E-3$ ),  $\beta$ -NADH ( $p=5.28E-6$ ), FAD ( $p=3.34E-5$ ), L-tryptophan ( $p=2.89E-2$ ), elastin ( $p=2.82E-5$ ), pyridoxal 5'-phosphate ( $p=3.87E-4$ ), and water ( $p=0.33$ ) while higher fit coefficients belonging to hematoporphyrin ( $p=3.84E-3$ ), 4-pyridoxic acid ( $p=7.46E-3$ ), as compared to normal tissues. Compared with the fitting results for *in vivo* colonic tissue, the relative concentration for each biochemical changed accordingly. For instance, the decreased concentrations of  $\beta$ -NADH, FAD, L-tryptophan are probability due to the changed metabolic activities that are affected by resection. However, the trend in biochemical changes between normal and cancer

colonic tissue are the same for *ex vivo* and *in vivo* colonic tissues, except water. For the *ex vivo* condition, normal tissues have the higher water concentration than cancer colonic tissue. The trend in the change of water concentration is reverse for *in vivo* condition. This might be attributed to the artifacts induced by storage and measurements of *ex vivo* colonic tissues. For example, the specimens are stored in the saline solution after resection and measured with water in order to keep the moisture.

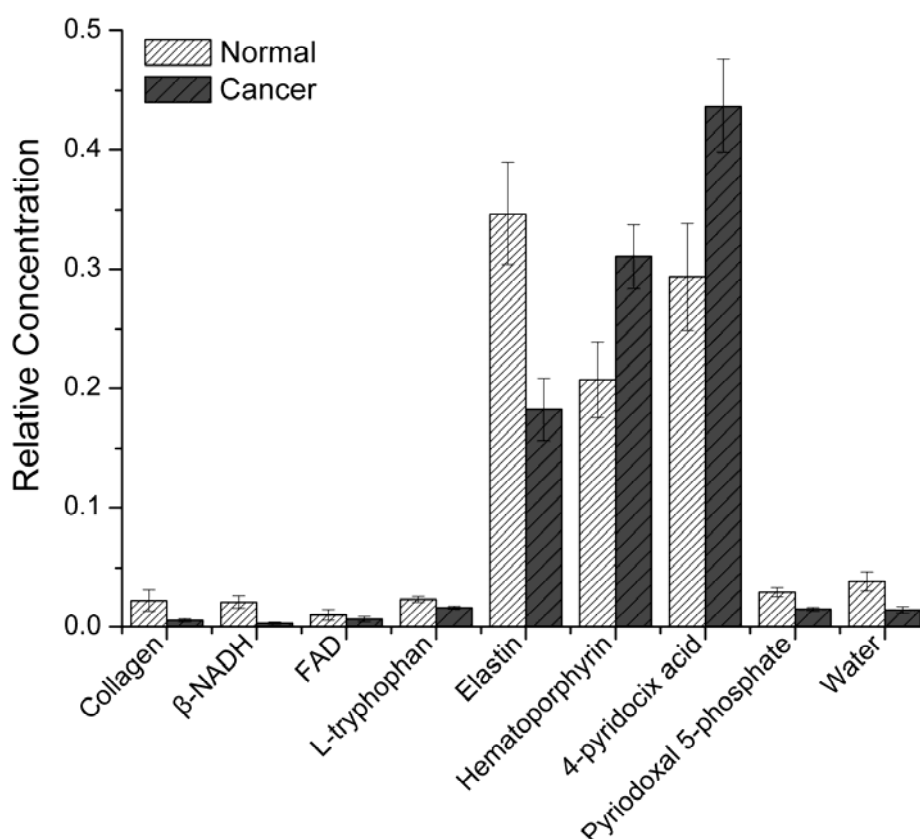


**Fig. 5.7** Histograms displaying the average compositions of the tissues diagnosed as normal and cancer. The one standard error (SE) confidence intervals as shown for each model component. All biochemicals are significant for discriminating two different type of colonic tissues ( $p < 0.05$ ).

Nine significant biochemicals are loaded into the LDA model to develop effective diagnostic algorithms for diagnosis of colon cancer. Fig. 5.8 shows the classification results of NIR AF spectra of *ex vivo* paired normal and cancer colonic

tissue using LDA together with the leave-one spectra-out, cross validation techniques. Based on the relative concentration of biochemicals, the LDA algorithm provides a diagnostic sensitivity 84.3% (27/32) and specificity of 88.2% (60/68) for distinguish cancer from normal colonic tissue. We further evaluate the performance of the LDA diagnostic algorithm derived from nine significant biochemicals for ex vivo colonic NIR AF datasets. Fig. 5.9 shows the receiver operation characteristic (ROC) curve that is generated from the scatter plot in Fig. 5.8 at different threshold levels. The ROC curve displays the discrimination results using LDA diagnostic algorithms together with the leave-one spectrum-out, cross validation method. The integration area under the ROC curve is 0.945.

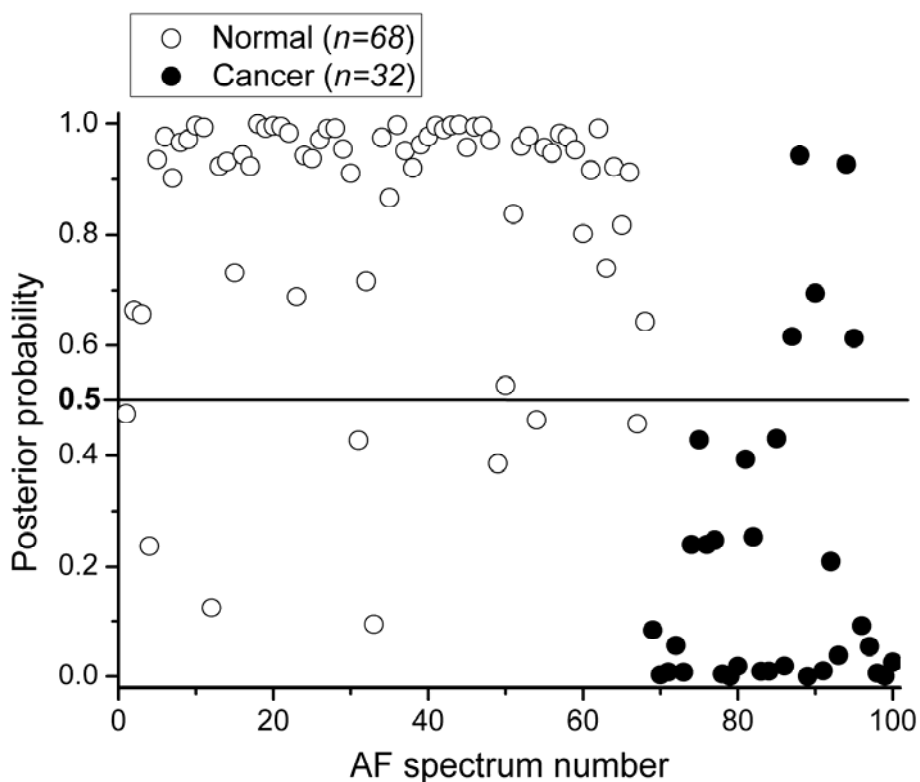


**Fig. 5.8** Scatter plot of the posterior probabilities belongs to normal and cancer colonic tissue using the LDA algorithms. The separate line yields a diagnostic sensitivity of 84.3% (27/32) and 88.2% (60/68) for distinguishing cancer from normal colon tissues.

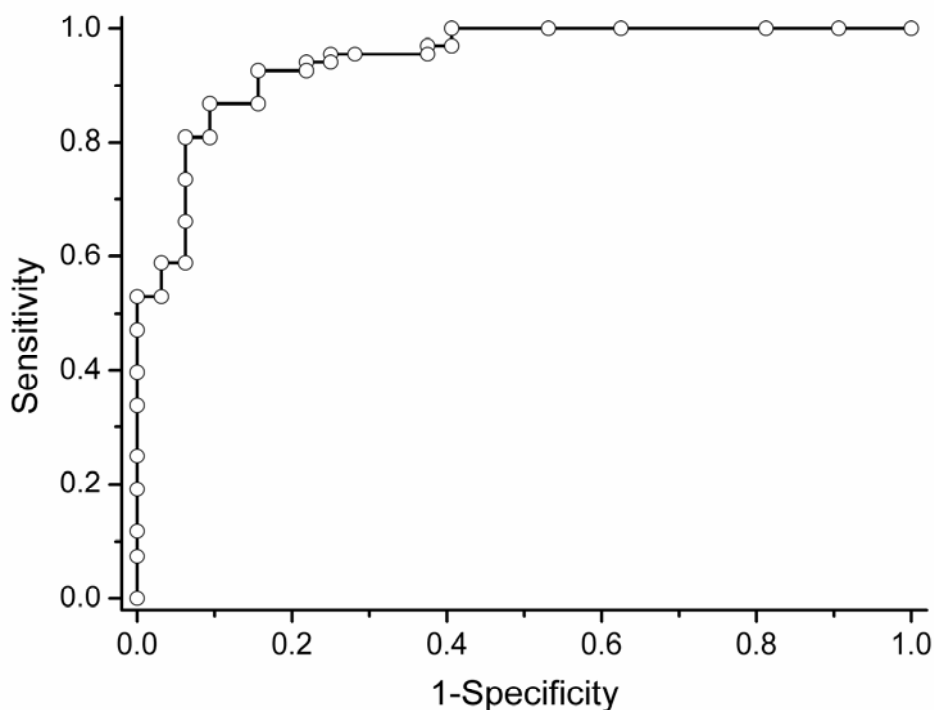


**Fig. 5.9** Receiver operating characteristic (ROC) curve of discrimination results of normal and cancer colonic tissue using the LDA algorithm based on relative concentration for nine biochemicals. The integration areas under the ROC curves are 94.5.

## 5.4 Conclusion

Based on the high quality NIR AF spectra acquired from different types of colonic tissues, The NNCSLM fitting model was implemented to estimate the relative concentration of biochemicals for *ex vivo* normal and cancerous colonic tissue, and *in vivo* normal, hyperplastic polyp, adenomatous polyp, and cancerous colonic tissue. The AF spectral biochemical analysis shows significant differences among different types of colonic tissues and provides new insights into biochemical origins of NIR AF for diagnosis and characterization of colonic precancer and cancer. In this chapter, we investigate for first time (to our knowledge) the potential endogenous fluorophores responsible for the colonic NIR AF spectrum and explore the changes of endogenous fluorophores associated with cancer transformation. We further

employ LDA diagnostic algorithms to distinguish precancer (adenomatous polyp) and cancer from normal tissue. The good classification results demonstrate the potential of NIR AF spectroscopy to be a technique to be a clinical complement to conventional WLR endoscopy for improving *in vivo* detection and diagnosis of colonic precancer and cancer at molecular level.

One noted that the NNCLSM modeling of NIR AF spectra only served as a semi-quantitative estimation of biochemical compositions of colonic tissue and the results obtained should be interpreted with caution. This is because: (i) the NNCLSM modeling only includes the most essential endogenous fluorophores that are known to be associated with the structural matrix of tissues or involved in cellular metabolic processes; (ii) the *in vitro* biochemical conformations may not truly reflect the *in vivo* conditions; (iii) the spectral reconstruction does not take into account for the effects of tissue optical properties (e.g., tissue absorption and scattering), the nonuniform fluorophore distribution in tissue and, in particular, the depth-associated variations of NIR AF signals. To better understand the relationships between the tissue morphologic/biochemical changes and the tissue NIR AF spectra for further improving tissue diagnosis and classification, confocal NIR AF microspectroscopy should be explored on the colonic tissue *in vivo* and *in vitro*, by measuring the complete NIR AF spectra of specific tissue microstructures, or alternatively by mapping the distributions of some specific NIR AF peaks or principal components within a tissue, or even mapping the biochemical distributions at different tissue depths for association with neoplastic transformation in colonic tissue. In addition, how the absorbers (e.g., hemoglobin) in tissue attenuate the NIR excitation light, and thus attenuating tissue NIR AF emission and modulating NIR

AF spectral shape should be studied further. Thus, a more complete NNCLSM biochemical modeling integrated with tissue optical properties (e.g., absorption and scattering coefficients, anisotropy, tissue thickness, etc.), and light propagation in multilayer tissue model with Monte Carlo simulation warrants further investigation. Nevertheless, within these limits, we have shown that *in vivo* estimation of colonic intrinsic biochemicals compositions can be largely realized with highly representative biochemicals responsible for tissue NIR AF emission, and the fitting results correlate well with histopathological findings. Therefore, the distinctive differences in NIR AF spectra among benign, precancer, and cancer colonic tissues confirm the potential role of endoscopic image-guided NIR AF spectroscopy for improving *in vivo* diagnosis of colonic precancer and cancer during clinical colonoscopic screenings.

# **Chapter 6 Integrated Visible and Near-infrared Diffuse Reflectance Spectroscopy for Improving Colonic Cancer Diagnosis**

## **6.1 Introduction of Diffuse Reflectance Spectroscopy**

In recent years, a range of spectroscopies have been investigated for distinguishing malignant tissue in real time to minimize the artifacts by sampling errors, such as elastic-scattering [183-184], fluorescence [115, 154, 185], and Raman spectroscopies [114, 126, 146, 151]. Diffuse reflectance (DR) spectroscopy is one of the simplest elastic-scattering spectroscopic techniques for studying biological tissue and it is the technique that measures the diffuse reflection from the tissue surface to determine absorption and scattering properties of sampled tissues [186]. DR spectroscopy, which is able to noninvasively and quantitatively determine the optical absorption and scattering properties of a turbid medium, can provide pathologically relevant information about living tissues, including tissue morphology, as well as the size, shape and, density of cells [187]. The changes of tissue optical property associated with the malignant transformation directly affect tissues diffuse reflectance. For instance, during the progression from normal to neoplastic, an increase in blood absorption below 600 nm, which is due to the development of neo-vascularization inherent to tumor tissue, would be the most obvious change within a diffuse reflectance spectrum. Hence, DR spectroscopy can help to track architectural and morphological changes associated with malignant transformation in tissue [188].

Currently, DR spectroscopy has been widely exploited in several applications

related to diagnosis, prognosis, and assessing treatment response of cancers in different organs [189-195]. These studies only focused on the visible (VIS) range. In VIS range, the absorption coefficient of tissue is assumed to be a linear combination of absorbers specific to the tissue type sampled such as hemoglobin in blood, beta-carotene, and melanin [196]. However, a pronounced water absorption peak, which appears in the near-infrared (NIR) range around 970 nm [197], has been disregarded in these VIS DR studies. Water, which is one of the main components in the tissue and cells, has also been used to probe cancers [198]. By measuring the broadband DR, additional information regarding the disposition of tissue water can be obtained to improve the detection and classification accuracy of the suspected lesions [199].

In this study, we extend the previous VIS DR work to a wide range of wavelength including the NIR domain (with the spectral ranges of 400-1000 nm). A rapid-acquisition DR spectroscopy system developed in house was used to acquire both VIS and NIR DR spectra at the same time from colonic normal and cancer tissue. Principal component analysis (PCA) and linear discriminant analysis (LDA) were then used to test and compare the performance of integrated VIS and NIR (VIS-NIR), VIS, and NIR DR spectroscopy for colonic tissue classification.

## **6.2 Diffuse Reflectance Spectroscopy System**

The system comprised a tungsten halogen light source (HL-2000, Ocean Optics Inc., Dunedin, FL), a bifurcated fiber (R400-7-VIS/NIR, Ocean Optics Inc., Dunedin, FL) for delivery and collection, and spectrometers (QE65000-FL, FWHM=6nm, Ocean Optics, Dunedin, FL). The white light source is coupled into a bifurcated fiber to illuminate the tissue directly. The fiber probe (2 m in length; 6.33 mm in outer

diameter), consists of 6 delivery fibers (core diameter of 400  $\mu\text{m}$ ) surrounding the central light collection fiber (core diameter of 400  $\mu\text{m}$ , NA=0.22). Tissue diffuse reflectance signals collected by the bifurcated fiber and were fed into a scientific-grade spectrometer. The tissue DR spectra were displayed on the computer screen in real time and could be saved for further analysis. The system acquired spectra over the wavelength range of 400-1000 nm and each tissue DR spectra were acquired in 8 ms.

### **6.3 Results and Discussion**

106 integrated VIS-NIR DR spectra of colonic tissue were acquired from 7 paired colonic tissues, in which 48 were from cancer tissues and 58 were from normal tissues. Fig. 6.1 shows the mean DR spectra  $\pm 1$  standard error (SE) of normal ( $n=58$ ) and cancer ( $n=48$ ) colonic tissues in the colon. The paired Student's *t*-test on the mean differences of spectral intensities point by point in the ranges 400-1000 nm between normal and cancer tissue revealed that the integrated VIS-NIR DR intensity differences between normal and cancer tissues were significant with a  $p < 0.05$ . The ratios of DR spectra of normal and cancer tissues are not flat horizontal lines but decrease from 400 to 500 nm and then have two obvious peaks near 540 nm, 580 nm and finally increase till 1000 nm (data not shown). The spectral shape differences from 400 to 1000 nm are apparent for DR spectra between colonic normal and cancer tissues. Three pronounced valleys near 420 nm, 540 nm, and 580 nm, which are attributed to strong oxy- and deoxy-hemoglobin absorption [196], can be clearly identified for both normal and cancer colonic tissues. The two hemoglobin absorption valleys around 540 nm and 580 are larger and more obvious on the cancer tissue spectral curve than on the normal one. The colonic normal tissues

possessed absorption peaks around 420 nm which were slightly red-shifted compared to the corresponding peak within the mean cancer spectra. In the NIR range, we also observe variations between normal and cancer tissues. The water absorption valley around 970 nm [200] is more obvious on the cancer spectral curve than on the normal one. All of these line-shape differences were therefore explored in greater details for tissue classification through principal components analysis (PCA) and linear discriminant analysis (LDA).

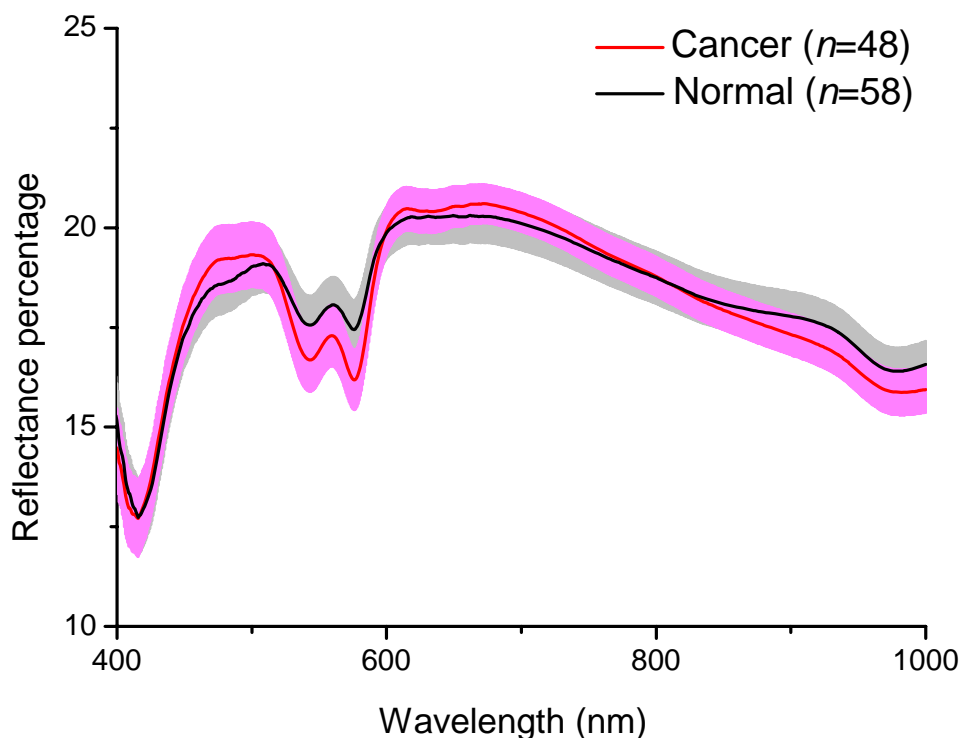


**Fig. 6.1** The mean integrated visible and near-infrared (VIS-NIR) diffuse reflectance (DR) spectra  $\pm 1$  standard error (SE) of normal ( $n=58$ ) and cancer ( $n=48$ ) colonic tissue. The shaded areas in tissue DR spectra stand for the respective standard error.

The differences of DR spectra between colonic normal and cancer tissue could be attributed to the changes of tissue optical properties in the colon [84], for example the higher absorption may reflect the increase in the percentage of hemoglobin and water in colonic cancer tissues associated with dysplastic transformation. The colonic tissue DR spectra are dominated by the characteristic

hemoglobin and water absorption bands, near 420 nm, 540 nm, 580 nm and 1000 nm. There are distinctive DR spectral differences between normal and cancer tissues in the whole spectral region (400-1000 nm). To understand and interpret these spectral differences between normal and cancer tissues, it is important to know where the spectral signals come from within the tissue. In the VIS region of the DR spectra, Hemoglobin, which is present in vascularized tissues, has two primary bands of absorption: Soret (peak=420 nm), and Q-bands (peaks=542 and 577 nm) [55]. Hemoglobin is considered the most important absorber for differentiating normal from malignant tissues [185]. The intrinsic absorption spectral fingerprint of oxyhemoglobin (HbO<sub>2</sub>) and deoxyhemoglobin (Hb) at the VIS wavelength range allows optical methods to quantitative tissue angiogenesis and hypoxia noninvasively [201]. Our results showed that colonic cancer tissue has higher absorption than normal tissues near 540 nm, 580 nm. These findings are in agreement with previous reports that demonstrate an increase in blood absorption during colon carcinogenesis from normal to malignant tumors [201]. The significant increase in the blood volume fraction of the malignant lesions could be attributed to the increased microvasculature of malignant tumors and accordingly the increased blood content and poor oxygenation [202]. The observation of the change of 420 nm absorption band position between normal and cancer colonic tissue are consistent with reports that normal colonic tissue possessed absorption peaks at 430 nm which were red-shifted compared to the adenomatous spectra with a band at 415 nm [195]. Moreover, in the NIR region we also observe that colon cancer also has higher water absorption in the NIR around 970 nm compared to normal tissues. Water have a pronounced absorption peak in the NIR around 970 nm [197], that is due to the

combination of the first harmonic of the O-H symmetric stretch vibration and the fundamental anti-symmetric stretch vibration from hydrogen bound O-H [200]. The characteristics of this peak (970 nm) are sensitive indicator of the local environment of water molecules [199]. This phenomenon strongly reflects the changes of the metabolic rate in cancer since water provides the conversion of mechanical energy developed by contractile proteins into the chemical energy useful in cell process [178]. Our observations that higher water absorption in colonic cancer is in agreement with our studies of biochemical modeling of colon tissues, which shows the increased water content of colon tissue compared to the benign tissues [154]. In addition, the changes of tissue microstructure scattering properties (e.g. nucleus size) could also contribute to the significant differences of DR spectra between normal and colonic cancer tissues [203]. However, it still poorly understood due to the complex nature of the tissue scattering process and it warrants further investigation.

We have also employed the multivariate statistical technique [i.e., PCA and LDA] by utilizing the integrated VIS-NIR DR spectra (400-1000 nm) to determine the most diagnostically significant DR features for colonic tissue classification. Fig. 6.2 shows the ten principal components (PCs) loadings calculated from PCA on the integrated VIS-NIR DR spectra (400-1000 nm). Some PC features (Fig. 6.2) with peaks and troughs at positions similar to those of absorption of hemoglobin and water in tissue DR spectra (Fig. 6.1). The first PC accounts for the largest variance (93.14%), whereas successive PCs describe features that contribute progressively smaller variances. The unpaired, two sided Student's test on the obtained principal components (PCs) shows that only seven PCs (PC3, PC4, PC5, PC7, PC8, PC9, and PC10) that were diagnostically significant ( $p < 0.05$ ) for discriminating cancer from

normal colonic tissue. Then all these seven significant PCs were loaded into LDA model to develop effective diagnostic for colonic tissue diagnosis.

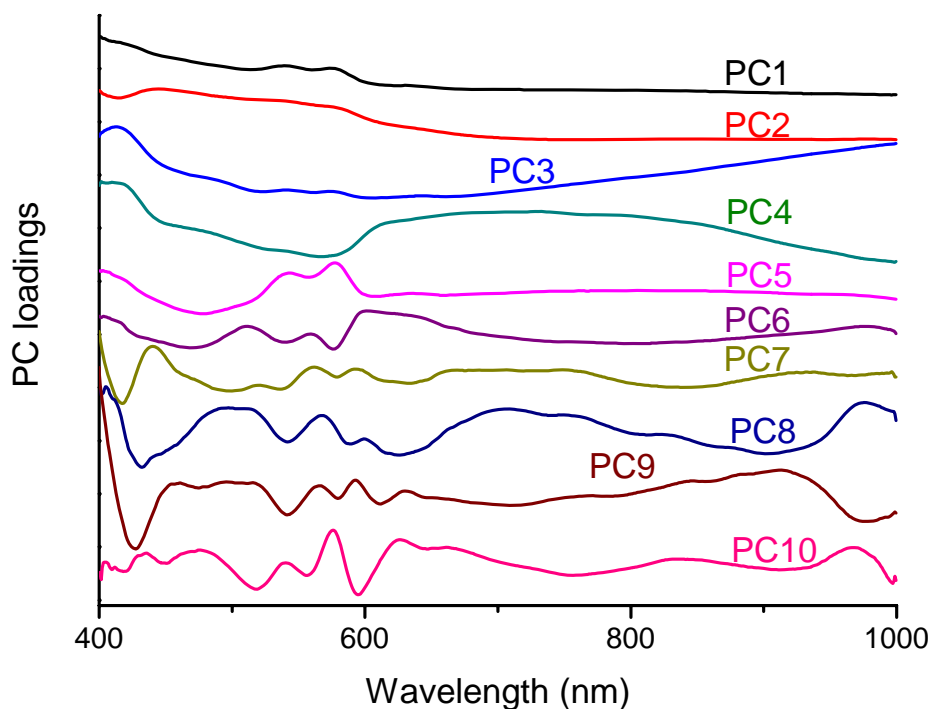


**Fig. 6.2** The ten principal components (PCs) accounting more than 99% of the total variance calculated from the integrated VIS/NIR DR spectra (PC1~93.14%, PC2~4.64%, PC3~1.38%, PC4~0.48%, PC5~0.23%, PC6~0.06%, PC7~0.02%, PC8~0.014%, PC9~0.01%, PC10~0.01%).

To compare the diagnostic capability of integrated VIS-NIR DR, VIS, and NIR DR spectra, we employ the PCA-LDA-based spectral classification with the leave-one spectrum-out, cross validation method on these three data set respectively. Fig. 6.3 shows the posterior probabilities of belonging to the normal and cancer groups as calculated for (a) integrated VIS-NIR (400-1000 nm), (b) VIS (400-700 nm), and (c) NIR (700-1000 nm) DR spectra. The classification results showed that 87.5% (42/48), 85.4% (41/48), and 83.3% (40/48) of cancer tissues were correctly classified (diagnostic sensitivity) using the three spectral data sets (*i.e.* integrated VIS-NIR, VIS, and NIR DR spectra), respectively. The diagnostic specificities were 94.8%, 81.03%, and 74.1%, and overall diagnostic accuracies were 91.5%, 83.02%,

and 78.3% for the integrated VIS-NIR, VIS, and NIR DR spectra, respectively.

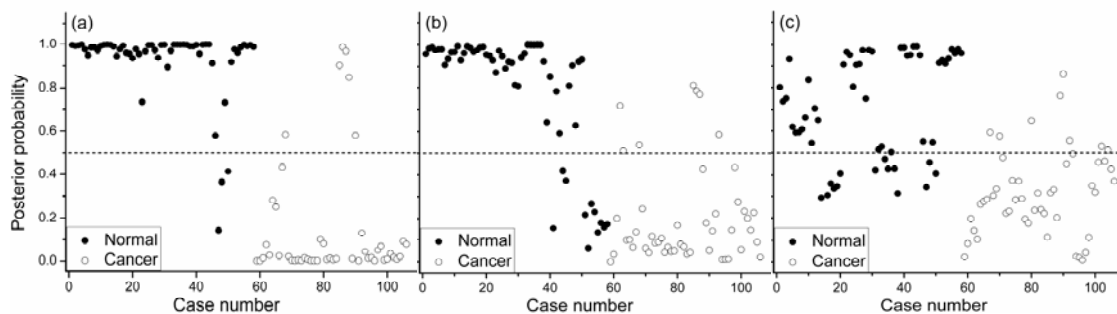


**Fig. 6.3** Scatter plot of the posterior probability belonging to the normal and cancer colonic tissue calculated from the data sets of (a) integrated VIS/NIR, (b) VIS, and (c) NIR, respectively, using the PCA-LDA algorithms, together with the leave-one tissue site-out, cross validation method with three different spectral spaces.

To further evaluate and compare the performance of the PCA-LDA based diagnostic algorithms derived from three data sets for tissue classification, ROC curve (Fig. 6.4) were generated from the scatter plot in Fig. 6.3 at different threshold levels, displaying the discrimination results using the integrated VIS-NIR, VIS, and NIR DR spectra, respectively. The integration area under the ROC curve is 0.97, 0.93, and 0.878, for integrated VIS-NIR, VIS, NIR DR spectra, respectively. A comparative evaluation of the ROC curves indicates that the either VIS or NIR DR spectra alone can be used for tissue diagnosis with high diagnostic sensitivity and specificity. Among these three diagnostic algorithms derived from the three spectral data sets, the integrated VIS-NIR DR spectra, which contains both hemoglobin and water signatures, generated better diagnostic accuracy than the single VIS and NIR spectral ranges, as illustrated by the improvement in the sensitivity and specificity (Fig. 6.4).

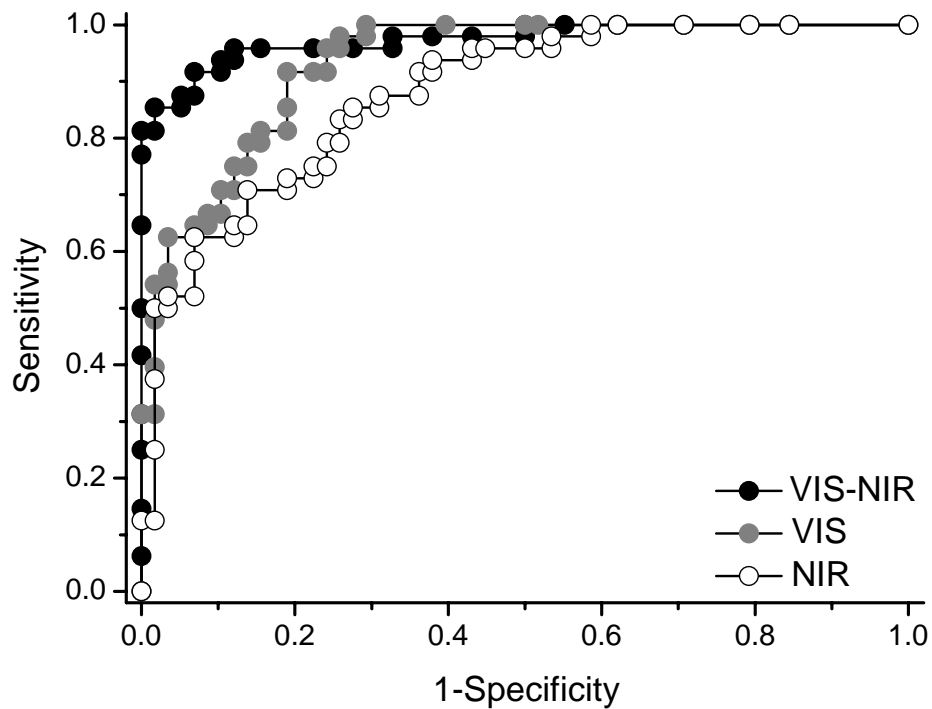


**Fig. 6.4** Receiver operating characteristic (ROC) curve of discrimination results for integrated VIS-NIR, VIS, and NIR DR spectra, respectively, using PCA-LDA algorithms, together with the leave-one tissue site-out, cross validation method. The integration areas under the ROC curve are 0.973, 0.93, and 0.878, respectively, for integrated VIS-NIR, VIS, and NIR DR spectra.

In summary, we have demonstrated that high-quality integrated VIS-NIR DR spectra can be acquired from colonic tissue within 8 ms. The results suggest that cancer tissue had greater absorption of hemoglobin and water than normal colonic tissue. The integrated VIS-NIR DR spectroscopy combined with PCA-LDA techniques can be used to capture the diagnostically important spectral features that maximize differentiation between colonic normal and cancer tissue. This model showed that, although the VIS or NIR spectroscopic technique alone, can be used to differentiate cancer tissue from colonic normal tissue with fairly high accuracy, the integrated VIS-NIR DR spectra, which contained both hemoglobin and water signatures, can further improve the diagnostic accuracy (Fig. 6.4). Despite the small

case number, the performances of the diagnostic algorithms derived from integrated visible and NIR in an unbiased manner with the leave-one-out, cross-validation method are very promising for improving colon cancer diagnosis (Fig. 6.3). Therefore, with the development of minimized size of fiber probe that can be coupled into the biopsy channel of commercial colonoscopy, we can combine the integrated VIS-NIR DR spectroscopy and AF spectroscopy for *in vivo* diagnosis of colon cancer during endoscopic examination.

To our knowledge, the use of the integrated VIS-NIR DR spectra together with the multivariate statistical techniques reported here is the first demonstration of principal this optical technique have potential to be applied to noninvasive *in vivo* tissue diagnosis. Best differentiation between normal and cancer colonic tissues can be achieved using the integrated VIS-NIR DR spectroscopy (400-1000 nm) as compared to VIS or NIR DR spectroscopy. Therefore, we conclude that the integrated VIS-NIR spectroscopy is a promising technique that may yield an effective and clinically useful diagnostic schema for improving early diagnosis of colonic cancer.

## Chapter 7 Conclusions and Future Directions

### 7.1 Conclusions

The motivation for research in this dissertation stemmed from the refinement of conventional colonoscopy for improving the detection of colon cancer. After a comparison of different advanced techniques used to complement the colonoscopy, AF technique shows a promising potential to provide the real-time information of endogenous fluorophores that are associated with morphological structure and metabolic processes. Most of AF studies, which used the UV or VIS wavelength for excitation, are not capable to detect lesions in deeper areas with the limited penetration depth. We, therefore, extended our AF work to the NIR domain and demonstrated the feasibility of using NIR AF/DR imaging and spectroscopy techniques for the early detection of precancer and cancer in the colon.

We have developed an integrated NIR AF and DR imaging system combined with polarization technique to detect the NIR AF emission under different polarization conditions of colonic tissues. A total of 48 paired colonic tissue specimens (normal *vs.* cancer) were measured using the integrated NIR DR (850-1100 nm) and NIR AF imaging at the 785 nm laser excitation. The results showed that NIR AF intensities of cancer tissues are significantly lower than those of normal tissues ( $p < 0.001$ , paired 2-sided Student's t-test,  $n=48$ ). In addition, NIR AF imaging under polarization conditions gives a higher diagnostic accuracy (of ~92-94%) compared to non-polarized NIR AF imaging or NIR DR imaging. Moreover, the ratio imaging of NIR DR to NIR AF with polarization provides the best diagnostic accuracy (of ~96%) among the NIR AF and NIR DR imaging techniques. This work

suggests that the integrated NIR AF/DR imaging under polarization condition has the potential to improve the early diagnosis and detection of malignant lesions in the colon.

Then, we integrated a novel flexible fiber probe into our NIR AF spectroscopy system to realize *in vivo* measurement of NIR AF spectra from different types of colonic tissues during the endoscopic examination. A total of 198 *in vivo* composite NIR AF and Raman spectra were acquired from normal (n=116), hyperplastic (n=48), and adenomatous polyp (n=34) colonic tissues at 785 nm laser excitation under white-light reflectance (WLR) endoscopic guidance. Significant differences ( $p < 0.05$ , ANOVA) in *in vivo* NIR AF spectra associated with Raman peaks are observed among colonic normal, hyperplastic, adenomatous polyps, and cancer tissues in the spectral ranges of 810-1050 nm. Multivariate statistical techniques, including PCA and LDA together with the leave-one tissue site-out, cross validation, were used to develop diagnostic algorithms for classification of subtypes of colonic polyp based on spectral characteristics. The diagnostic algorithms yield sensitivities of 83.6%, 77.1%, and 88.2%, and specificities of 96.3%, 88%, and 92.1% respectively, for classification of colonic normal, hyperplastic, and adenomatous polyps. Good classification among different types of colonic tissue can be achieved using PCA-LDA diagnostic algorithms, indicating the potential of NIR AF to be a clinically complement to conventional WLR endoscopy for the rapid, non-invasive, *in vivo* identification of precancer (adenomatous polyp) during clinical colonoscopic examination.

To further investigate the origins of tissue biochemicals responsible for the NIR AF differences among different types of colonic tissues, we have constructed a

non-negativity-constrained least squares minimization (NNCLSM) biochemical model to estimate the biochemical compositions of colonic tissues. The NIR AF spectra from the nine representative biochemicals (i.e., collagen I, elastin,  $\beta$ -NADH, FAD, L-tryptophan, hematoporphyrin, 4-pyridoxic acid, pyridoxal 5'-phosphate, and water) in colonic tissue were found to be the most significant for optimally fitting the measured *in vivo* NIR AF spectra of colonic tissue. Colonic precancer and cancer tissues show lower fit coefficients for collagen I, FAD,  $\beta$ -NADH, L-tryptophan, and pyridoxal 5'-phosphate, and higher fit coefficients for hematoporphyrin, 4-pyridoxic acid, and water as compared to benign tissues. We also compare the fitting results for the *ex vivo* and *in vivo* colonic specimens. Hence, NIR AF spectroscopy provides new insights into biochemical changes of colonic tissue associated with cell proliferation and metabolic rate during cancer progression.

We also evaluate the diagnostic ability of the integrated VIS-NIR DR spectroscopy technique for detection and diagnosis of colonic cancer. High-quality DR spectra with the spectral ranges of 400-1000 nm from normal and cancer colonic mucosal tissue were acquired. Significant differences were observed in DR spectra between normal ( $n=58$ ) and cancer ( $n=48$ ) colonic tissue, particularly in the spectral bands near 420, 540, 580 and 1000 nm, which are primarily correlated to absorption of hemoglobin and water. By using PCA-LDA algorithm, classification results of three spectral data sets (*i.e.* integrated VIS-NIR, VIS, and NIR DR spectra) showed diagnostic sensitivities of 87.5%, 85.4%, and 83.3%; specificities of 94.8%, 81.03%, and 74.1%; and overall diagnostic accuracy of 91.5%, 83.02%, and 78.3% respectively, for colonic cancer identification. This study suggests that the integrated

VIS-NIR DR spectroscopy associated with PCA-LDA diagnostic algorithms has the potential for improving the early diagnosis and detection of colonic cancer.

## **7.2 Future Directions**

While the works in the thesis contributed to the advancement of NIR AF/DR imaging and spectroscopy for the detection of colon cancer, they do suffer from some limitations, and thus, provide the directions for future studies.

### **i). Integration of NIR AF/DR imaging and spectroscopy system**

Our NIR AF imaging system is limited for the *ex vivo* measurements due to its experimental setup. With further miniaturization of the current NIR excitation and detection devices, we plan to couple the NIR AF imaging system into conventional endoscopes and realize *in vivo* measurement during colonoscopic screening in the future. Moreover, with the development of the endoscope-based fiber probe, we can also integrate the NIR AF and DR spectroscopy to the commercial endoscopy system. As a complement to conventional white-light endoscopy, NIR AF/DR imaging and spectroscopy system can provide wealth of morphological and biochemical information for improving *in vivo* detection and diagnosis of precancer and cancer in the colon and it can further assist doctor to minimize incision and dissection inaccuracies, and permit real-time confirmation of complete resection.

### **ii). On-line classification of different types of colonic tissues**

In this thesis, we only run all the multivariate statistical analysis off-line. In the clinical, the real-time biopsy is critical for effectively removing the lesions with cancerous potential during colonoscopic screening. Therefore, we aim to develop an algorithm that can classify the subtype so colonic polyps on-line. This real-time

classification function would assist endoscopists for accurate biopsy, and consequently reduce the risk and cost for polypectomy. However, in this thesis, we have only evaluated the classification of hyperplastic and adenomatous colonic polyp. In pathology, adenomatous polyps can be further divided into tubal, villous, and tubulo-villous different types. Thus, to realize real-time classifying of different types of colonic polyps during colonoscopic examination, the multivariate statistical algorithm needs more complicated training.

### **iii). Multi-layer colonic tissue model for chemical analysis**

Currently, our biochemical modeling only served as a semi-quantitative estimation of biochemical compositions of colonic tissue. The NNCLSM modeling only includes the most essential endogenous fluorophores which are known to be associated with the structural matrix of tissues or involved in cellular metabolic processes. Thus, this *in vitro* biochemical conformation may not truly reflect the *in vivo* conditions. Moreover, the spectral reconstruction does not take into account for the effects of tissue optical properties, such as absorption and scattering. To better understand the relationships between the tissue morphologic/biochemical changes and the tissue NIR AF spectra for further improving tissue diagnosis and classification, confocal NIR AF microspectroscopy should be explored on the colonic tissue *in vivo* and *in vitro*, by measuring the complete NIR AF spectra of specific tissue microstructures, or alternatively by mapping the distributions of some specific NIR AF peaks or principal components within a tissue, or even mapping the biochemical distributions at different tissue depths for association with neoplastic transformation in colonic tissue. Thus, a more complete NNCLSM biochemical modeling integrated with tissue optical properties (e.g., absorption and scattering

coefficients, anisotropy, tissue thickness, etc.), and light propagation in multilayer tissue model with Monte Carlo simulation warrants further investigation.

# List of Publications

## Peer-Reviewed Journal Articles

1. Z. Huang, S. K. Teh, W. Zheng, J. Mo, K. Lin, **X. Shao**, K. Y. Ho, M. Teh, and K. G. Yeoh, "Integrated Raman spectroscopy and trimodal wide-field imaging techniques for real-time in vivo tissue Raman measurements at endoscopy," *Opt. Lett.* **34**, 758-760 (2009).
2. **X. Shao**, W. Zheng, and Z. Huang, "Polarized near-infrared autofluorescence imaging combined with near-infrared diffuse reflectance imaging for improving colonic cancer detection," *Opt. Express* **18**, 24293-24300 (2010).
3. **X. Shao**, W. Zheng, and Z. Huang, "In vivo diagnosis of colonic precancer and cancer using near-infrared autofluorescence spectroscopy and biochemical modeling," *J. Biomed. Opt.* **16**, 067005 (2011).
4. **X. Shao**, W. Zheng and Z. Huang, "Near-infrared autofluorescence spectroscopy for *in vivo* identification of hyperplastic and adenomatous polyps in the colon," *Biosens. Bioelectron.* **30**, 118-122 (2011).
5. **X. Shao**, W. Zheng and Z. Huang, "Integrated visible and near-infrared diffuse reflectance spectroscopy for improving colonic cancer diagnosis," In preparation.
6. **X. Shao**, W. Zheng and Z. Huang, "Polarized NIR autofluorescence and diffuse reflectance imaging for diagnosis of colonic cancer," In preparation.

## Conference Presentations

1. **X. Shao**, W. Zheng, and Z. Huang, "Near-infrared fluorescence polarization imaging for cancer detection in the colon," in *Optics Within Life Science-10*, (Singapore, 2008).
2. **X. Shao**, J. Mo, W. Zheng, Z. Huang, "Near-infrared fluorescence imaging for colonic cancer detection," in *SPIE Photonics West* (USA, 2008).
3. **X. Shao**, W. Zheng, Huang Zhiwei, "Near-infrared autofluorescence polarization imaging for colonic cancer detection," in *ACP* (Shanghai, 2009).

## References

1. A. C. Society, "Colorectal cancer facts & figures 2008-2010," American Cancer Society (2008).
2. "The basis of rectal cancer," [www.kfo179.de/english/information/](http://www.kfo179.de/english/information/).
3. K. Soreide, and H. S oiland, *Clinical, Genetic and Molecular Precursor Features in Colorectal Neoplasia* (Nova Science Publishers, 2008).
4. W. Grady, "Genomic instability and colon cancer," *Cancer Metastasis Rev.* **23**, 11-27 (2004).
5. T. Muto, H. Nagawa, T. Watanabe, T. Masaki, and T. Sawada, "Colorectal carcinogenesis: historical review," *Dis. Colon Rectum.* **40**, S80 (1997).
6. M. Konishi, R. Kikuchi-Yanoshita, K. Tanaka, M. Muraoka, A. Onda, Y. Okumura, N. Kishi, T. Iwama, T. Mori, and M. Koike, "Molecular nature of colon tumors in hereditary nonpolyposis colon cancer, familial polyposis, and sporadic colon cancer," *Gastroenterology* **111**, 307-317 (1996).
7. J. H. Bond, "Update on colorectal polyps: management and follow-up surveillance," *Endoscopy* **35**, S35-S40 (2003).
8. S. L. Gearhart, and N. Ahuja, *Colorectal cancer* (W.B. Saunders Company, Philadelphia, 2011).
9. A. Jemal, R. Siegel, J. Xu, and E. Ward, "Cancer Statistics, 2010," *CA. Cancer J. Clin.*, 20073 (2010).
10. P. Rozen, G. P. Young, B. Levin, and S. J. Spann, *Colorectal cancer in clinical practice* (Taylor & francis, London, 2006).
11. A. Jemal, F. Bray, M. M. Center, J. Ferlay, E. Ward, and D. Forman, "Global cancer statistics," *CA. Cancer J. Clin.* (2011).
12. W. Du, J. T. L. Mah, J. Lee, R. Sankila, R. Sankaranarayanan, and K.-S. Chia, "Incidence and survival of mucinous adenocarcinoma of the colorectum: a population-based study from an asian country," *Dis. Colon Rectum.* **47**, 78-85 (2004).
13. S. Winawer, A. Zauber, M. Ho, M. O'Brien, L. Gottlieb, S. Sternberg, J. Wayne, M. Schapiro, J. Bond, and J. Panish, "Prevention of colorectal cancer

- by colonoscopic polypectomy," *New Engl. J. Med.* **329**, 1977 (1993).
14. S. B. Edge, and D. R. Byrd, *AJCC Cancer Staging Manual* (Springer, 2009).
  15. A. Jemal, L. Clegg, E. Ward, L. Ries, X. Wu, P. Jamison, P. Wingo, H. Howe, R. Anderson, and B. Edwards, "Annual report to the nation on the status of cancer, 1975–2001, with a special feature regarding survival," *Cancer* **101**, 3-27 (2004).
  16. F. Jenkinson, and R. J. C. Steele, "Colorectal cancer screening - Methodology," *Surgeon* **8**, 164-171 (2010).
  17. D. Lieberman, "Progress and challenges in colorectal cancer screening and surveillance," *Gastroenterology* **138**, 2115-2126 (2010).
  18. G. Young, "Fecal immunochemical tests (FIT) vs. office-based guaiac fecal occult blood test (FOBT)," *Pract Gastroenterol* **18**, 46-56 (2004).
  19. A. Smith, G. Young, S. Cole, and P. Bampton, "Comparison of a brush sampling fecal immunochemical test for hemoglobin with a sensitive guaiac based fecal occult blood test in detection of colorectal neoplasia," *Cancer* **107**, 2152-2159 (2006).
  20. J. Hardcastle, J. Chamberlain, M. Robinson, S. Moss, S. Amar, T. Balfour, P. James, and C. Mangham, "Randomised controlled trial of faecal-occult-blood screening for colorectal cancer," *Lancet.* **348**, 1472-1477 (1996).
  21. L. Sun, H. Wu, and Y. Guan, "Colonography by CT, MRI and PET/CT combined with conventional colonoscopy in colorectal cancer screening and staging," *World J Gastroenterol.* **14**, 853 (2008).
  22. R. van Gelder, C. Nio, J. Florie, J. Bartelsman, P. Snel, S. de Jager, S. van Deventer, J. Laméris, P. Bossuyt, and J. Stoker, "Computed tomographic colonography compared with colonoscopy in patients at increased risk for colorectal cancer," *Gastroenterology* **127**, 41-48 (2004).
  23. P. Cotton, V. Durkalski, B. Pineau, Y. Palesch, P. Mauldin, B. Hoffman, D. Vining, W. Small, J. Affronti, and D. Rex, "Computed tomographic colonography (virtual colonoscopy): a multicenter comparison with standard colonoscopy for detection of colorectal neoplasia," *JAMA.* **291**, 1713 (2004).
  24. J. Church, *Endoscopy of the colon, rectum, and anus* (Igaku-Shoin, 1995).

25. P. Newcomb, R. Norfleet, B. Storer, T. Surawicz, and P. Marcus, "Screening sigmoidoscopy and colorectal cancer mortality," *J Natl Cancer Inst.* **84**, 1572 (1992).
26. J. Selby, G. Friedman, C. Quesenberry Jr, and N. Weiss, "A case-control study of screening sigmoidoscopy and mortality from colorectal cancer," *New Engl. J. Med.* **326**, 653-657 (1992).
27. K. E. Kim, ed. *Early detection and prevention in colorectal cancer* (SLACK incorporated, 2009).
28. W. Wolff, and H. Shinya, "Colonofiberoscopy," *JAMA.* **217**, 1509 (1971).
29. M. Sivak Jr, and D. Fleischer, "Colonoscopy with a VideoEndoscope (TM): preliminary experience," *Gastrointest. Endosc.* **30**, 1-5 (1984).
30. G. J. E. Brown, and B. P. Saunders, "Advances in colonic imaging: technical improvements in colonoscopy," *Eur. J. Gastroenterol. Hepatol.* **17**, 785-792 (2005).
31. D. Rex, C. Cutler, G. Lemmel, E. Rahmani, D. Clark, D. Helper, G. Lehman, and D. Mark, "Colonoscopic miss rates of adenomas determined by back-to-back colonoscopies," *Gastroenterology* **112**, 24-28 (1997).
32. I. Heiskanen, T. Luostarinen, and H. Järvinen, "Impact of screening examinations on survival in familial adenomatous polyposis," *Scand. J. Gastroenterol.* **35**, 1284-1287 (2000).
33. M. Fennerty, "Tissue staining," *Gastrointest. Endosc. Clin. N. Am.* **4**, 297 (1994).
34. R. Dacosta, B. Wilson, and N. Marcon, "New optical technologies for earlier endoscopic diagnosis of premalignant gastrointestinal lesions," *J. Gastroenterol. Hepatol.* **17**, S85-S104 (2002).
35. Y. Saitoh, I. Waxman, A. West, N. Popnikolov, Z. Gatalica, J. Watari, T. Obara, Y. Kohgo, and P. Pasricha, "Prevalence and distinctive biologic features of flat colorectal adenomas in a North American population," *Gastroenterology* **120**, 1657-1665 (2001).
36. F. Van Den Broek, P. Fockens, and E. Dekker, "Review article: new developments in colonic imaging," *Aliment. Pharmacol. Ther.* **26**, 91-99

- (2007).
37. L. M. Wong Kee Song, D. G. Adler, B. Chand, J. D. Conway, J. M. B. Croffie, J. A. DiSario, D. S. Mishkin, R. J. Shah, L. Somogyi, W. M. Tierney, and B. T. Petersen, "Chromoendoscopy," *Gastrointest. Endosc.* **66**, 639-649 (2007).
  38. J. B. Pawley, ed. *Handbook of biological confocal microscopy* (Springer, Berlin, 2006).
  39. H. Makhoulf, A. Gmitro, A. Tanbakuchi, J. Udovich, and A. Rouse, "Multispectral confocal microendoscope for in vivo and in situ imaging," *J. Biomed. Opt.* **13**, 044016 (2008).
  40. R. Kiesslich, A. Hoffman, and M. F. Neurath, "Colonoscopy, tumors, and inflammatory bowel disease - new diagnostic methods," *Endoscopy* **38**, 5-10 (2006).
  41. T. Wang, "Confocal microscopy from the bench to the bedside," *Gastrointest. Endosc.* **62**, 696 (2005).
  42. M. Pennazio, R. Santucci, E. Rondonotti, C. Abbiati, G. Beccari, F. Rossini, and R. De Franchis, "Outcome of patients with obscure gastrointestinal bleeding after capsule endoscopy: Report of 100 consecutive cases," *Gastroenterology* **126**, 643-653 (2004).
  43. A. Van Gossum, M. Munoz-Navas, I. Fernandez-Urien, C. Carretero, G. Gay, M. Delvaux, M. Lapalus, T. Ponchon, H. Neuhaus, and M. Philipper, "Capsule endoscopy versus colonoscopy for the detection of polyps and cancer," *New Engl. J. Med.* **361**, 264 (2009).
  44. R. DaCosta, B. Wilson, and N. Marcon, "Optical techniques for the endoscopic detection of dysplastic colonic lesions," *Curr. Opin. Gastroenterol.* **21**, 70 (2005).
  45. H. Zeng, A. McWilliams, and S. Lam, "Optical spectroscopy and imaging for early lung cancer detection: a review," *Photodiag. Photody. Ther.* **1**, 111-122 (2004).
  46. H. Aihara, K. Sumiyama, S. Saito, H. Tajiri, and M. Ikegami, "Numerical analysis of the autofluorescence intensity of neoplastic and non-neoplastic colorectal lesions by using a novel videoendoscopy system," *Gastrointest. Endosc.* **69**, 726-733 (2009).

47. R. M. Cothren, J. M. V. Sivak, J. Van Dam, R. E. Petras, M. Fitzmaurice, J. M. Crawford, J. Wu, J. F. Brennan, R. P. Rava, R. Manoharan, and M. S. Feld, "Detection of dysplasia at colonoscopy using laser-induced fluorescence: a blinded study," *Gastrointest. Endosc.* **44**, 168-176 (1996).
48. R. S. DaCosta, B. C. Wilson, and N. E. Marcon, "Fluorescence and spectral imaging," *ScientificWorldJournal* **7**, 2046-2071 (2007).
49. B. Bressler, L. Paszat, C. Vinden, C. Li, H. JINGSONG, and L. Rabeneck, "Colonoscopic miss rates for right-sided colon cancer: a population-based analysis," *Gastroenterology* **127**, 452-456 (2004).
50. F. Graham-Smith, T. A. King, and D. Wilkins, *Optics and photonics: an introduction* (J. Wiley, 2007).
51. D. Jameson, J. Croney, and P. Moens, "[1] Fluorescence: Basic concepts, practical aspects, and some anecdotes," *Methods Enzymol.* **360**, 1-43 (2003).
52. A. Evenson, "The characteristics of sound and light waves," (1999), <http://www.cord.edu/faculty/manning/physics215/studentpages/angieevanson.html>.
53. R. Richards-Kortum, and E. Sevick-Muraca, "Quantitative optical spectroscopy for tissue diagnosis," *Annu. Rev. Phys. Chem.* **47**, 555-606 (1996).
54. J. R. Lakowicz, ed. *Principles of Fluorescence Spectroscopy* (Springer, New York, 2006).
55. M. Mycek, and B. Pogue, *Handbook of biomedical fluorescence* (Marcel Dekker, 2003).
56. J. R. Lackowicz, ed. *Principles of Fluorescence Spectroscopy* (Springer, New York, 2006).
57. T. Vo-Dinh, *Biomedical photonics handbook* (CRC Press, 2003).
58. J. R. Albani, "Fluorescence polarization," in *Principles and applications of fluorescence spectroscopy* (Blackwell Publishing, Oxford, 2007).
59. S. L. Jacques, and J. C. Ramella-Roman, "Polarized light imaging of tissues," in *Laers and current optical techniques in biology*, G. Palumbo, and R. Pratesi, eds. (The Royal Society of Chemistry, Northampton, 2004).

60. F. Perrin, "Polarisation de la lumière de fluorescence. Vie moyenne des molécules dans l'état excité," (1926).
61. S. G. Demos, and R. R. Alfano, "Optical polarization imaging," *Appl. Opt.* **36**, 150-155 (1997).
62. S. L. Jacques, J. R. Roman, and K. Lee, "Imaging superficial tissues with polarized light," *Lasers Surg. Med.* **26**, 119-129 (2000).
63. H. Staveren, M. Keijzer, T. Keesmaat, H. Jansen, W. Kirkel, J. Beek, and W. Star, "Integrating sphere effect in whole-bladder-wall photodynamic therapy: III. Fluence multiplication, optical penetration and light distribution with an eccentric source for human bladder optical properties," *Phys. Med. Biol.* **41**, 579 (1996).
64. R. Haskell, L. Svaasand, T. Tsay, T. Feng, M. McAdams, and B. Tromberg, "Boundary conditions for the diffusion equation in radiative transfer," *J. Opt. Soc. Am. A. Opt. Image Sci. Vis.* **11**, 2727-2741 (1994).
65. W. Cheong, S. Prahl, and A. Welch, "A review of the optical properties of biological tissues," *IEEE J. Quantum Electron.* **26**, 2166-2185 (1990).
66. F. P. Bolin, L. E. Preuss, R. C. Taylor, and R. J. Ference, "Refractive index of some mammalian tissues using a fiber optic cladding method," *Appl. Opt.* **28**, 2297-2303 (1989).
67. S. L. Jacques, and S. A. Prahl, "Absorption spectra for biological tissues," (1998), <http://omlc.ogi.edu/classroom/ece532/class3/muaspectra.html>.
68. E. Silva, and R. Richards-Kortum, "Fluorescence spectroscopy: a diagnostic tool for cervical intraepithelial neoplasia (CIN)," *Gynecol. Oncol.* **52**, 31-38 (1994).
69. M. Zellweger, P. Grosjean, D. Goujon, P. Monnier, H. van den Bergh, and G. Wagnières, "In vivo autofluorescence spectroscopy of human bronchial tissue to optimize the detection and imaging of early cancers," *J. Biomed. Opt.* **6**, 41 (2001).
70. D. Zaak, H. Stepp, R. Baumgartner, P. Schneede, R. Waidelich, D. Frimberger, A. Hartmann, R. KNUCHEL, A. Hofstetter, and A. Hohla, "Ultraviolet-excited (308 nm) autofluorescence for bladder cancer detection," *Urology* **60**, 1029-1033 (2002).

71. Z. Kulas, E. Beres-Pawlik, and T. Krecicki, "Numerical analysis of endoscopic autofluorescence imaging for cancerous tissue detection," *J. Non-Cryst. Solids* **352**, 2468-2475 (2006).
72. E. M. Goldys, ed. *Fluorescence application in biotechnology and life sciences* (Wiley Blackwell, New Jersey, 2008).
73. E. Borotto, J. Englender, J. C. Pourny, S. Naveau, J. C. Chaput, and Y. Lecarpentier, "Detection of the fluorescence of GI vessels in rats using a CCD camera or a near-infrared video endoscope," *Gastrointest. Endosc.* **50**, 684-688 (1999).
74. E. Sevick-Muraca, J. Houston, and M. Gurfinkel, "Fluorescence-enhanced, near infrared diagnostic imaging with contrast agents," *Curr. Opin. Chem. Biol.* **6**, 642-650 (2002).
75. J. Frangioni, "In vivo near-infrared fluorescence imaging," *Curr. Opin. Chem. Biol.* **7**, 626-634 (2003).
76. J. Rao, A. Dragulescu-Andrasi, and H. Yao, "Fluorescence imaging in vivo: recent advances," *Curr. Opin. Biotechnol.* **18**, 17-25 (2007).
77. S. Kim, Y. Lim, E. Soltesz, A. De Grand, J. Lee, A. Nakayama, J. Parker, T. Mihaljevic, R. Laurence, and D. Dor, "Near-infrared fluorescent type II quantum dots for sentinel lymph node mapping," *Nature* **22**, 93-97 (2004).
78. I. Medintz, H. Uyeda, E. Goldman, and H. Mattoussi, "Quantum dot bioconjugates for imaging, labelling and sensing," *Nature Materials* **4**, 435-446 (2005).
79. X. Huang, P. K. Jain, I. H. El-Sayed, and M. A. El-Sayed, "Determination of the minimum temperature required for selective photothermal destruction of cancer cells with the use of Immunotargeted gold nanoparticles," *Photochem. Photobiol.* **82**, 412-417 (2006).
80. D. W. Thomas, and T. George, "Autofluorescence imaging: have we finally seen the light?," *Gastrointest. Endosc.* **61**, 686-688 (2005).
81. G. Bottiroli, and A. C. Croce, "Autofluorescence spectroscopy of cells and tissues as a tool for biomedical diagnosis," in *Lasers and current optical techniques in biology* (Royal society of chemistry, Cambridge, 2004).

82. P. Andersson, S. Montan, and S. Svanberg, "Multispectral system for medical fluorescence imaging," *IEEE J. Quantum Electron.* **23**, 1798-1805 (2002).
83. R. Marchesini, E. Pignoli, S. Tomatis, S. Fumagalli, A. Sichirollo, S. Palma, M. Fante, P. Spinelli, A. Croce, and G. Bottiroli, "Ex vivo optical properties of human colon tissue," *Lasers Surg. Med.* **15**, 351-357 (1994).
84. G. I. Zonios, R. M. Cothren, J. T. Arendt, W. Jun, J. Van Dam, J. M. Crawford, R. Manoharan, and M. S. Feld, "Morphological model of human colon tissue fluorescence," *IEEE Trans Biomed Eng.* **43**, 113-122 (1996).
85. R. Alfano, D. Tata, J. Cordero, P. Tomashefsky, F. Longo, and M. Alfano, "Laser induced fluorescence spectroscopy from native cancerous and normal tissue," *IEEE J. Quantum Electron.* **20**, 1507-1511 (1984).
86. J. Mourant, I. Bigio, J. Boyer, R. Conn, T. Johnson, and T. Shimada, "Spectroscopic diagnosis of bladder cancer with elastic light scattering," *Lasers Surg. Med.* **17**, 350-357 (1995).
87. K. Schomacker, J. Frisoli, C. Compton, T. Flotte, J. Richter, N. Nishioka, and T. Deutsch, "Ultraviolet laser-induced fluorescence of colonic tissue: basic biology and diagnostic potential," *Lasers Surg. Med.* **12**, 63-78 (1992).
88. S. Demos, R. Gandour-Edwards, R. Ramsamooj, and R. deVere White, "Spectroscopic detection of bladder cancer using near-infrared imaging techniques," *J. Biomed. Opt.* **9**, 767 (2004).
89. F. Koenig, F. McGovern, H. Enquist, R. Larne, T. Deutsch, and K. Schomacher, "Autofluorescence guided biopsy for the early diagnosis of bladder carcinoma," *J Urol.* **159**, 1871-1875 (1998).
90. C. Kittrell, R. Willett, C. de Los Santos-Pacheo, N. Ratliff, J. Kramer, E. Malk, and M. Feld, "Diagnosis of fibrous arterial atherosclerosis using fluorescence," *Appl. Opt.* **24**, 2280-2281 (1985).
91. E. B. Hanlon, I. Itzkan, R. R. Dasari, M. S. Feld, R. J. Ferrante, A. C. McKee, D. Lathi, and N. W. Kowall, "Near-infrared fluorescence spectroscopy detects Alzheimer's disease in vitro," *Photochem. Photobiol.* **70**, 236-242 (1999).
92. J. Hung, S. Lam, J. C. Leriche, and B. Palcic, "Autofluorescence of normal and malignant bronchial tissue," *Lasers Surg. Med.* **11**, 99-105 (1991).

93. D. Goujon, M. Zellweger, A. Radu, P. Grosjean, B. Weber, H. van den Bergh, P. Monnier, and G. Wagnières, "In vivo autofluorescence imaging of early cancers in the human tracheobronchial tree with a spectrally optimized system," *J. Biomed. Opt.* **8**, 17 (2003).
94. F. Hirsch, S. Prindiville, Y. Miller, W. Franklin, E. Dempsey, J. Murphy, P. Bunn Jr, and T. Kennedy, "Fluorescence versus white-light bronchoscopy for detection of preneoplastic lesions: a randomized study," *J Natl Cancer Inst.* **93**, 1385 (2001).
95. H. Zeng, M. Petek, M. Zorman, A. McWilliams, B. Palcic, and S. Lam, "Integrated endoscopy system for simultaneous imaging and spectroscopy for early lung cancer detection," *Opt. Lett.* **29**, 587-589 (2004).
96. W. R. Kessler, "Autofluorescence colonoscopy: a green light on the long road to "real-time" histology," *Gastrointest. Endosc.* **68**, 291-293 (2008).
97. L. Fournier, V. Lucidi, K. Berejnoi, T. Miller, S. Demos, and R. Brasch, "In-vivo NIR autofluorescence imaging of rat mammary tumors," *Opt. Express* **14**, 6713-6723 (2006).
98. C. Lieber, S. Urayama, N. Rahim, R. Tu, R. Saroufeem, B. Reubner, and S. Demos, "Multimodal near infrared spectral imaging as an exploratory tool for dysplastic esophageal lesion identification," *Opt. Express* **14**, 2211-2219 (2006).
99. V. Kondepati, J. Zimmermann, M. Keese, J. Sturm, B. Manegold, and J. Backhaus, "Near-infrared fiber optic spectroscopy as a novel diagnostic tool for the detection of pancreatic cancer," *J. Biomed. Opt.* **10**, 054016 (2005).
100. S. Demos, R. Bold, R. White, and R. Ramsamooj, "Investigation of near-infrared autofluorescence imaging for the detection of breast cancer," *IEEE Journal of Selected Topics in Quantum Electronics* **11**, 791-798 (2005).
101. S. Demos, R. Gandour-Edwards, R. Ramsamooj, and R. deVere White, "Near-infrared autofluorescence imaging for detection of cancer," *J. Biomed. Opt.* **9**, 587 (2004).
102. R. V. Belcher, and S. G. Smith, "Study of porphyrins present in hepatoma tissue," *Biochem. J.* **119**, 16 (1970).
103. B. Chance, E. Anday, S. Nioka, S. Zhou, L. Hong, K. Worden, C. Li, T.

- Murray, Y. Ovetsky, and D. Pidikiti, "A novel method for fast imaging of brain function, non-invasively, with light," *Opt. Express* **2**, 411-423 (1998).
104. S. Coyle, T. Ward, C. Markham, and G. McDarby, "On the suitability of near-infrared (NIR) systems for next-generation brain-computer interfaces," *Physiol. Meas.* **25**, 815 (2004).
105. A. L. McCallum, J. T. Jenkins, D. Gillen, and R. G. Molloy, "Evaluation of autofluorescence colonoscopy for the detection and diagnosis of colonic polyps," *Gastrointest. Endosc.* **68**, 283-290 (2008).
106. S. Anandasabapathy, "Endoscopic imaging: emerging optical techniques for the detection of colorectal neoplasia," *Curr. Opin. Gastroenterol.* **24**, 64-69 (2008).
107. D. Roblyer, R. Richards-Kortum, K. Sokolov, A. K. El-Naggar, M. D. Williams, C. Kurachi, and A. M. Gillenwater, "Multispectral optical imaging device for in vivo detection of oral neoplasia," *J. Biomed. Opt.* **13**, 024019-024011 (2008).
108. D. Pantalone, F. Andreoli, F. Fusi, V. Basile, G. Romano, G. Giustozzi, L. Rigacci, R. Alterini, and M. Monici, "Multispectral imaging autofluorescence microscopy in colonic and gastric cancer metastatic lymph nodes," *Clin. Gastroenterol. Hepatol.* **5**, 230-236 (2007).
109. R. Richards-Kortum, R. Rava, R. Petras, M. Fitzmaurice, M. Sivak, and M. Feld, "Spectroscopic diagnosis of colonic dysplasia," *Photochem. Photobiol.* **53**, 777-786 (1991).
110. K. T. Schomacker, J. K. Frisoli, C. C. Compton, T. J. Flotte, J. M. Richter, N. S. Nishioka, and T. F. Deutsch, "Ultraviolet laser-induced fluorescence of colonic tissue: basic biology and diagnostic potential," *Lasers Surg. Med.* **12**, 63-78 (1992).
111. M. A. Kara, F. P. Peters, F. J. W. ten Kate, S. J. van Deventer, P. Fockens, and J. J. G. H. M. Bergman, "Endoscopic video autofluorescence imaging may improve the detection of early neoplasia in patients with Barrett's esophagus," *Gastrointest. Endosc.* **61**, 679-685 (2005).
112. X. Han, H. Lui, D. I. McLean, and H. Zeng, "Near-infrared autofluorescence imaging of cutaneous melanins and human skin in vivo," *J. Biomed. Opt.* **14**,

- 024017 (2009).
113. Z. Huang, H. Zeng, I. Hamzavi, A. Alajlan, E. Tan, D. I. McLean, and H. Lui, "Cutaneous melanin exhibiting fluorescence emission under near-infrared light excitation," *J. Biomed. Opt.* **11**, 034010 (2006).
  114. Z. Huang, H. Lui, D. I. McLean, M. Korbelik, and H. Zeng, "Raman spectroscopy in combination with background near-infrared autofluorescence enhances the in vivo assessment of malignant tissues," *Photochem. Photobiol.* **81**, 1219-1226 (2005).
  115. Z. Huang, W. Zheng, S. Xie, R. Chen, H. Zeng, D. Mclean, and H. Lui, "Laser-induced autofluorescence microscopy of normal and tumor human colonic tissue," *Int. J. Oncol.* **24**, 59-63 (2004).
  116. R. Weersink, M. S. Patterson, K. Diamond, S. Silver, and N. Padgett, "Noninvasive measurement of fluorophore concentration in turbid media with a simple fluorescence/reflectance ratio technique," *Appl. Opt.* **40**, 6389-6395 (2001).
  117. M. Janko, P. Davydovskaya, M. Bauer, A. Zink, and R. W. Stark, "Anisotropic Raman scattering in collagen bundles," *Opt. Lett.* **35** (2010).
  118. "American National Standard for the Safe Use of Lasers: ANSI Standard 2136.1-1986 " in *American National Standards Institute* (Washington D.C. , 1986).
  119. R. Drezek, K. Sokolov, U. Utzinger, I. Boiko, A. Malpica, M. Follen, and R. Richards-Kortum, "Understanding the contributions of NADH and collagen to cervical tissue fluorescence spectra: modeling, measurements, and implications," *J. Biomed. Opt.* **6**, 385-396 (2001).
  120. X. Wang, and L. V. Wang, "Propagation of polarized light in birefringent turbid media: a Monte Carlo study," *J. Biomed. Opt.* **7**, 279-290 (2002).
  121. J. Y. Qu, J. Hua, and Z. Huang, "Correction of geometrical effects on fluorescence imaging of tissue," *Opt. Commun.* **176**, 319-326 (2000).
  122. B. C. Morson, "Evolution of cancer of the colon and rectum," *Cancer* **34**, 845-849 (1974).
  123. T. Muto, H. Bussey, and B. Morson, "The evolution of cancer of the colon

- and rectum," *Cancer* **36**, 2251-2270 (1975).
124. T. M. Yeung, and N. J. Mortensen, "Advances in endoscopic visualisation of colorectal polyps," *Colorectal Disease* **13**, 352-359 (2011).
  125. P. R. Pfau, and M. V. Sivak Jr, "Endoscopic diagnostics," *Gastroenterology* **120**, 763-781 (2001).
  126. Z. Huang, S. K. Teh, W. Zheng, J. Mo, K. Lin, X. Shao, K. Y. Ho, M. Teh, and K. G. Yeoh, "Integrated Raman spectroscopy and trimodal wide-field imaging techniques for real-time in vivo tissue Raman measurements at endoscopy," *Opt. Lett.* **34**, 758-760 (2009).
  127. Z. Huang, M. S. Bergholt, W. Zheng, K. Lin, K. Y. Ho, M. Teh, and K. G. Yeoh, "In vivo early diagnosis of gastric dysplasia using narrow-band image-guided Raman endoscopy," *J. Biomed. Opt.* **15**, 037017-037015 (2010).
  128. U. Peitz, and P. Malfertheiner, "Chromoendoscopy: from a research tool to clinical progress," *Dig. Dis.* **20**, 111-119 (2002).
  129. M. Konerding, E. Fait, and A. Gaumann, "3D microvascular architecture of pre-cancerous lesions and invasive carcinomas of the colon," *Br. J. Cancer* **84**, 1354 (2001).
  130. A. Molckovsky, L.-M. W. K. Song, M. G. Shim, N. E. Marcon, and B. C. Wilson, "Diagnostic potential of near-infrared Raman spectroscopy in the colon: differentiating adenomatous from hyperplastic polyps," *Gastrointest. Endosc.* **57**, 396-402 (2003).
  131. R. S. DaCosta, H. Andersson, M. Cirocco, N. E. Marcon, and B. C. Wilson, "Autofluorescence characterisation of isolated whole crypts and primary cultured human epithelial cells from normal, hyperplastic, and adenomatous colonic mucosa," *J. Clin. Pathol.* **58**, 766-774 (2005).
  132. Z. Benes, and Z. Antos, "Optical biopsy system distinguishing between hyperplastic and adenomatous polyps in the colon during colonoscopy," *Anticancer Res.* **29**, 4737-4739 (2009).
  133. M.-A. Mycek, K. T. Schomacker, and N. S. Nishioka, "Colonic polyp differentiation using time-resolved autofluorescence spectroscopy," *Gastrointest. Endosc.* **48**, 390-394 (1998).

134. T. D. Wang, J. M. Crawford, M. S. Feld, Y. Wang, I. Itzkan, and J. Van Dam, "In vivo identification of colonic dysplasia using fluorescence endoscopic imaging," *Gastrointest. Endosc.* **49**, 447-455 (1999).
135. W. Dillon, and M. Goldstein, *Multivariate analysis: methods and applications* (Wiley, New York, 1984).
136. S. K. Teh, W. Zheng, K. Y. Ho, M. Teh, K. G. Yeoh, and Z. Huang, "Near-infrared Raman spectroscopy for early diagnosis and typing of adenocarcinoma in the stomach," *Br. J. Surg.* **97**, 550-557 (2010).
137. F. R. Dollish, W. G. Fateley, and F. F. Bentley, *Characteristic Raman frequencies of organic compounds* (Wiley New York, 1974).
138. T. C. Bakker Schut, M. Witjes, H. Sterenborg, O. Speelman, J. Roodenburg, E. Marple, H. Bruining, and G. Puppels, "In vivo detection of dysplastic tissue by Raman spectroscopy," *Anal. Chem.* **72**, 6010-6018 (2000).
139. P. J. Caspers, G. W. Lucassen, and G. J. Puppels, "Combined in vivo confocal Raman spectroscopy and confocal microscopy of human skin," *Biophys. J.* **85**, 572-580 (2003).
140. C. J. Frank, R. L. McCreery, and D. C. B. Redd, "Raman spectroscopy of normal and diseased human breast tissues," *Anal. Chem.* **67**, 777-783 (1995).
141. M. Gniadecka, H. C. Wulf, O. F. Nielsen, D. H. Christensen, and J. Hercogova, "Distinctive molecular abnormalities in benign and malignant skin lesions: studies by Raman spectroscopy," *Photochem. Photobiol.* **66**, 418-423 (1997).
142. Z. Huang, H. Zeng, I. Hamzavi, D. I. McLean, and H. Lui, "Rapid near-infrared Raman spectroscopy system for real-time in vivo skin measurements," *Opt. Lett.* **26**, 1782-1784 (2001).
143. Z. Huang, A. McWilliams, H. Lui, D. McLean, S. Lam, and H. Zeng, "Near infrared Raman spectroscopy for optical diagnosis of lung cancer," *Int. J. Cancer* **107**, 1047-1052 (2003).
144. A. Mahadevan-Jansen, M. F. Mitchell, N. Ramanujam, U. Utzinger, and R. Richards-Kortum, "Development of a fiber optic probe to measure NIR Raman spectra of cervical tissue in vivo," *Photochem. Photobiol.* **68**, 427-431 (1998).

145. A. Mizuno, H. Kitajima, K. Kawauchi, S. Muraishi, and Y. Ozaki, "Near-infrared Fourier transform Raman spectroscopic study of human brain tissues and tumours," *J. Raman Spectrosc.* **25**, 25-29 (1994).
146. J. Mo, W. Zheng, J. J. H. Low, J. Ng, A. Ilancheran, and Z. Huang, "High wavenumber raman spectroscopy for in vivo detection of cervical dysplasia," *Anal. Chem.* **81**, 8908-8915 (2009).
147. M. G. Shim, L.-M. Wong Kee Song, N. E. Marcon, and B. C. Wilson, "In vivo near-infrared raman spectroscopy: demonstration of feasibility during clinical gastrointestinal endoscopy," *Photochem. Photobiol.* **72**, 146-150 (2000).
148. N. Stone, P. Stavroulaki, C. Kendall, M. Birchall, and H. Barr, "Raman spectroscopy for early detection of laryngeal malignancy: preliminary results," *Laryngoscope.* **110**, 1756-1763 (2000).
149. N. Stone, C. Kendall, N. Shepherd, P. Crow, and H. Barr, "Near infrared Raman spectroscopy for the classification of epithelial pre cancers and cancers," *J. Raman Spectrosc.* **33**, 564-573 (2002).
150. U. Utzinger, D. L. Heintzelman, A. Mahadevan-Jansen, A. Malpica, M. Follen, and R. Richards-Kortum, "Near-infrared raman spectroscopy for in vivo detection of cervical precancers," *Appl. Spectrosc.* **55**, 955-959 (2001).
151. E. Widjaja, W. Zheng, and Z. Huang, "Classification of colonic tissues using near-infrared Raman spectroscopy and support vector machines," *Int. J. Oncol.* **32**, 653-662 (2008).
152. G. Zhang, S. Demos, and R. Alfano, "Far-red and NIR spectral wing emission from tissues under 532 and 632 nm photo-excitation," *Lasers Life Sci.* **9**, 1-16 (1999).
153. G. Wagnieres, W. Star, and B. Wilson, "In vivo fluorescence spectroscopy and imaging for oncological applications," *Photochem. Photobiol.* **68**, 603-632 (1998).
154. X. Shao, W. Zheng, and Z. Huang, "In vivo diagnosis of colonic precancer and cancer using near-infrared autofluorescence spectroscopy and biochemical modeling," *J. Biomed. Opt.* **16**, 067005 (2011).
155. B. Barry, H. Edwards, and A. Williams, "Fourier transform Raman and

- infrared vibrational study of human skin: assignment of spectral bands," *J. Raman Spectrosc.* **23**, 641-645 (1992).
156. S. K. Teh, W. Zheng, K. Y. Ho, M. Teh, K. G. Yeoh, and Z. Huang, "Diagnostic potential of near-infrared Raman spectroscopy in the stomach: differentiating dysplasia from normal tissue," *Br. J. Cancer* **98**, 457-465 (2008).
  157. J. Berg, J. Tymoczko, and L. Stryer, *Biochemistry, Fifth Edition Lecture Notebook* (W. H. Freeman, 2002).
  158. F. Teale, and G. Weber, "Ultraviolet fluorescence of the aromatic amino acids," *Biochem. J* **65**, 476 (1957).
  159. B. Banerjee, B. Miedema, and H. Chandrasekhar, "Role of basement membrane collagen and elastin in the autofluorescence spectra of the colon," *J. Investig. Med.* **47**, 326 (1999).
  160. G. Bottioli, A. C. Croce, D. Locatelli, R. Marchesini, E. Pignoli, S. Tomatis, C. Cuzzoni, S. Di Palma, M. Dalfante, and P. Spinelli, "Natural fluorescence of normal and neoplastic human colon: a comprehensive "ex vivo" study," *Lasers Surg. Med.* **16**, 48-60 (1995).
  161. R. Marchesini, E. Pignoli, S. Tomatis, S. Fumagalli, A. E. Sichirollo, S. D. Palma, M. D. Fante, P. Spinelli, A. C. Croce, and G. Bottioli, "Ex vivo optical properties of human colon tissue," *Lasers Surg. Med.* **15**, 351-357 (1994).
  162. L. Stryer, *Biochemistry* (W. H. Freeman, 1981).
  163. N. Ramanujam, M. Mitchell, A. Mahadevan, S. Warren, S. Thomsen, E. Silva, and R. Richards-Kortum, "In vivo diagnosis of cervical intraepithelial neoplasia using 337-nm-excited laser-induced fluorescence," *Proc. Natl. Acad. Sci. USA.* **91**, 10193 (1994).
  164. A. Policard, "Etude sur les aspects offerts par des tumeurs experimentales examinees a la lumiere de Wood," *CR Soc Biol* **91**, 1423-1424 (1924).
  165. F. Ghadially, and W. Neish, "Porphyrin fluorescence of experimentally produced squamous cell carcinoma," (1960).
  166. J. Kennedy, R. Pottier, and D. Pross, "Photodynamic therapy with

- endogenous protoporphyrin IX: Basic principles and present clinical experience," *J. Photochem. Photobiol. B: Biol.* **6**, 143-148 (1990).
167. C. Sun, E. Duzman, J. Mellott, L. Liaw, and M. Berns, "Spectroscopic, morphologic, and cytotoxic studies on major fractions of hematoporphyrin derivative and photofrin II," *Lasers Surg. Med.* **7**, 171-179 (1987).
  168. L. Marchand, T. Donlon, J. Hankin, L. Kolonel, L. Wilkens, and A. Seifried, "B-vitamin intake, metabolic genes, and colorectal cancer risk (United States)," *Cancer Causes Control* **13**, 239-248 (2002).
  169. D. M. Haaland, and E. V. Thomas, "Partial least-squares methods for spectral analyses. 1. Relation to other quantitative calibration methods and the extraction of qualitative information," *Anal. Chem.* **60**, 1193-1202 (1988).
  170. A. Haka, K. Shafer-Peltier, M. Fitzmaurice, J. Crowe, R. Dasari, and M. Feld, "Diagnosing breast cancer by using Raman spectroscopy," *Proc. Natl. Acad. Sci. USA.* **102**, 12371-12376 (2005).
  171. I. Georgakoudi, B. Jacobson, M. Müller, E. Sheets, K. Badizadegan, D. Carr-Locke, C. Crum, C. Boone, R. Dasari, and J. Van Dam, "NAD (P) H and collagen as in vivo quantitative fluorescent biomarkers of epithelial precancerous changes," *Cancer Res.* **62**, 682-687 (2002).
  172. R. S. Wooten, D. A. Ahlquist, R. E. Anderson, H. A. Carpenter, J. H. Pemberton, D. A. Cortese, and D. M. Ilstrup, "Localization of hematoporphyrin. Derivative to human colorectal cancer," *Cancer* **64**, 1569-1576 (1989).
  173. B. Mayinger, M. Jordan, P. Horner, C. Gerlach, S. Muehldorfer, B. Bittorf, K. Matzel, W. Hohenberger, E. Hahn, and K. Guenther, "Endoscopic light-induced autofluorescence spectroscopy for the diagnosis of colorectal cancer and adenoma," *J. Photochem. Photobiol. B: Biol.* **70**, 13-20 (2003).
  174. E. Wynder, and B. Reddy, "Metabolic epidemiology of colorectal cancer," *Cancer* **34**, 801-806 (1974).
  175. A. Merrill Jr, and J. Henderson, "Diseases associated with defects in vitamin B6 metabolism or utilization," *Annu. Rev. Nutr.* **7**, 137-156 (1987).
  176. J. Schwartz, J. Passonneau, G. Johnson, and I. Pastan, "The effect of growth conditions on NAD<sup>+</sup> and NADH concentrations and the NAD<sup>+</sup>: NADH ratio

- in normal and transformed fibroblasts," *J. Biol. Chem.* **249**, 4138 (1974).
177. D. Bent, and E. Hayon, "Excited state chemistry of aromatic amino acids and related peptides. III. Tryptophan," *J. Am. Chem. Soc.* **97**, 2612-2619 (1975).
  178. J. Ali, W. Wang, M. Zevallos, and R. Alfano, "Near infrared spectroscopy and imaging to probe differences in water content in normal and cancer human prostate tissues," *Technol Cancer Res Treat.* **3**, 491 (2004).
  179. C. Gullledge, and M. Dewhirst, "Tumor oxygenation: a matter of supply and demand," *Anticancer Res.* **16**, 741-750 (1996).
  180. A. Huang, D. Fuchs, B. Widner, C. Glover, D. Henderson, and T. Allen-Mersh, "Serum tryptophan decrease correlates with immune activation and impaired quality of life in colorectal cancer," *Br. J. Cancer* **86**, 1691-1696 (2002).
  181. E. Wei, E. Giovannucci, J. Selhub, C. Fuchs, S. Hankinson, and J. Ma, "Plasma vitamin B<sub>6</sub> and the risk of colorectal cancer and adenoma in women," *JNCI Cancer Spectrum* **97**, 684-692 (2005).
  182. C. Potera, D. Rose, and R. Brown, "Vitamin B<sub>6</sub> deficiency in cancer patients," *Am. J. Clin. Nutr.* **30**, 1677 (1977).
  183. J. R. Mourant, I. J. Bigio, J. Boyer, T. M. Johnson, J. Lacey, A. G. Bohorfoush, and M. Mellow, "Elastic scattering spectroscopy as a diagnostic tool for differentiating pathologies in the gastrointestinal tract: preliminary testing," *J. Biomed. Opt.* **1**, 192-199 (1996).
  184. K. Lin, W. Zheng, and Z. Huang, "Integrated autofluorescence endoscopic imaging and point-wise spectroscopy for real-time in vivo tissue measurements," *J. Biomed. Opt.* **15**, 040507 (2010).
  185. D. Ferreira, P. Coutinho, E. Castanheira, J. Correia, and G. Minas, "Fluorescence and diffuse reflectance spectroscopy for early cancer detection using a new strategy towards the development of a miniaturized system," in *Conf Proc IEEE Eng Med Biol Soc.*, 1210-1213(2010).
  186. M. Chandra, K. Vishwanath, G. D. Fichter, E. Liao, S. J. Hollister, and M. A. Mycek, "Quantitative molecular sensing in biological tissues: an approach to non-invasive optical characterization," *Opt. Express* **14**, 6157-6171 (2006).

187. B. C. Wilson, and S. L. Jacques, "Optical reflectance and transmittance of tissues: principles and applications," *IEEE J. Quantum Electron.* **26**, 2186-2199 (1990).
188. S. Gebhart, W. Lin, and A. Mahadevan-Jansen, "In vitro determination of normal and neoplastic human brain tissue optical properties using inverse adding-doubling," *Phys. Med. Biol.* **51**, 2011 (2006).
189. T. Vo-Dinh, M. Panjehpour, and B. F. Overholt, "Laser induced fluorescence for esophageal cancer and dysplasia diagnosis," *Ann. N.Y. Acad. Sci.* **838**, 116-122 (1998).
190. G. Zonios, L. T. Perelman, V. Backman, R. Manoharan, M. Fitzmaurice, J. Van Dam, and M. S. Feld, "Diffuse reflectance spectroscopy of human adenomatous colon polyps *in vivo*," *Appl. Opt.* **38**, 6628-6637 (1999).
191. I. J. Bigio, S. G. Bown, G. Briggs, C. Kelley, S. Lakhani, D. Pickard, P. M. Ripley, I. G. Rose, and C. Saunders, "Diagnosis of breast cancer using elastic-scattering spectroscopy: preliminary clinical results," *J. Biomed. Opt.* **5**, 221 (2000).
192. M. Chandra, J. Scheiman, D. Heidt, D. Simeone, B. McKenna, and M. A. Mycek, "Probing pancreatic disease using tissue optical spectroscopy," *J. Biomed. Opt.* **12**, 060501 (2007).
193. R. Marchesini, M. Brambilla, C. Clemente, M. Maniezzo, A. E. Sichirollo, A. Testori, D. R. Venturoli, and N. Cascinelli, "In vivo spectrophotometric evaluation of neoplastic and non neoplastic skin pigmented lesions – I. reflectance measurements," *Photochem. Photobiol.* **53**, 77-84 (1991).
194. J. R. Mourant, I. J. Bigio, J. Boyer, R. L. Conn, T. Johnson, and T. Shimada, "Spectroscopic diagnosis of bladder cancer with elastic light scattering," *Lasers Surg. Med.* **17**, 350-357 (1995).
195. Z. Ge, K. T. Schomacker, and N. S. Nishioka, "Identification of colonic dysplasia and neoplasia by diffuse reflectance spectroscopy and pattern recognition techniques," *Appl. Spectrosc.* **52**, 833-839 (1998).
196. N. Rajaram, A. Gopal, X. Zhang, and J. W. Tunnell, "Experimental validation of the effects of microvasculature pigment packaging on *in vivo* diffuse reflectance spectroscopy," *Lasers Surg. Med.* **42**, 680-688 (2010).

197. J. A. Curcio, and C. C. Petty, "The near infrared absorption spectrum of liquid water," *J. Opt. Soc. Am* **41**, 302-304 (1951).
198. H. Arimoto, M. Egawa, and Y. Yamada, "Depth profile of diffuse reflectance near infrared spectroscopy for measurement of water content in skin," *Skin Res. Technol.* **11**, 27-35 (2005).
199. S. Chung, A. Cerussi, S. Merritt, J. Ruth, and B. Tromberg, "Non-invasive tissue temperature measurements based on quantitative diffuse optical spectroscopy (DOS) of water," *Phys. Med. Biol.* **55**, 3753 (2010).
200. J. Bayly, V. Kartha, and W. Stevens, "The absorption spectra of liquid phase H<sub>2</sub>O, HDO and D<sub>2</sub>O from 0.7  $\mu$ m to 10  $\mu$ m," *Infrared Physics* **3**, 211-222 (1963).
201. H. W. Wang, J. K. Jiang, C. H. Lin, J. K. Lin, G. J. Huang, and J. S. Yu, "Diffuse reflectance spectroscopy detects increased hemoglobin concentration and decreased oxygenation during colon carcinogenesis from normal to malignant tumors," *Opt. Express* **17**, 2805-2817 (2009).
202. Y. S. Fawzy, M. Petek, M. Tercelj, and H. Zeng, "In vivo assessment and evaluation of lung tissue morphologic and physiological changes from non-contact endoscopic reflectance spectroscopy for improving lung cancer detection," *J. Biomed. Opt.* **11**, 044003 (2006).
203. Y. S. Fawzy, and H. Zeng, "Determination of scattering volume fraction and particle size distribution in the superficial layer of a turbid medium by using diffuse reflectance spectroscopy," *Appl. Opt.* **45**, 3902-3912 (2006).

# Appendix

## A.1 American Joint committee on Cancer Staging of Colon Cancer [14]

The tumor-node-metastasis (TNM) systems of the American Joint Committee on Cancer (AJCC), the four stages are based on the depth of invasion of the primary tumor (T), lymph node status (N), and distant metastasis (M). Approximately 39% of colon and rectum cancer cases are diagnosed while the cancer is still confined to the primary site (localized stage or stage I/IIa), 36% are diagnosed after the cancer has spread to regional lymph nodes (stage III) or directly beyond the primary site (stage IIb) and 19% are diagnosed after the cancer metastasized (distant stage or stage IV).

| Stage      | T     | N     | M   |
|------------|-------|-------|-----|
| Stage I    | T1-2  | N0    | M0  |
| Stage IIA  | T3    | N0    | M0  |
| Stage IIB  | T4a   | N0    | M0  |
| Stage IIC  | T4b   | N0    | M0  |
| Stage IIIA | T1-2  | N1    | M0  |
|            | T1    | N2a   | M0  |
| Stage IIIB | T3-T4 | N1    | M0  |
|            | T2-3  | N2a   | M0  |
|            | T1-2  | N2b   | M0  |
| Stage IIIC | T4a   | N2a   | M0  |
|            | T3-4a | N2b   | M0  |
|            | T4b   | N1-2  | M0  |
| Stage IVA  | Any T | Any N | M1a |
| Stage IVB  | Any T | Any N | M1b |

**A.2 Table 1 Some known tissue endogenous fluorophores and wavelengths of their excitation and emission maxima [34, 81]**

| Endogenous fluorophore | Biological source                                                 | Wavelength of max. Fluorescence excitation (nm) | Wavelength of max. Fluorescence emission (nm) |
|------------------------|-------------------------------------------------------------------|-------------------------------------------------|-----------------------------------------------|
| Tryptophan             | Amino acids                                                       | 280                                             | 350                                           |
| Phenylalanine          |                                                                   | 260                                             | 280                                           |
| Tyrosine               |                                                                   | 275                                             | 330                                           |
| Collagen               | Connective tissue                                                 | 330-340                                         | 400-410                                       |
| Elastin                | Extracellular matrix                                              | 350,420                                         | 420,510                                       |
| NADH                   | Metabolic cofactors                                               | 340                                             | 450                                           |
| FAD, flavins           |                                                                   | 450                                             | 515                                           |
| Pyridoxine             | Vitamin B6 compounds                                              | 330,340                                         | 400                                           |
| Pyridoxal-5'-phosphate |                                                                   | 330                                             | 400                                           |
| Porphyrins             | By-product of heme biosynthesis;<br>bacterial fauna               | 400-450                                         | 635,690                                       |
| Ceroid, lipofuscin     | Lipopigment granules;<br>age related;<br>lipid oxidation products | 340-395                                         | 430-460,540-640                               |